DESIGN AND FABRICATION OF A DNA ELECTROPHORESIS CHIP BASED ON MEMS TECHNOLOGY

A THESIS SUBMITTED TO
THE GRADUATE SCHOOL OF NATURAL AND APPLIED SCIENCES
OF
MIDDLE EAST TECHNICAL UNIVERSITY

BY

SERTAN SUKAS

IN PARTIAL FULFILLMENT OF THE REQUIREMENTS
FOR
THE DEGREE OF MASTER OF SCIENCE
IN
MECHANICAL ENGINEERING

SEPTEMBER 2007

Approval of the thesis:

DESIGN AND FABRICATION OF A DNA ELECTROPHORESIS CHIP BASED ON MEMS TECHNOLOGY

submitted by **SERTAN SUKAS** in partial fulfillment of the requirements for the degree of **Master of Science in Mechanical Engineering Department, Middle East Technical University** by,

Prof. Dr. Canan Özgen
Dean, Graduate School of **Natural and Applied Sciences** _____

Prof. Dr. Kemal İder
Head of Department, **Mechanical Engineering** _____

Asst. Prof. Dr. Cüneyt Sert
Supervisor, **Mechanical Engineering Dept., METU** _____

Asst. Prof. Dr. Haluk Külah
Co-Supervisor, **Electrical and Electronics Engineering Dept., METU** _____

Examining Committee Members:

Prof. Dr. Tuna Balkan
Mechanical Engineering Dept., METU _____

Asst. Prof. Dr. Cüneyt Sert
Mechanical Engineering Dept., METU _____

Asst. Prof. Dr. Haluk Külah
Electrical and Electronics Engineering Dept., METU _____

Asst. Prof. Dr. Ayşe Elif Erson
Biology Dept., METU _____

Asst. Prof. Dr. Tuba Okutucu
Mechanical Engineering Dept., METU _____

Date: 17.09.2007

I hereby declare that all information in this document has been obtained and presented in accordance with academic rules and ethical conduct. I also declare that, as required by these rules and conduct, I have fully cited and referenced all material and results that are not original to this work.

Name, Last Name : Sertan SUKAS

Signature :

ABSTRACT

DESIGN AND FABRICATION OF A DNA ELECTROPHORESIS CHIP BASED ON MEMS TECHNOLOGY

SUKAS, Sertan

M.Sc., Department of Mechanical Engineering

Supervisor: Asst. Prof. Dr. Cüneyt Sert

Co-Supervisor: Asst. Prof. Dr. Haluk Külah

September 2007, 138 pages

This thesis reports design, fabrication, and implementation of two different micro electrophoresis system architectures for DNA analyses. The first architecture is traditional single channel layout with several design alternatives for size-based separation of DNA fragments. The second one is novel double channel architecture specialized for rapid mutation detection using heteroduplex analysis (HDA) method with an application of a newly designed injection technique. Besides achieving high resolution separations within the length of 1 mm with single channel arrangement, HDA was successfully applied for 590 base pair (bp) long PCR sample with 3 bp mutations in a separation length of 50 μm in less than 3 minutes with double channel structure.

Microchannels were formed using parylene-C due to its conformal deposition, no surface treatment requirement, transparency, biocompatibility, low background fluorescence, etc. Using the advantage of parylene in fabrication, the microchannels were fabricated with an only three-mask process. New double channel architecture is obtained by dividing the 200 μm-wide separation channel into two parts by a 20 μm-thick wall between them.

For sample injection, various techniques, such as traditional cross, double-T, and double-L were investigated and optimized for single channel architecture assisting with pullback injection method. For double channel architecture, a novel, u-turn injection technique was applied. Precise control of sample amount by adjusting the injection time was accomplished by this new technique.

Using high resolution cross-linked polyacrylamide gel as sieving material, separations were achieved in a very short length and time. Electrophoresis was performed in both channels of the double channel microchips simultaneously under the same conditions. This gives the chance of having a control channel in microchip format, which is very critical for the accuracy and reliability of the results in genetic analyses.

Keywords: Microchip Capillary Electrophoresis, Mutation Detection, Heteroduplex Analysis, DNA, Parylene.

ÖZ

MEMS TABANLI DNA ELEKTROFOREZ ÇİP TASARIMI VE ÜRETİMİ

SUKAS, Sertan
Yüksek Lisans, Makina Mühendisliği Bölümü
Tez Yöneticisi: Y. Doç. Dr. Cüneyt Sert
Ortak Tez Yöneticisi: Y. Doç. Dr. Haluk Külah

Eylül 2007, 138 sayfa

Bu tezde DNA analizleri için geliştirilmiş iki farklı mikro elektroforez sistem modellerinin tasarımları, üretimleri ve uygulamaları sunulmuştur. İlk model, DNA fragmanlarının uzunluğa bağlı olarak ayrıştırılması için birçok alternatif ile tasarlanan geleneksel tek kanallı yapıdır. İkinci model, yeni tasarlanmış bir enjeksiyon tekniği ile heteroduplex analiz (HDA) metodu kullanılarak hızlı mutasyon taraması için özelleştirilmiş, özgün çift kanallı yapıdır. Tek kanallı yapı ile 1 mm mertebesinde yüksek çözünürlüklü ayrıştırmaların başarılmasının yanısıra; heteroduplex analizi, 590 bp uzunluğunda 3 bp mutasyon içeren PCR örneği ile çift kanallı yapı kullanılarak 50 μm ayrıştırma uzunluğunda, 3 dakikadan daha kısa bir sürede başarıyla uygulanmıştır.

Parylene-C, konformal kaplanma, yüzey işlemesine ihtiyaç duymama, şeffaflık, biyolojik uygulamalara uygunluk, düşük arka plan floresanı v.b. avantajları sebebiyle mikrokanalların oluşturulmasında ana malzeme olarak kullanılmıştır. Parylene maddesinin üretimdeki avantajlarından faydalanılarak mikrokanallar sadece üç maskelik bir süreç sonunda üretilmiştir. Yeni tasarım olan çift kanallı yapılar, 200 µm genişliğindeki ayrıştırma kanalı 20 µm kalınlığındaki bir duvar ile ikiye bölünerek elde edilmiştir.

Örnek enjeksiyonu için tek kanallı yapılarda haç, çift-T ve çift-L olmak üzere değişik enjeksiyon teknikleri, geri-çekim yardımcı metodu ile uygulanmış ve optimize edilmiştir. Çift kanallı yapılar için özgün u-dönüş enjeksiyon tekniği uygulanmıştır. Bu yeni teknikle enjeksiyon zamanı ile oynanarak örnek miktarının hassas bir şekilde kontrolü sağlanmıştır.

Elek malzemesi olarak yüksek çözünürlüklü, düşük akışkanlıkta polyacrylamide jeli kullanılarak ayrıştırmalar çok kısa mesafelerde ve çok kısa sürelerde gerçekleştirilmiştir. Elektroforez uygulaması, çift kanallı yapıların herbir kanalında eşzamanlı olarak aynı şartlarda yapılabilmiştir. Bu, genetik analizlerde alınan sonuçların kesinliği ve güvenilirliği açısından çok kritik bir öneme sahip olan kontrol kanalına mikroçip formatında sahip olunmasını sağlamıştır.

Anahtar Kelimeler: Mikroçip Kılcal Kanal Elektroforezi, Mutasyon Taraması, Heteroduplex Analizi, DNA, Parylene.

To My Angel

ACKNOWLEDGMENTS

I would like to express my appreciation and thanks to my project supervisor and co-advisor Asst. Prof. Dr. Haluk Külah, and my supervisor Asst. Prof. Dr. Cüneyt Sert for their guidance and support during my graduate study. I would also thank to Haluk Külah for supplying me a high quality research environment.

I would also like to thank to Asst. Prof. Dr. Ayşe Elif Erson for her guidance throughout my thesis work and supplying the biological samples that I need.

Special thanks to Fehmi Çivitci for shearing his time with me in any place that I worked throughout my graduate study. Sharing my working environment with him and our endless stress relief sessions were so exceptional for me.

I wish to thank to Orhan Akar for his guidance, support and spending his time for me to teach everything in METU-MET facility. Also thanks to Mahmud Yusuf Tanrıkulu for answering all my questions.

I also want to thank to Ata Tuna Çiftlik for his last moment supports and all members of METU-BioMEMS and METU-MEMS research groups.

I would like to thank to my family for being always with me in any condition. Last but not least, I would like to express my deepest gratitude to my fiancée, Özlem for her love and endless support.

This work was supported by TÜBİTAK with grant number 104S605.

TABLE OF CONTENTS

LIST OF TABLES

TABLES

LIST OF FIGURES

FIGURES

CHAPTER 1

INTRODUCTION

One of the greatest mysteries of all times is the genetic code of mankind which is believed to reveal all the secrets of human beings. Since the first determination of complete genome of a virus in 1976 by Walter Fiers [1], the most important attempt to understand the genetic makeup of human species was the "Human Genome Project" which was started in 1990 and planned to be finished in 15 years. The aim was to completely decode the genomic code of human. In addition to this three billion dollars project, many researchers from different countries have been working for years for the ultimate goal of revealing the secrets of the human body. Due to these huge efforts and advances in the field of genomics, it was announced in 2003 that the main tasks of the project were accomplished two years earlier than planned. Although these studies triggered gigantic developments in existing research methods and also initiated the development of new technologies, it is obvious that accomplishing the goals of sequencing other organism's or single individuals' genomes need more efforts for feasible, faster and lower cost applications. The leading technology will definitely be the microarray technology which has been very rapidly growing for last decades.

The aim of such efforts is to serve medicine and health sciences as well as genetics. Several techniques are applied for analyzing human DNA either with conventional methods or in micro scale for various purposes such as sequencing and mutation

detection. Electrophoresis is one of the most popular techniques being used for DNA analyses since the 30s.

After the impact of the micro electromechanical systems (MEMS) in many technological fields with rapid developments in microfabrication technologies, microfluidic systems started to play an important role in chemical and genetic analyses, as well as electrophoresis. Such systems are called as micro total analysis systems (μ-TAS). This research area is called BioMEMS and these multipurpose microsystems are named as lab-on-a-chip systems.

Miniaturization was the starting point of integrating microsystems in the field of electrophoresis. Due to this fact, taking the advantage of the knowledge gained through the early methods, the popularity of micro capillary electrophoresis systems has been continuously increasing since they were first introduced in early 90s. Application of micro-fabricated analysis tools is obviously a revolution in electrophoresis like many other chemical analysis techniques in a number of aspects, which are discussed in the next sections.

This thesis reports design, fabrication, and implementation of two different micro electrophoresis systems for DNA analyses. The first system is a traditional single channel microchip for size-based separation of DNA fragments. The other is a novel double channel architecture specialized for rapid mutation detection with an application of a newly designed injection technique. The design, fabrication, and the experimentation procedures are discussed in the following chapters. In this chapter, Section 1.1 explains conventional electrophoresis techniques for DNA analyses, Section 1.2 describes micro scale electrophoresis systems while comparing them with conventional methods, Section 1.3 gives details about the fabrication techniques used for constructing microchips, Section 1.4 gives information about the applications of micro electrophoresis systems, and Section 1.5 summarizes the objective and gives organization of the thesis.

1.1. Conventional Electrophoresis Techniques

Since the first recorded successful application in the 30s, electrophoresis is a widely used technique for DNA analyses. The technique is based on separating charged molecules in a fluidic medium under the influence of an electric field. Figure 1.1 describes the basic theory of electrophoresis.

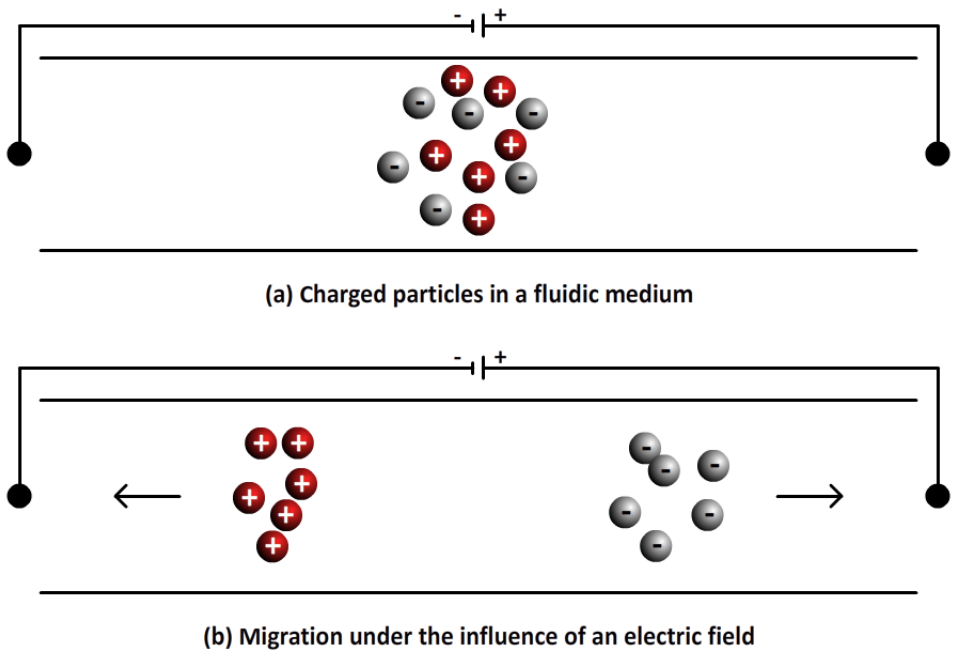

Figure 1.1: Basic electrophoresis theory.

Besides its easy application in separation of inversely charged particles as shown in Figure 1.1, electrophoresis is not used only for this purpose. Analytes, which carry the same charge, are separated due to differences in their electrophoretic mobilities. The separands of different sizes show different mobilities in a special medium such as a semisolid slab-gel, which serves as a sieving material. Size-based

separations of DNA, RNA and proteins with different sizes can be performed using this method.

Alternative techniques without gel medium were also applied. Cellulose acetate membrane electrophoresis [2] was first applied in 1957. Since these membranes have large pores, they do not serve as a sieving medium. Paper and thin-layer electrophoresis [3] was first applied in 1990, in which thin layer silica gel-plates were used for linking buffer tanks. However, these methods failed to survive against gel electrophoresis method due to its several advantages over them, such as improved separation capability and higher sample loading capacity. Nevertheless, after the implementation of high performance capillary electrophoresis (HPCE) systems for genomic analyses [4, 5], they became another strong alternative for electrophoresis applications. Slab-gel and capillary electrophoresis techniques are described in subsequent sections.

1.1.1. Slab-gel Electrophoresis

In slab-gel or gel electrophoresis, a gel slab is placed into a tank filled with buffer solution with two electrodes immersed at the two ends of the solution and connected to the power supply. When high voltage is applied, DNA moves towards the higher potential because it is naturally negatively charged due to the phosphate groups of its nucleotides. Figure 1.2 shows the picture of a typical gel electrophoresis system.

The gel provides physical support and mechanical stability for the fluidic buffer system. But the main role of the gel is its sieving effect. Molecular sieving effect makes size based separation possible because DNA fragments have constant mass-to-charge ratio in free solution, except for the short fragments (smaller than 400 bp). In other words, it is not possible to separate DNA fragments in free solution without using a sieving medium. Figure 1.3 summarizes the technique.

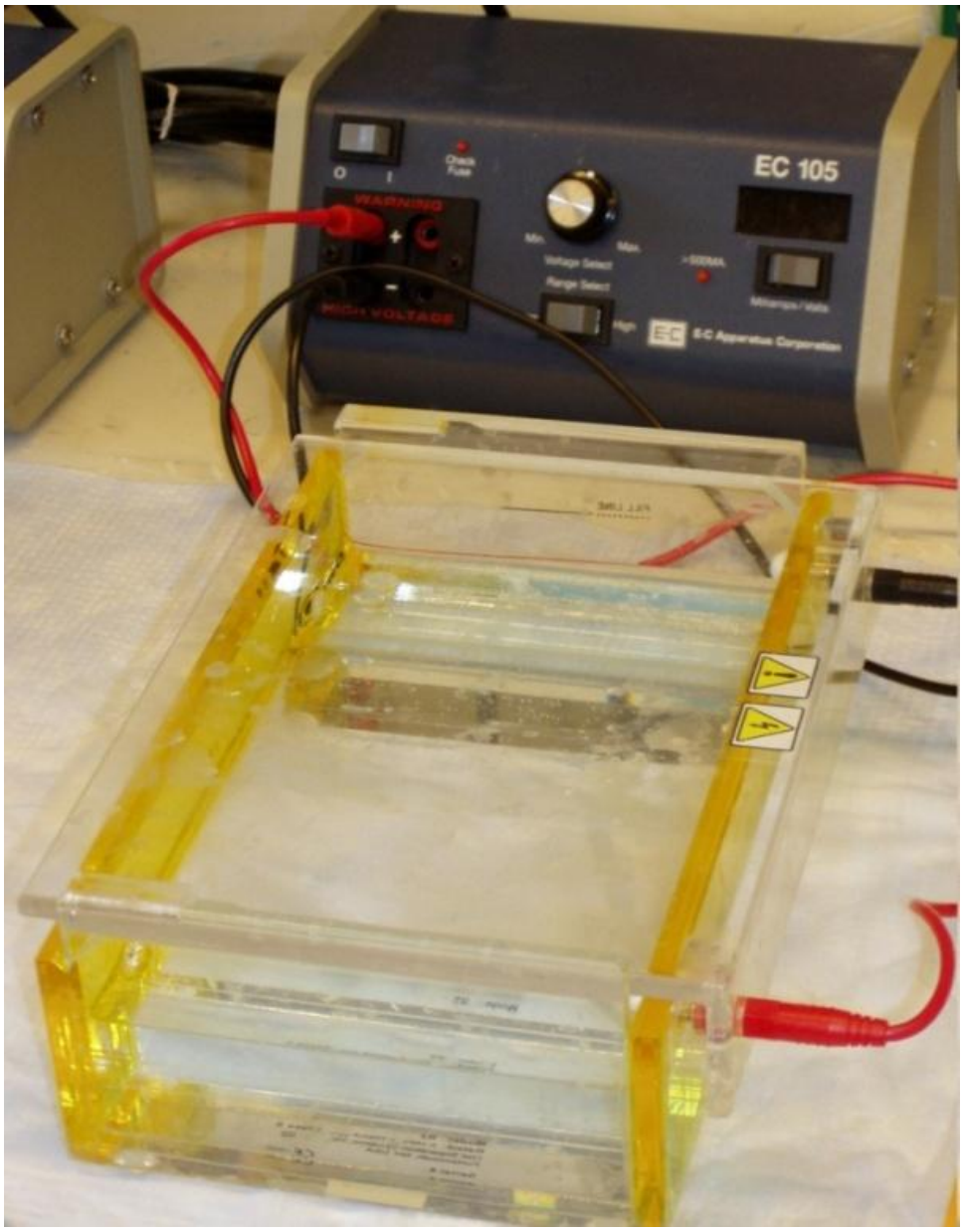

Figure 1.2: A typical gel electrophoresis setup.

Typically, agarose is used for low resolution separations of DNA whereas polyacrylamide is used for higher resolution with relatively shorter fragments.

Buffer, which is also called background electrolyte (BGE), is used as a carrier electrolyte solution. Buffer maintains the pH of the solution around the suitable

values for the analysis and provides sufficient conductivity for the separation to be performed. Generally, various concentrations of TBE (Tris, Boric acid, EDTA) are used as a buffer solution for standard agarose gel electrophoresis.

For visualization purposes, analytes are marked with a dye such as ethidium bromide which binds to DNA and is responsive to ultraviolet (UV) light. After the electrophoresis run, the gel slab is exposed to UV light and the separated fragments marked with a dye are visualized. Figure 1.4 shows the picture of a gel slab taken under the UV light after the separation.

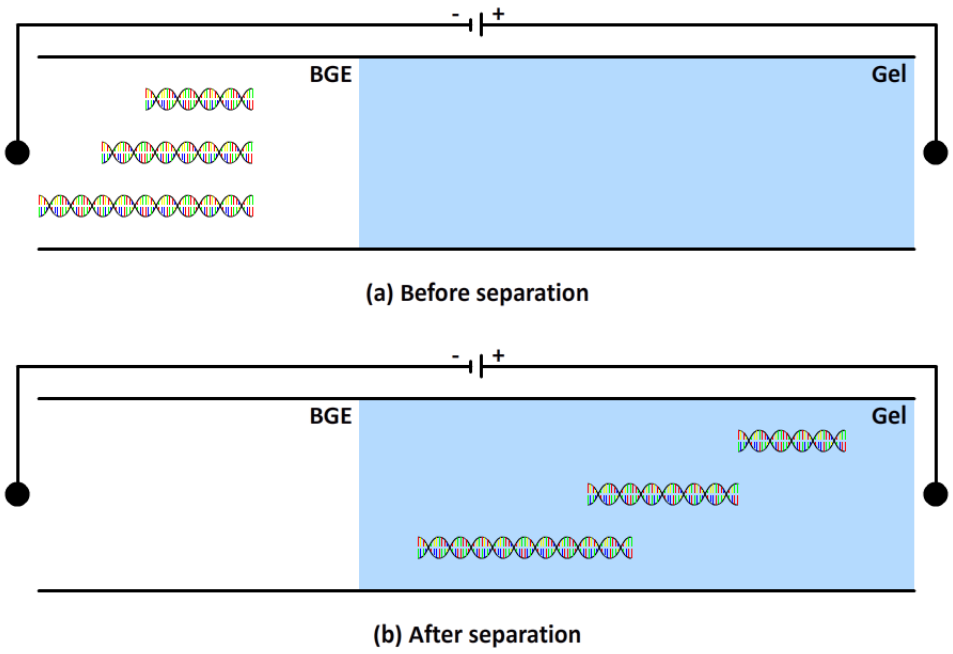

Figure 1.3: DNA gel electrophoresis.

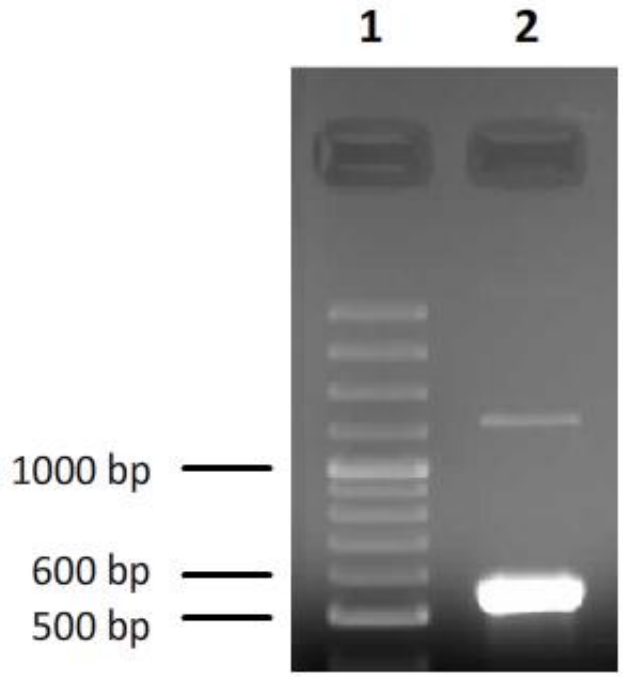

Figure 1.4: Results of a typical DNA gel electrophoresis run. Lane 1: DNA ladder, lane 2: 560 bp long PCR sample.

1.1.2. Capillary Electrophoresis (CE)

In this technique, separation is performed in the fused silica capillaries typically 20 to 30 cm long and with an internal diameter of 50 to 100 µm. Both ends of the capillary are immersed into the buffer solution and are in contact with the electrodes. Schematic view of a typical capillary electrophoresis setup is given in Figure 1.5.

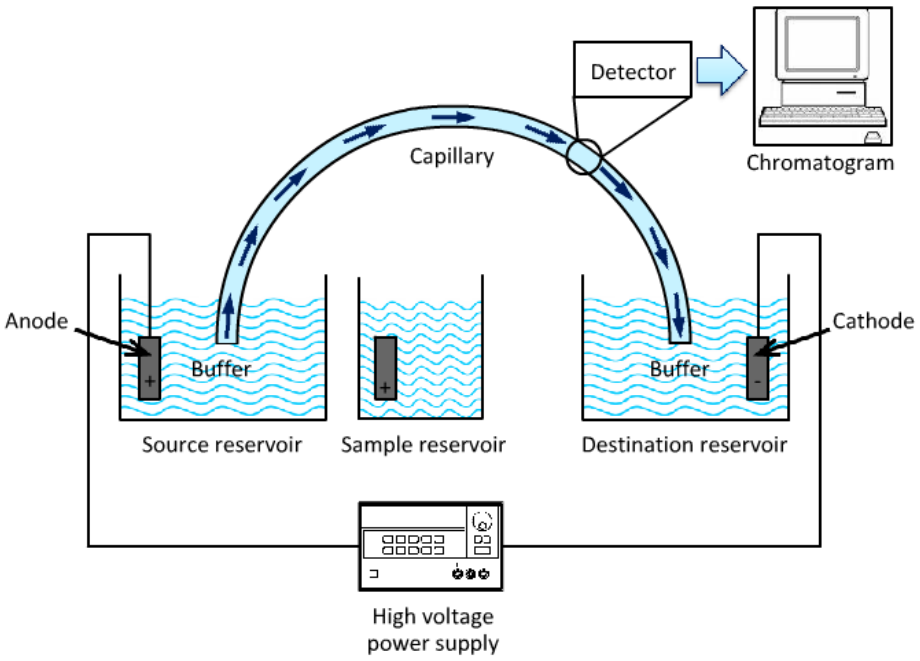

Figure 1.5: A typical capillary electrophoresis setup.

Application of CE introduced many advantages over the slab-gel electrophoresis. The capillary walls mechanically support the buffer solution instead of a gel material. Sample loading (injection) can be performed in a repeatable manner with very low sample amounts. Detection is performed on-line and the output is a chromatogram instead of a picture. Use of the capillaries allows the application of higher voltages because of efficient heat dissipation. The possibility of applying higher voltages makes the analysis time shorter than the slab-gel electrophoresis because the analysis speed is directly proportional to the amount of differential potential applied between the two electrodes placed at both ends of the capillaries. On the other hand, only one sample can be analyzed in a single run with CE, while multiple samples can be analyzed in a single run with multiple lanes in slab-gel electrophoresis. In order to solve this problem, capillary array electrophoresis (CAE) systems were proposed for high throughput analyses [6, 7].

However, miniaturization of CE devices to micro scale puts the above mentioned advantages one step further. Microchip capillary electrophoresis (CE) systems offer many advantages compared to macro scale devices such as compact geometry, low cost, ease of use, less labor, and short separation times. Following sections discuss the micro scale electrophoresis systems.

1.2. Electrophoresis in Micro Scale

Although an excitement was generated with the first implementation of a microfabricated gas chromatography device in 1979 [8], the interaction between micro technology and separation technology started with the first reported microfabricated liquid chromatography system in 1990 [9]. Following these, with the introduction of the first microchip CE device in 1992 [10], microsystems became an excellent candidate for electrophoresis applications because of their various advantages, such as requirement of very little sample amount for operation and providing fast, high performance separations with efficient heat dissipation. Starting with early 90s, micro CE technology has grown dramatically and today it is used in several applications, which are described briefly in the next sections.

The theory and physical mechanisms of microchip CE systems are based on the knowledge gained from conventional CE devices. The key parameter which describes the movement of the analyte is *mobility*. There are two phenomena affecting the motion of the analyte in electrophoresis: Electroosmosis and electrophoresis. The presence of electroosmotic flow (EOF) in electrophoresis applications is a well known fact since the first reported CE system [5]. Electroosmosis is a bulk fluid flow (typically a buffer solution) that occurs when a voltage difference is applied across the channel. This type of flow is a result of charge on the inside of the channel wall. As a result, the velocity of a particle under the effect of an applied electrical field is given by

$$v = (\mu_{ep} + \mu_{eof})E \quad (1.1)$$

where v is the velocity of the particle, μ_{ep} is the electrophoretic mobility of the analyte, μ_{eof} is the electroosmotic mobility (the contribution of the electroosmotic flow to mobility), and E is the electrical field strength. The effect of electroosmosis does not change for a specified system. In other words, it is a system parameter. Then the dominating parameter for describing the analyte motion becomes the electrophoretic mobility, which is defined as

$$\mu = \frac{qE}{6\pi\eta r} \quad (1.2)$$

where μ is the mobility, q is the charge on the analyte, E is the applied electrical field strength, η is the dynamic viscosity, and r is the radius of the analyte. As seen in Equation (1.2), the most important parameter in describing the mobility is the net charge on the analyte and its ratio to the mass of the analyte, which is represented with the radius term in the equation. Like the radius term, the fragment length of a DNA molecule represents its mass. The fragment length is defined as the number of base pairs (bp). As stated in the previous section, DNA molecules have constant mass-to-charge ratio. Thus, their mobilities become independent of their fragment lengths. This makes the application of the electrophoresis more complex. Several studies were performed in order to describe the DNA electrophoresis. Details of the theory and the physical mechanisms of microchip CE of DNA molecules are discussed in the next chapter.

Micro CE technology is an excellent platform for not only developing and applying new techniques, but also applying or combining the conventional CE techniques for preserving their advantages while eliminating the disadvantages by miniaturization. Macro scale devices are being rapidly replaced with micro CE systems due to number of aspects. The most important advantages of micro CE systems are:

1. The implementation and usage of the microsystems are easy since their compact geometry.
2. Micro CE devices need less amount of sample to be analyzed, in the order of picoliters. Since the extraction and amplification of DNA is not an easy process, this feature is very important considering the decrease in the labor time before the application.
3. Heat dissipation is very efficient in micro scale. Thus, high voltages in kV range can be applied within very short lengths, yielding high resolution applications.
4. Taking the advantage of application of high potentials, the analysis time decreases from days to minutes. Therefore, labor time is not only decreased for sample preparation stage, but also for the analysis.
5. Due to the exponential improvements in microfabrication techniques, the cost of microfabricated devices per analysis is enormously less than the macro-sized counterparts.
6. In addition to their low cost, microfabricated devices are flexible, enabling the integration of various external systems and further development in terms of many aspects, such as combinating with integrated circuits.

The fabrication methods for micro CE devices are discussed in the following sections.

1.3. Fabrication Techniques for Micro-Electrophoresis Systems

The first microchip CE systems, were constructed using glass as a substrate material [10, 11]. Glass is a silicon compound and the readily developed fabrication technology in the MEMS field was applied for the fabrication of glass microchips. An important advantage of glass as a channel material is its excellent transparency which is vital for detection purposes. Having the same surface chemical properties with the fused silica capillaries used in conventional CE systems; glass is an excellent

material for constructing microchips in order to take advantage of previous experiences gained with CE systems.

In spite of the above mentioned advantages, glass has some drawbacks. Glass microchips yield very high manufacturing costs per device since not only one can fabricate only one device per run, but also high quality glass is very expensive. In addition, glass microchips are so fragile that extreme care should be taken during the operation. Because of these disadvantages, polymers have gained significant popularity in microchip fabrication as a substrate material. Polymer microchips are cheaper and easy to fabricate, making them suitable for constructing disposable chips. Hence, several microfabrication techniques were developed for polymer micro CE chips. The following sections describe the fabrication techniques for glass and polymer materials.

1.3.1. Glass Microchips

Glass microchips are fabricated using common lithography and wet etch techniques. Final device is constructed by assembling the top and bottom substrates after processing them separately. The channels are formed on the base substrate by wet etching. In order to define the channel layout on the base substrate, it is coated with a sacrificial layer, which is mostly a metal layer, at the first step. Then the sacrificial layer is patterned with photolithography and etching steps, respectively. At the final step, the glass substrate is etched isotropically by wet etching in order to create the channels. After creating the channels, the etch mask is removed. The access holes are drilled either on the base substrate or the blank glass wafer. Then these two wafers are bonded together to form the complete micro device. On the covering glass substrate, the on-chip electrodes can be constructed if necessary. The fabrication method is the same as for the creation of the etch mask for channel formation. A typical fabrication process flow is shown in Figure 1.6.

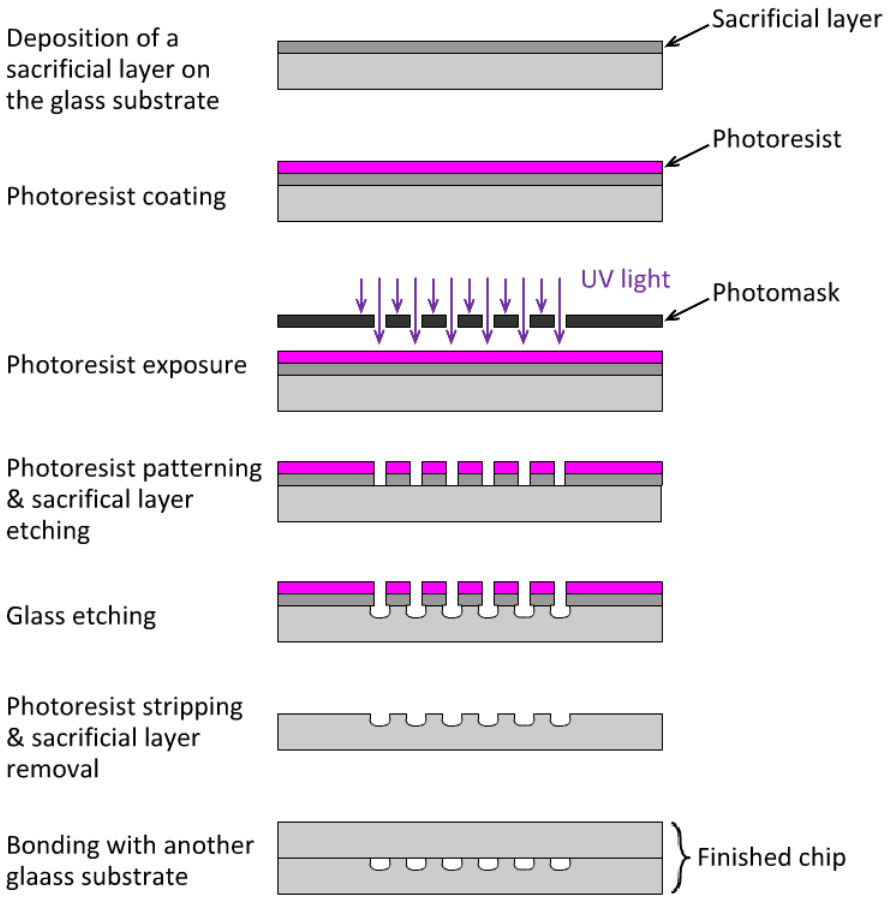

Figure 1.6: Typical fabrication process flow for glass microchips [12].

1.3.2. Polymer Microchips

The fabrication techniques used for construction of polymer microchips can be categorized into two main sections: bulk micromachining and surface micromachining. The most widely used techniques in both categories are discussed in the subsequent sections.

1.3.2.1. Bulk Micromachining

In bulk micromachining of polymers, the most common fabrication techniques are laser ablation [13], injection molding [14], casting [15], and hot embossing [16].

1.3.2.1.1. Laser Ablation

Many commercially available polymers are known to be photoablated when interacted with UV laser radiation. They include polycarbonate, poly-(methyl methacrylate) (PMMA), polystyrene, nitrocellulose, poly-(ethylene terephthalate) (PET or Melinex), and poly(tetrafluoroethylene) (Teflon) [13, 17]. During the photoablation process, the polymer is exposed to a UV radiation. Due to the short wave length laser pulses in UV region, the covalent bonds in long polymer chains are broken in the exposed parts of the polymer [17]. At this stage, a shock wave is generated. Then it removes the decomposed polymer fragments, yielding a photoablated cavity. As shown in Figure 1.7, the laser energy can be patterned using a mask with the succeeding creation of micro cavities and channels in various geometries or by controlling position of the laser with manipulator setups. The resulting structures mostly have little thermal damage, straight vertical walls, and well-defined depth [13, 18]. However, this technique is not suitable for mass production.

1.3.2.1.2. Injection Molding, Hot Embossing and Casting

The creation of microchannels and other structures using molding techniques are performed in two main steps: Fabrication of mold (or master), and pattern transfer from the mold to polymer substrates [12]. Microchip fabrication using these techniques is performed by replicating the mold pattern on the polymer substrate. The mold replication is accomplished by injection molding, embossing, or casting.

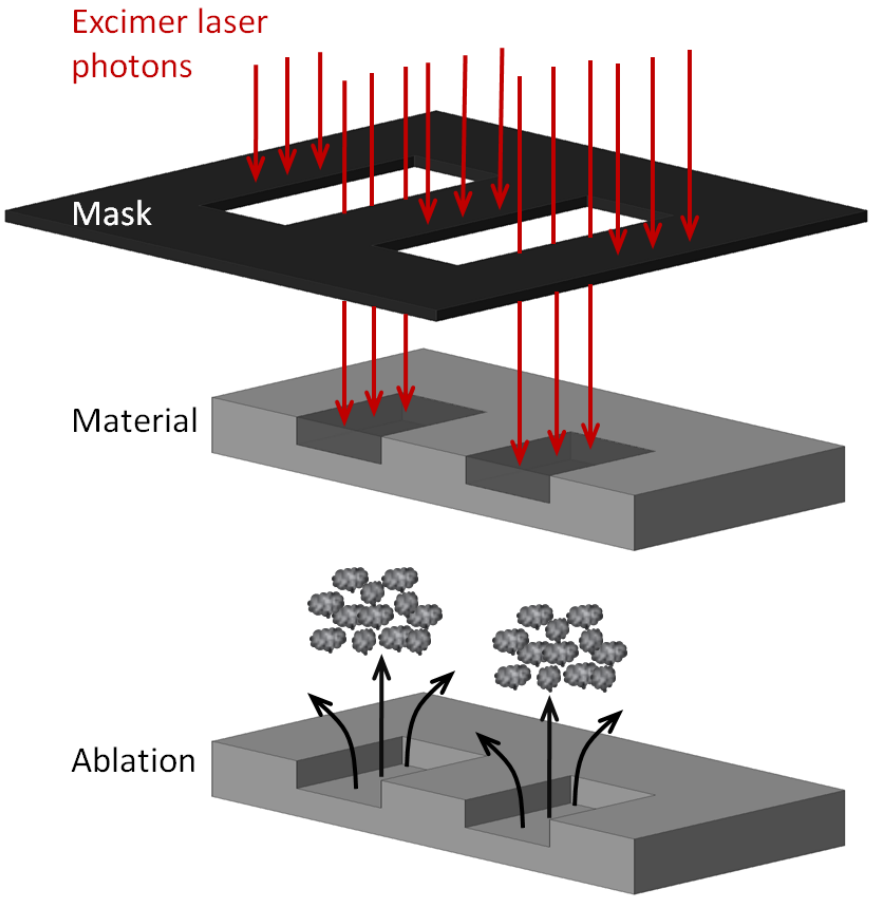

Figure 1.7: UV laser micromachining process. UV laser pulse rapidly breaks chemical bonds within a restricted volume to cause a mini explosion and ejection of ablated material [13].

In the injection molding process [14], polymer is melted and injected into a mold in a molding chamber. Injection molding allows very high-throughput and low cost production, because total process time for molding and releasing is about 5 to 10 seconds per device.

In the hot embossing process [16], the embossing tool (or stamp) and the polymer substrate are heated separately under vacuum conditions to a temperature just above the glass transition temperature of the polymer material. The stamp is then

taken into contact with the substrate and embossing is performed. This operation usually takes several minutes per device and can be considered as a useful tool in rapid prototyping devices.

In the casting process [15], polymer material such as poly(dimethylsiloxane) (PDMS) is usually spilled on top of the master and then cured (or hardened) at atmospheric pressure and room temperature. Elevating the temperature can accelerate curing. Finally, the hardened thick polymer slab is peeled off from the master piece and placed on another polymer substrate if necessary. The method is summarized in Figure 1.8. Casting is the simplest and easiest method to apply among these three molding processes, but requires contact with the master for minutes to hours.

1.3.2.2. Surface Micromachining

Surface micromachining is a fabrication process, in which the microchannels are formed on the surface of the substrates (silicon or glass), rather than etching, embossing or casting the substrate material. As a first step, the substrate is coated with either a structural polymer (parylene) or an isolation layer (oxide) for the purposes of thermal, electrical or mechanical isolations. For the cases, where the material of isolation layer is not selected as the structural polymer, the deposition of the structural layer is performed onto this isolation layer for biocompatibility and/or surface chemistry requirements. For construction of the microchannels, a sacrificial layer (photoresist) (PR) is spin-coated onto the isolated substrate first and patterned afterwards. The height of the sacrificial layer determines the height of the channels. Second, the structural polymer layer is deposited onto the sacrificial layer with chemical vapor deposition (CVD). After dry etching (plasma ashing) of the release holes, the sacrificial layer is etched away and the suspended channel structure is formed. Figure 1.9 shows the described fabrication process flow.

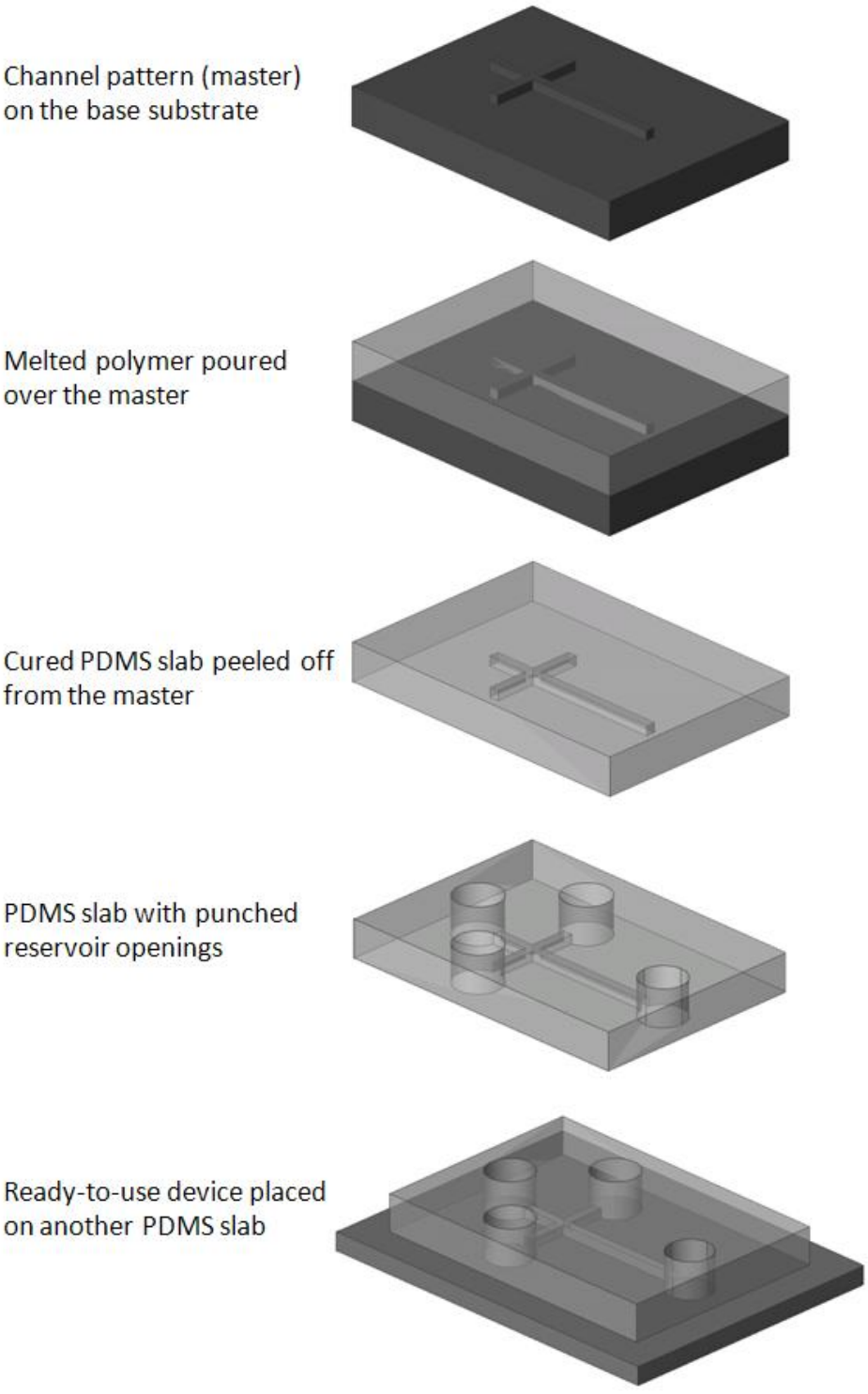

Figure 1.8: Fabrication process flow for PDMS chip with casting [15].

Bulk micromachining techniques are advantageous due to the simplicity of fabrication, and therefore enable the formation of very long channels. However, these techniques require the bonding of a cover substrate onto the one, within which the microchannels are formed. Anodic and thermal bonding techniques are not reliable for non-planar surfaces. For such cases, glues or adhesives are used.

Using these materials is rather problematic both in the bonding process because of the bubble formation at the interface of the substrates and in the experimentation because of the biocompatibility issues. Another drawback of the bulk micromachining techniques is non-batch drilling of holes on one of the substrates. On the other hand, all fabrication steps can be performed in a batch process and bonding of substrates is no longer necessary with surface micromachining.

The most important and unique aspect of surface micromachining technology is the ability of leaving the base substrate intact during the whole fabrication process. This feature gives the capability of constructing the microfluidic systems onto the readily fabricated circuits on a wafer (silicon), making the assembled system quite versatile.

The major disadvantage of surface micromachining is that the fabrication technology is naturally a two-dimensional planar process which can limit the flexibility of the design. On the other hand, low cost and batch fabrication capabilities, and integrability with the integrated circuits will make the surface micromachining technology a leading fabrication technique in near future.

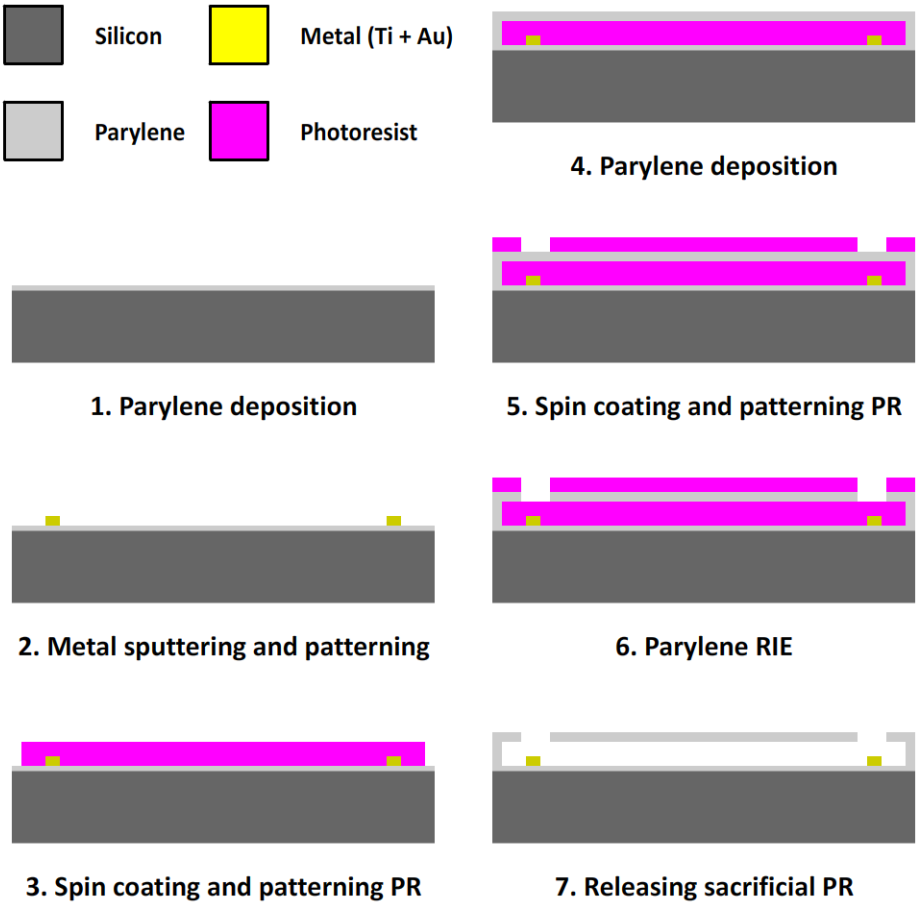

Figure 1.9: Fabrication process flow for parylene microchip [19].

1.4. Size-based DNA Separations with Micro Capillary Electrophoresis Systems

Similar to the conventional methods, DNA is the most popular analyte to be examined in micro technology in the field of genetics. The easiness of the application of the micro devices with high performance in short separation times make them being widely used in various DNA analyses, such as sequencing and mutation detection.

DNA sequence information for genes and genomes is useful for many purposes in molecular genetics. Since its importance, rapid sequencing has been brought into focus with the Human Genome Project. However, it is not the only method for genetic analyses and may not always be the most feasible tool. There are several other popular genotyping methods.

Since time is a very important concern in genetic analyses, the methods which can be applied as high throughput analyses are one step ahead of the other ones. The most widely used techniques for DNA analysis with electrophoresis other than sequencing are single-stranded conformation polymorphism (SSCP), and heteroduplex analysis (HDA). In these methods, separation of the samples is based on differences in their size and/or conformations. Following sections give brief information about these methods.

1.4.1. Sequencing

Sequencing is determining the order of the nucleotide bases in a DNA oligonucleotide [20]. DNA sequencing is performed in two steps: A polymerase chain reaction (PCR) modified by Sanger dideoxy chain termination reaction [21] is followed by a high resolution electrophoresis run. PCR reaction is briefly an enzymatic replication of DNA fragments using DNA polymerase enzyme with controlled annealing and cooling stages.

For sample preparation, a mixture is prepared by adding the following items to the template DNA, which is aimed to be sequenced: (i) DNA primer, which is complementary to the template DNA; (ii) DNA polymerase enzyme, and nucleotides (dNTPs) for constructing the complementary strand; (iii) the artificial nucleotides (di-deoxynucleotides) (didNTPs). These didNTPs are fluorescently labeled in four different colors for four different types of nucleotides and they interrupt PCR process when they are used as building blocks. When the solution is heated up, two

complementary strands of template DNA separate. By cooling the solution, the primer finds its complementary strand in the template DNA. Then the temperature of the solution is slightly raised for binding DNA polymerase enzyme to the template DNA and creating the new strand. While creating the new complementary strand, both dNTPs and didNTPs are used. The synthesis stops when a didNTP is incorporated into the newly synthesized strand. Since the huge amount (billions) of sample is present in the mixture, this reaction can take place in number of times and yields a collection of DNA strands of many different lengths. Figure 1.10 summarizes this technique.

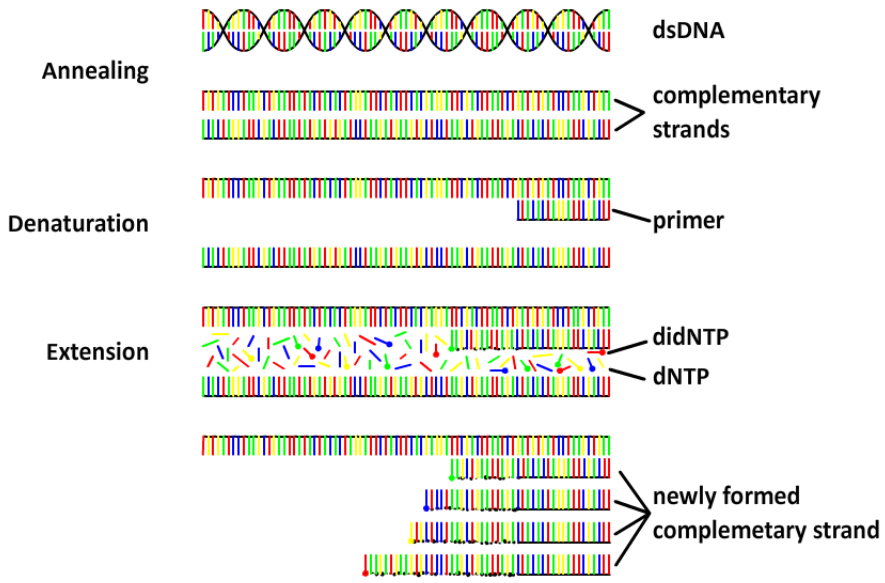

Figure 1.10: Basic steps of sample preparation stage of DNA sequencing before electrophoresis run.

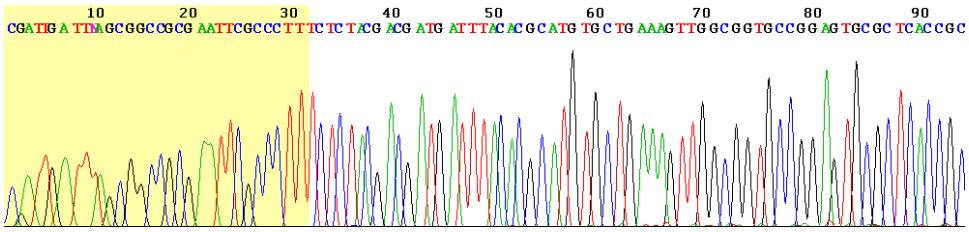

Figure 1.11: A typical chromatogram of the results for DNA sequencing run.

In the second stage, the sample prepared with the method described above is separated with high performance sieving matrices with one base resolution. Detecting the base specific unique fluorescence labels and processing the data, the sequencing analysis is completed. Figure 1.11 shows a typical chromatogram obtained after the sequencing run.

Although sequencing has the highest resolution, it may not be preferred in certain circumstances where it becomes costly with increasing sample amount and sizes. Therefore, researchers use other mutation detection tools for screening high number of patients' samples or very large genes to find out mutations that may be responsible for the disease phenotype. SSCP and HDA analyses are such techniques.

1.4.2. Single-stranded Conformation Polymorphism

The method is based on detecting the abnormal migration of single stranded DNA (ssDNA), which has a disordered structure because of mutation, in non-denaturing sieving materials [22]. Like many ssDNA applications, this technique needs high resolution applications. The most important disadvantage of this method is that its performance highly depends on the operation temperature [23]. So, in order to achieve a successful analysis, precise control of temperature with both heating and cooling capabilities is required.

1.4.3. Heteroduplex Analysis

HDA is one of the simplest and most widely used mutation screening methods [24]. The technique is based on electrophoretic conformational separation of double-stranded DNA (dsDNA) fragments with perfect sequence complementarities (homoduplexes) from the ones with one or more mismatches (heteroduplexes). These mismatches cause a distortion in usual conformation of dsDNA molecules when run on high resolution separation matrices (e.g. polyacrylamide) resulting with slower migration patterns for heteroduplex samples. Heteroduplex samples with even one mismatch show a different mobility compared to homoduplex counterparts. Therefore, ideally a wild type sample forming a homoduplex or a DNA size ladder should be run together with the test sample for research or diagnostic purposes to easily distinguish a heteroduplex structure.

For sample preparation, wild type and test sample, which is being investigated for the absence of mutation, are mixed and heated up to 95 °C for denaturation. At this step, the double stranded structures of the mixed samples are separated into single stranded form. Then cooling the solution to 68 °C, all single strands are matched each other, bind together randomly and construct double stranded homoduplex and heteroduplex pairs. After the sample preparation stage, a high resolution electrophoresis is performed for separating the homoduplexes and heteroduplexes. Figure 1.12 illustrates the application of the HDA.

Since CAE systems are required for reliable analyses with this method, conventional slab-gel electrophoresis systems are widely used for the application of HDA. However, applying HDA in micro scale has many advantages such as very low sample and reagent consumption, ease of use, versatility, simplicity of the protocol, elimination of special sample preparation steps, and low number of parameters and system constraints while operation [25].

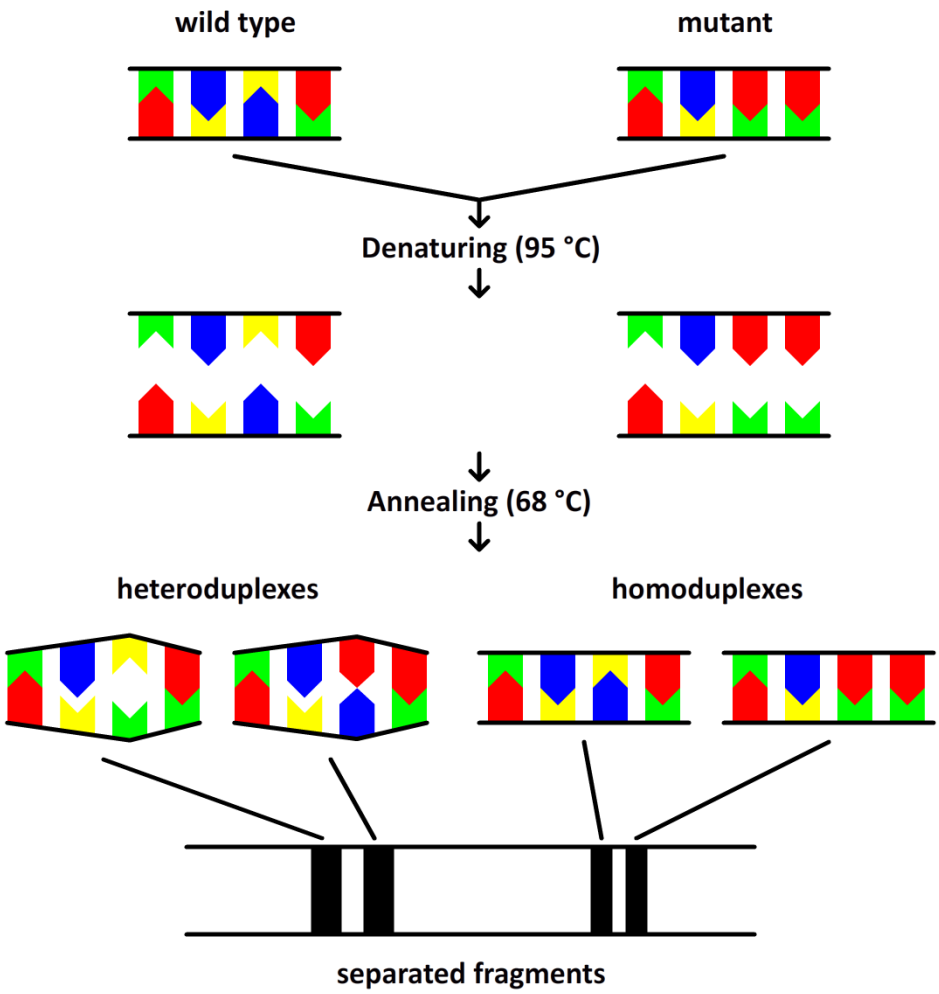

Figure 1.12: Heteroduplex analysis.

1.5. The Objective and Organization of the Thesis

Within the framework of this study, design, fabrication, and implementation of polymeric micro electrophoresis systems for DNA analyses based on MEMS technology are aimed to be performed. Regarding this purpose, following are the objectives to be completed in this thesis work:

1. **Design of polymer based micro electrophoresis systems:** Flow simulations are performed for the analyses of injection techniques. Determining the injection technique, channel dimensions and separation channel length are determined. According to the geometry determination, different channel layouts are defined and required shape optimizations for increasing device performance are made with flow simulations. Designs are finalized and layouts are created for fabrication.

2. **Development of fabrication process flow for parylene:** The desired fabrication process flow is determined for parylene based microchip. The microfabrication steps are optimized for successful fabrication of devices with desired specifications.

3. **Constructing the experimental setup and experimental work:** Experimental setup is constructed for testing and fluorescence based detection. Materials and methods, such as sample to be separated, sieving material for device testing are determined. The fabricated devices are tested for successful size-based separations of DNA. The parameters, such as applied voltages during injection and separation, gel polymerization time etc. are optimized for best performance and the highest resolution.

4. **Development of a novel double channel microchip for heteroduplex analysis:** Double channel layout is determined according to the needs of successful HDA application. An injection method for the new system is designed and its applicability is proved with the flow simulations. Further optimizations are made in case they are necessary.

5. **Application of heteroduplex analysis with double channel structure:** Using the practical knowledge gained from the performed experiments, successful

application of HDA is performed with the novel double channel design with high performance.

The rest of the thesis is organized as:

In Chapter 2, DNA electrophoresis theory is explained in details. The properties of DNA and the flow parameters, which determine the motion of the DNA molecules, are described. The migration theories of DNA fragments in polymer matrices are discussed. Performance metrics of DNA separations are stated.

In Chapter 3, the design methodology for both single and double channel architectures is explained. For single channel layout, flow simulation results for various injection techniques are discussed. Creation of the double channel layout is described and the details of the design procedure for the injection system for the double channel architecture are given. The flow simulations for geometry optimization are discussed. Final designs are listed and described in this chapter.

In Chapter 4, the fabrication method for parylene and its properties are described. The characteristics of parylene based systems are also discussed for BioMEMS applications. Layout and mask creation processes are explained. Finally, the details of the fabrication process flow and the fabricated structures are described.

In Chapter 5, the constructed experimental setup is described. The details of material and sample preparation processes for both single and double channel experiments are given. Results of both single channel separations and the HDA application with the double channel structure are given with the details of the procedure applied in electrophoresis runs.

In Chapter 6, the performed studies and the accomplishments are discussed. After making a conclusion, the future works are stated.

CHAPTER 2

DNA ELECTROPHORESIS THEORY

Electric field based techniques are most widely used in bioanalyses because of their versatility. In chromatography field, electrophoresis is one of the most popular techniques especially in micro scale, since there is no moving parts, no need for mechanical work during the application. Therefore, electrophoresis is the most suitable technique for separation of biomolecules with the fragile microchips. Since the maturity of conventional electrophoresis techniques, the application of electrophoresis in micro scale has not yet been able to go beyond being miniaturized applications of the conventional methods. So, the theory of electrophoresis does not differ much from macro scale. The following sections describe the theory of electrophoresis in micro scale (mostly applies for both micro and macro scales).

2.1. Fundamentals of Electrophoresis

Electrophoresis is briefly defined as applying an external electric field to charged objects in a solution and making them to get into motion. The velocity of the particle depends on several parameters, which are described in the following sections. This technique was first reported in the literature by A. Tiselius [26], who got the Nobel Prize in 1948 for his work on protein electrophoresis.

2.1.1. A Charged Particle in a Solution

When a particle is immersed in a solution, it bears a surface charge. A charged particle should not be considered as naked in the solvent, which contains mobile ions. It is always surrounded by counter ions, so that its total charge is strictly zero (electroneutrality). It remains in an equilibrium state due to the balance between electrostatic and Brownian forces but disturbs the distribution of ions in its surroundings in the solution. Then a layer of the fluid is generated on its surrounding, called *electric double layer* (EDL). EDL consists of two layers: The inner region, in which the attracted ions may be considered as permanently absorbed and immobile, called *Stern layer;* the outer region, in which the ions remain mobile, called *diffuse layer.* However, the distinction between these two layers is arbitrary and depends on the time scale. The thickness of the Stern layer is roughly given by the *Bjerrum length*, defined as [27]

$$l_B = \frac{e^2}{4\pi\varepsilon_b\varepsilon_0 kT} \tag{2.1}$$

where l_B is *Bjerrum length, e* is the elementary charge, ε_b and ε_0 are the dielectric constants of the fluid and vacuum, respectively, k is the Boltzmann constant, and T is temperature (in Kelvin). At room temperature, l_B is in the order of 0.7 nm for water.

In mean-field theory, the equilibrium distributions of mobile ions may be found using the Poisson-Boltzmann Equation [27],

$$\varepsilon_b\varepsilon_0\nabla^2 V_p = -e\sum_k Z_k C_k \exp(-ez_k V_p/kT) \tag{2.2}$$

where V_p is electrostatic potential, C_k and ez_k are the bulk concentration and the charge of ions of species k, respectively. The linearized equation gives the Debye-

Hückel theory and is applicable to the diffuse layer. According to the Debye-Hückel theory, external fields are screened in the electrolyte with the potential $V_p(x)$ decreasing exponentially from its value on the boundary V_s [27],

$$V_p(x) = V_s \exp(-\kappa X) \tag{2.3}$$

Then the Debye screening length is defined as [27]

$$\kappa^{-1} = \left(\frac{\varepsilon_b \varepsilon_0 kT}{e^2 \sum_k z_k{}^2 C_k} \right)^{1/2} \tag{2.4}$$

Consider an external electric field is applied with a uniform current. This field exerts a pulling force on the charged particle and the surrounding ions. The surrounding ion cloud, typically having a thickness of κ^{-1}, contains an excess of counter-ions, which are dragged in the opposite direction and interact with the particle hydrodynamically as shown in Figure 1.2. Then the *electrophoretic mobility* is defined as [28]

$$\mu = \frac{|\vec{\mathbf{v}}|}{|\vec{\mathbf{E}}|} \tag{2.5}$$

where μ is the electrophoretic mobility, $\vec{\mathbf{v}}$ is the velocity of ion, and $\vec{\mathbf{E}}$ is the applied electrical field. Since the exact solution is rather complex, simpler solutions are applied for two limiting cases: Debye layer is much thicker than the particle size, $\kappa^{-1} \gg R$, or much thinner, $\kappa^{-1} \ll R$. In the former case, the electric and viscous drag forces equilibrate each other, yielding [29]

$$\mu = \frac{Q}{6\pi\eta R} \tag{2.6}$$

where $6\pi\eta R$ denotes the frictional effect for a spherical particle. In the latter case, shear effect is restricted with the Debye length and zero outside.

Then velocity becomes independent of particle size and shape. In this case, mobility is defined as [30]

$$\mu = \frac{\varepsilon_b \varepsilon_0 \zeta}{\eta} \tag{2.7}$$

where ζ is called zeta potential, representing the potential on the surface at which shear appears and in the surrounding fluid, and η is the solvent viscosity. The mobility can also be defined in terms of surface charge density as [28]

$$\mu = \frac{\sigma}{4\pi\eta\kappa} \tag{2.8}$$

where σ is the surface charge density.

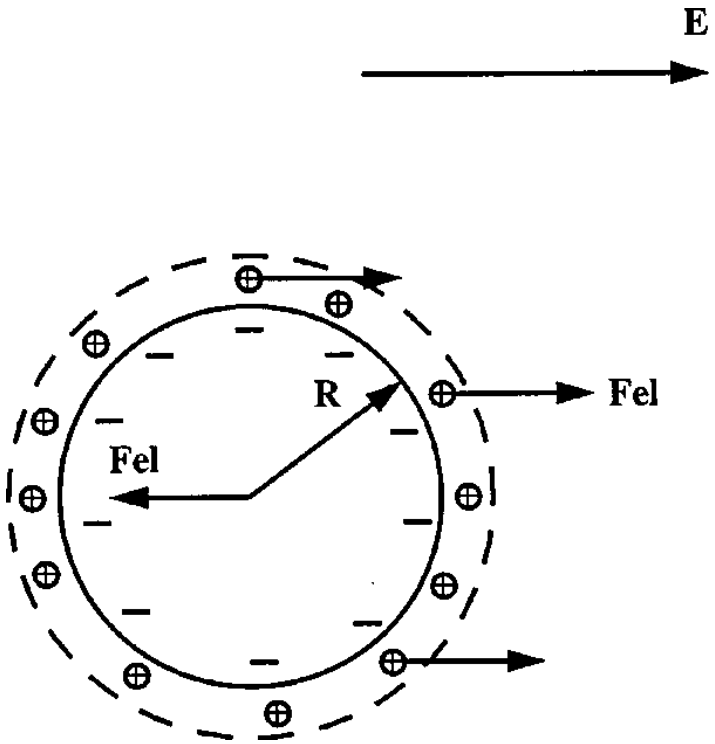

Figure 2.1: Schematic view of a negatively charged spherical particle of radius $R > \kappa^{-1}$ during electrophoresis in an electrolyte [27]

2.1.2. DNA as a Polymer Chain in a Solution

DNA is a polyelectrolyte, which is a polymer chain whose monomers bear a charge. Considering a polyelectrolyte of monomers of size d, it is represented as a persistent chain with a persistence length of l_p, significantly larger than its monomer size. For simplification, it is modeled as a flexible cylinder of diameter d and contour length, L. The first important parameter to be defined is *Khun length:*

$$l = 2l_p \tag{2.9}$$

For L larger than l, the conformation of the polymer is a random walk of step l, with an average end-to-end distance R_N and a radius of gyration R_g are related by [27]

$$R_N = \sqrt{6}R_g = l\sqrt{N_k} = (lL)^{1/2} \tag{2.10}$$

where N_k is the total number of Khun segments and defines as [27]

$$N_k = \frac{L}{l} \tag{2.11}$$

For very long chains, *excluded-volume interactions,* which states that a position in space cannot be occupied by two monomers simultaneously, introduce an extra repulsive effect, which expands the chain. These interactions are characterized by the excluded-volume parameter, v_F, which is defined as [27]

$$v_F = l^2 d \tag{2.12}$$

The crossover to this excluded-volume behavior occurs for a critical end-to-end distance [27],

$$R_v = \frac{l^2}{d} \tag{2.13}$$

And for a chain size of order [27]

$$N_v = \left(\frac{l}{d}\right)^2 \tag{2.14}$$

For larger chains, the end-to-end distance defined as [27]

$$\begin{aligned} R_F &= l{N_k}^{1/2} && N_k < N_v \\ R_F &= R_v(N_k/N_v)^v && N_k > N_v \end{aligned} \tag{2.15}$$

where v is the Flory exponent (typically equals to 0.6).

Considering the external electric field is applied onto this model polyelectrolyte, which is in a buffer solution, since the Debye length is small and counter-ions screen the hydrodynamic interactions over distances larger than it. Shear effects are also restricted within the cylinder of diameter ($d + 2\kappa^{-1}$), and represented as in the Equation (2.7). This fact states that the electrophoretic mobility, μ_0 of a long flexible polyelectrolyte in free solution is independent of its total length. The independence of the electrophoretic mobility of uniformly charged polyelectrolytes prevents size-based separations in free solution. So that, sieving materials (gels) are being used for the purpose of creating a sieving effect.

2.1.3. Resolution and Dispersion Concepts

Resolution is a parameter which defines the performance of the electrophoresis. Although the key parameter seems to be mobility in the theory, the results always go one step ahead for experimentalists. The resolution is measured from a chromatogram, which is briefly the graph of monitored fluorescence intensity of the separated bands. In usual, the chromatogram is a plot of the signal magnitude versus time monitored at a specified detection point. But it can also be obtained by

plotting the intensity magnitude of separated bands versus the channel or lane length through the separation channel waiting for a specified period of time for separation, e.g. the photograph of separated fragments obtained from slab-gel electrophoresis. The resolution between two bands or peaks from a chromatogram is defined as [31]

$$R = \frac{t_2 - t_1}{(W_1 + W_2)/2} \tag{2.16}$$

where t_1 and t_2 are the retention times or the positions of the centers of each peak, W_1 and W_2 are the base widths of the peaks in time units or in length scale. These parameters are illustrated in Figure 2.2.

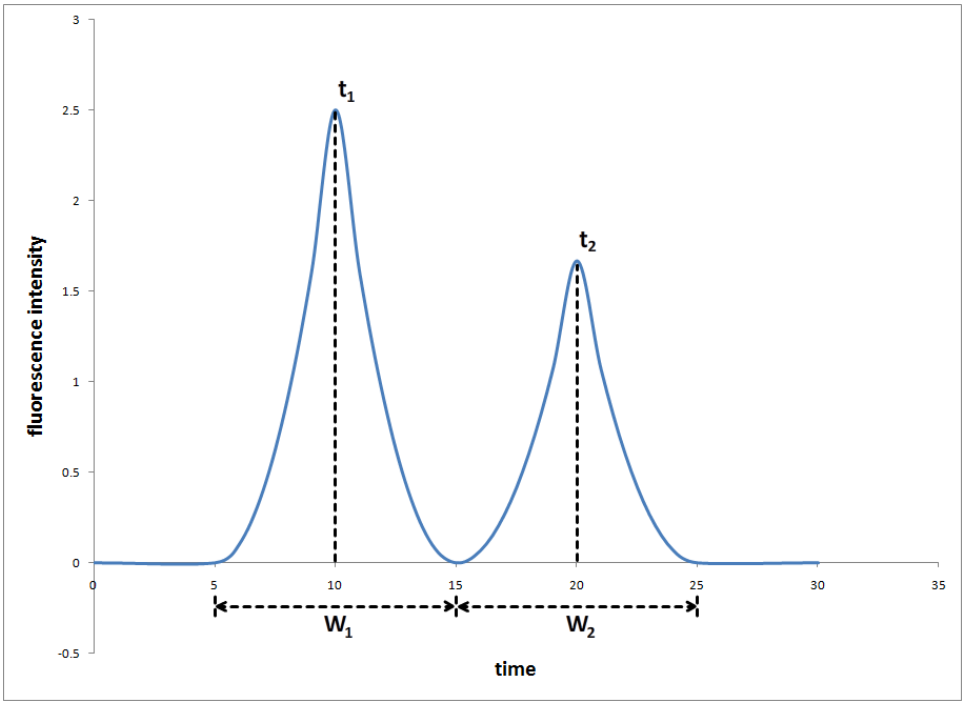

Figure 2.2: A sample chromatogram. Two neighboring peaks in Gaussian shape with the same with. Referring the Equation (2.16), the resolution is equal to 1.

In most cases, the noise in detector signals, the uncertainties in the base line or overlapping of the peaks make measurement of the base widths of the peaks problematic. Assuming the peak shapes as Gaussian, then the resolution is expressed using the definition of full width at half-maximum (hw) as [31]

$$R = \sqrt{2\ln 2}\,\frac{t_2 - t_1}{hw_1 + hw_2} \tag{2.17}$$

Re-expressing the retention times,

$$\Delta t = t_2 - t_1 = L\left(\frac{1}{v_2} - \frac{1}{v_1}\right) \tag{2.18}$$

where L is the distance between the injection and detection points, and v is the velocity of separated bands. Recalling the Equation (2.5),

$$\Delta t = \frac{L}{E}\left(\frac{\mu_1 - \mu_2}{\mu_1 \mu_2}\right) \tag{2.19}$$

In order to determine the full widths at half-maximum, the peak variance parameter needs to be defined. According to Luckey *et al.,* the variance is dependent on several sources. These dispersion sources are the electrokinetic injection, σ_{inj}^2, the finite detection volume, σ_{det}^2, thermal gradients across the capillary, $\sigma_{\Delta T}^2$, and diffusion of bands in the gel, σ_{diff}^2. Then the total variance is defined as [31]

$$\sigma_T^2 = \sigma_{inj}^2 + \sigma_{det}^2 + \sigma_{\Delta T}^2 + \sigma_{diff}^2 \tag{2.20}$$

Neglecting the effects of detector volume and thermal gradient, the other parameters are described as [31]

$$\sigma_{inj}^2 = \frac{l^2}{12} \tag{2.21}$$

where l is the length of the sample plug.

$$\sigma_{diff}^2 = \frac{2D^E L}{\mu E} = 2D^E t_r \tag{2.22}$$

where t_r is the retention time, and D^E is the longitudinal dispersion coefficient of the DNA fragments, which is dependent of the applied electric field.

Combining the above equations, the resolution in terms of observable parameters is defined as [31]

$$R = \frac{1}{4}\left(\frac{\mu_1 - \mu_2}{\mu_1}\right)\frac{L}{\sqrt{\frac{l^2}{12} + \frac{2D^E L}{\mu_1 E}}} \tag{2.23}$$

Resolution can be lost due to saturation of the mobility at a finite value independent of the size of the polyelectrolyte.

As can be seen from Equation (2.28), resolution is proportional approximately with the square root of the distance to the detection point, L. In one limiting case, when the sample plug size is large, the injection term dominates and resolution varies linearly with L. In other limiting case, when dispersion dominates, resolution is then varies with the square root of L.

2.2. DNA Migration in Polymer Matrices

Since the early applications of gel electrophoresis mostly involved relatively small polyelectrolytes, the ratio of the electrophoretic mobility in gel, μ, to the free-solution mobility, μ_0 was described as [32]

$$\ln\left(\frac{\mu}{\mu_0}\right) = -K_r c \tag{2.24}$$

where c is the gel concentration and K_r is the *retardation coefficient,* which is proportional to the particle radius squared. Although this approach was valid for macromolecules, it was not the case for large DNA fragments, whose mobility saturates after a specified value of the radius of gyration. This results from the flexibility of DNA and its ability to penetrate into the smaller pores by deforming its shape. So, more accurate models were described with the development of the electrophoresis technology. The following sections discuss these methods after describing the properties of polymer solutions.

2.2.1. Properties of Polymer Solutions

The fundamental structure of a polymer solution is basically described with its concentration. The concentration definition is categorized in three regimes: dilute, semi-dilute and concentrated (entangled). In dilute solutions, the polymer coils are hydrodynamically isolated from each other, but their spatial distribution is random and subject to fluctuations. As the polymer concentration increases, the polymer coils start colliding more frequently until the overlap concentration (c^*) is reached. Above the level of concentration of c^*, the polymer chains become entangled and form a dynamic network, which is illustrated in Figure 2.3

The overlap concentration is expected to be the same as the concentration inside a single coil, so that the discontinuity between the inside and the outside coil concentrations vanishes. Therefore, the overlap concentration is defined as [28]

$$c^* = \frac{M_w / N_A}{\frac{4}{3}\pi R_p^3} \tag{2.25}$$

where R_p is the gyration radius of the polymer, M_w is the average molecular mass, N_A is the Avogadro's number, and $M_w / N_A \sim N$, where N is degree of polymerization.

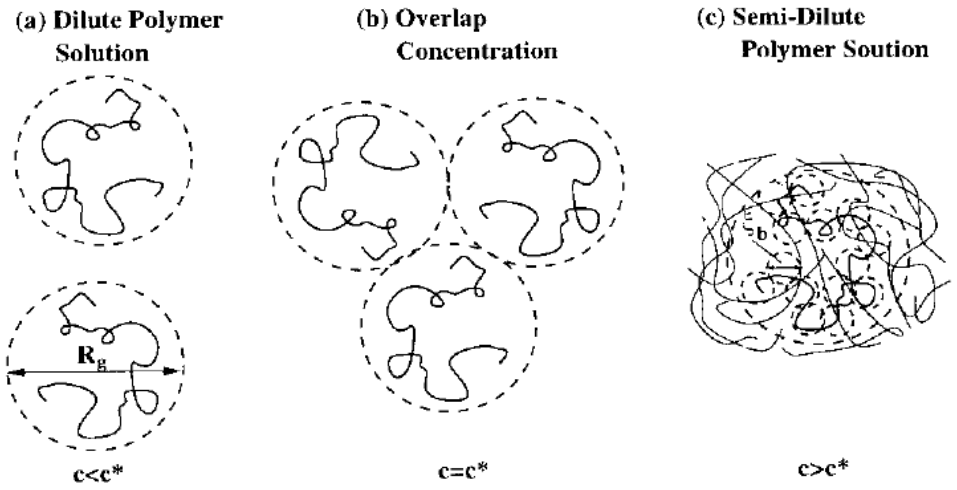

Figure 2.3: Schematic representation of polymer solutions. (a) Dilute, $c < c^*$; (b) overlap concentration, $c = c^*$; (c) semi-dilute, $c > c^*$ [28].

For a single polymer chain or an isolated chain in a dilute solution, the dimension of the polymer is determined by the square-averaged radius of gyration. Over a large range of sizes, it can be expressed by the Kratky-Porod formula [33]:

$$R_g = \langle R_p^2 \rangle^{1/2} = \left[\frac{1}{12} l^2 (2N_k - 1 + \exp 2N_k)\right]^{1/2} \tag{2.26}$$

Recall that l is the Khun length, and N_k is the total number of Khun segments.

A basic parameter in the definition of semi-dilute solutions is the screening length, which is the distance above which the excluded-volume interactions are screened by other chains. Basically, it can also be considered as the polymer mesh size. The *screening length* is defined by scaling theory as

$$\xi = 0.5 R_p \left(\frac{c}{c^*}\right)^{-0.75} \tag{2.27}$$

This parameter was stated to be an effective pore size for a transient network in electrophoresis [34]. Then a new parameter, blob size, was represented [35], which

is the dynamic equivalent of screening length. On scales much larger than ξ, a polymer chain can be viewed as a random walk of independent subunits of size ξ_b, called "blobs". The *blob size* is related to ξ by a universal pre-factor, which is defined as [36]

$$\xi_b = 2.86\xi = 1.43R_p \left(\frac{c}{c^*}\right)^{-0.75} \tag{2.28}$$

It is obvious that the blob size, ξ_b is defined by only re-scaling the screening length.

2.2.2. The Free Volume Model

In this rather simple approach, the gel is considered as a sieving material with a distribution of pores and the separation is defined as electric field driven motion through these pores. The modeling of the mobility is stated as the ratio of the electrophoretic mobility to the free solution mobility. This ratio is defined by the fractional volume available to the particle in gel. This relation is expressed as [27]

$$\frac{\mu}{\mu_0} = f \tag{2.29}$$

where μ is the mobility in the gel, μ_0 is the free solution mobility, and f is the fractional volume available to the particle in gel.

Considering the gel and the moving particles as randomly distributed objects and calculating the probability of coinciding of these objects gives the fractional free volume. Such a study was first performed by Ogston [37], for a sphere migrating in a suspension of long fibers. This model is known as the *free volume model*. The details of this model can be found in [27] with more generalized form for different types of objects. The case in Ogston model is for sheet-like obstacles, and the retardation coefficient in Equation (2.24) becomes,

$$K_r = \pi l^{'} (r + R_g)^2 \tag{2.30}$$

where $l^{'}$ is the gel polymer length per unit volume, and r is the radius of the spherical object. Since the validity of this model is strictly related to the size fraction of the migrating object and the pore sizes, only the migration of small-sized DNA fragments can be modeled with this method.

2.2.3. Diffusion and Reptation Concepts

The first theoretical model proposed to describe the dynamics of a polymer solution is the Rouse model [38]. The *Rouse diffusion coefficient* of the chain can be obtained from the Einstein relation,

$$D_R = \frac{kT}{\zeta_p} = \frac{kT}{6\pi\eta L} \sim \frac{1}{N} \tag{2.31}$$

According to this model, the *Rouse diffusion time*, which is described as the time necessary for a chain to diffuse by an average distance comparable to its end-to-end distance, is given as

$$\tau = \frac{R_p^2}{D_R} = \frac{a^2 \xi_b}{kT} N^2 \tag{2.32}$$

where a is the monomer size (re-defined here). When chains are considered to be in an interaction and interpenetration, the Rouse model is not sufficient to explain the chain dynamics. The dynamics of an entangled network of chains was determined by de Gennes [39] with *reptation theory*. Each chain is seen as moving by a Brownian curvilinear diffusion in an effective tube, of instant diameter of ξ_b, and a contour length defined as

$$L = N_{bl}\xi_b \tag{2.33}$$

where N_{bl} is the number of blobs in a chain.

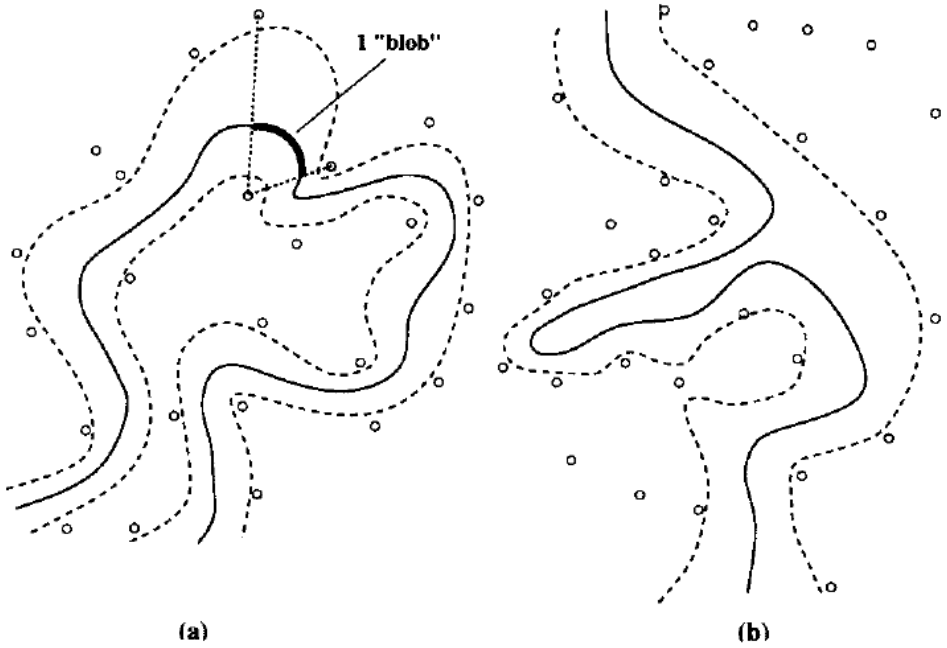

Figure 2.4: Schematic representation of the chain (solid line) and its "tube" (dotted lines) in the gel (small circles): (a) Chain without a loop; (b) chain with a loop [28].

The diffusing polymer is modeled as a linear chain, composed by N_{bl} blobs, of characteristic swollen size of ξ_b and of friction ζ_b stated by Stoke's law [28]:

$$\zeta_b = 6\pi\eta\xi_b \tag{2.34}$$

This states that each blob is dragged as a whole against the solvent flux (non-free-draining regime), whereas the whole polymer is free-draining on a scale larger than

the blob size in the Rouse model. Therefore, the total friction of the polymer can be expressed as a superposition of the single blob friction coefficients:

$$\zeta_p = N_{bl}\zeta_b \tag{2.35}$$

Then the tube diffusion coefficient is defined as [28]

$$D_t = \frac{kT}{\zeta_p} \tag{2.36}$$

The time for tube renewal is then expressed as [28]

$$\tau_{rep} = \frac{L^2}{D_t} = \frac{6\pi\eta}{kT} L^3 \sim \frac{6\pi\eta a^3}{kT} \left(\frac{c}{c^*}\right)^{1.5} N^3 \tag{2.37}$$

The value of τ_{rep} increases with the number of blobs per chain and the blob size. Therefore entangled solutions have a longer "memory" than non-entangled ones. Then the diffusion coefficient of the reptative chain in the tube is defined as [28]

$$D_{rep} = \frac{R_p^2}{\tau_{rep}} \sim \frac{1}{N^2} \tag{2.38}$$

2.2.4. Biased Reptation Models

After the inconsistency of Ogston model with experimental evidences, an alternative mechanism of migration, called the *Biased Reptation Model* (BRM), was independently proposed in 1982 by Lumpkin and Zimm [40] and Lerman and Frisch [41]. The model states that thin flexible chains can thread their way head-on through the pores of the gel by a reptative motion, which is biased in the direction of the applied electric field as shown in Figure 2.5. The BRM is a superposition of this biased motion to the random diffusional reptative movement of the polymer

chains. It shares with the original reptation model two basic assumptions: (i) no hernias or tube leakage; (ii) weakly fluctuating contour length (considered as constant).

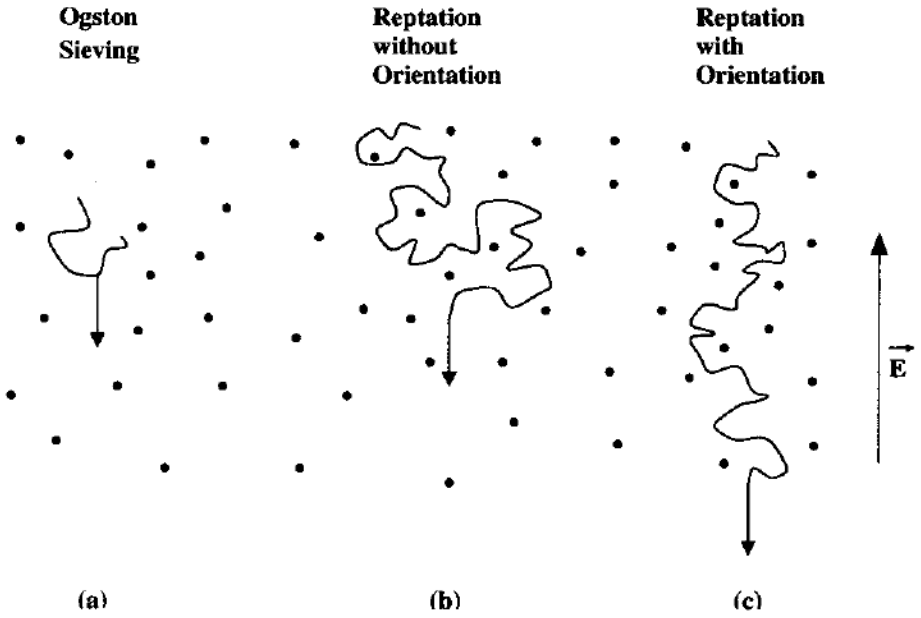

Figure 2.5: Different regimes of migration in constant electric field: (a) Ogston sieving; (b) reptation without orientation; (c) reptation with orientation [28].

Briefly explaining the idea behind the BRM, the electrophoretic mobility of a polyelectrolyte (e.g. DNA) is defined as [27]

$$\left(\frac{\mu}{\mu_0}\right)_{BRM} = \left(\frac{1}{3N} + \frac{\varepsilon^2}{9}\right) \tag{2.39}$$

Where μ_0 is the free solution mobility, and ε is the ratio to the thermal energy, of the electrostatic potential energy associated with the displacement of one blob by a

distance equal to its size. Defining this parameter with BRM which uses a local force picture, as [27]

$$\varepsilon_{BRM} = \frac{qE\xi_b}{kT} \tag{2.40}$$

Where q is the effective charge per blob.

For small N, the first (size-dependent) term dominates, accounting for the experimental dependence of the mobility with $1/N$. For large N, the second (field-dependent) term overcomes the size-dependent (Brownian) one, accounting from the fact that the mobility of large polyelectrolytes becomes independent of size and dependent on field. However, BRM predictions were not quantitatively correct for flexible chains at scaling level. For instance, the regime (c) in Figure 2.5 was never observed experimentally.

Duke and co-workers [42-44] reconsidered the assumption of fixed tube length during electrophoretic migration and demonstrated that rapid fluctuations in the positions of the ends, due to the elasticity of the charged polymer (e.g. DNA) inside its tube, play a vital role in the migration mechanism. The major consequence is that the electrophoretic mobility is linear in ε, and not in ε^2 as in the BRM. The validity of this theory of *Biased Reptation with Fluctuation* (BRF) was confirmed by experiments by Heller *et al.* [45] and by further theoretical work by Barkema *et al.* [46] and by Viovy [27], who proposed a convenient interpolation formula between the prediction for small DNA and the one for large DNA, valid at low fields [27]:

$$\left(\frac{\mu}{\mu_0}\right)_{BRF} = \left[\left(\frac{1}{3N}\right)^2 + \left(\frac{2\varepsilon}{5+2\alpha\varepsilon}\right)^2\right]^{1/2} \tag{2.41}$$

Where α is the ratio between the free mobility and the limiting in-gel mobility of DNA in strong fields (introduced phenomenologically to account for the saturation

of mobility at strong electric fields arising from non-reptative friction). This parameter is of order 3 in both experiments and simulations [27]. Defining the ratio ε,

$$\varepsilon = \frac{\eta \xi_b^2 \mu_0 E}{kT} \tag{2.42}$$

The cross-over from non-oriented reptation ($N < N^*$), where the mobility is field independent and dependent only on size, and oriented reptation ($N > N^*$) occurs around:

$$N^* = \frac{5}{6\varepsilon^2} \tag{2.43}$$

Reptation without orientation still occurs below a critical size N^*, but the mobility in this regime should be independent of pore size:

$$\left(\frac{\mu}{\mu_0}\right)_{rep} = \frac{1}{3N} \tag{2.44}$$

For large DNA ($N > N^*$), the existence of three different regimes with μ/μ_0 scaling with ε^1, $\varepsilon^{0.4}$, and ε^2 are observed [27].

2.3. Conclusion

In this chapter, the fundamental structure of DNA as a polyelectrolyte was defined with its migration theories in polymer matrices. The performance metrics, such as resolution and band broadening were also discussed. It can be concluded that mobility is inversely proportional with the fragment length to various powers according to different migration theories. The analyte velocity increases with the magnitude of applied electric field. Higher electric fields cause dispersion, hence decrease the resolution. The simplest approach for reaching higher resolution

degrees is increasing the separation length. The main drawback of this attitude is increased band broadening. In conclusion, as well as the theory, practical knowledge due to experimentation is quite important in electrophoresis applications for optimizing the operational parameters, such as applied voltages, separation length, etc.

CHAPTER 3

DESIGN AND OPTIMIZATION

In this work, two main tasks were stated: (i) Development and experimenting single-channel electrophoresis systems with common cross injection method; (ii) designing and implementation of novel double-channel architecture with a new injection method for the application of HDA.

In this chapter, following the statement of the design methodology, the design procedures are explained with device layout, injection system design, geometry optimization with flow simulations and finalization of designs for the single and the double channel architectures in two distinct sections. Finally, all designs are illustrated and explained for both single and double channel architectures.

3.1. Design Methodology

While designing microsystems, the micro-fabrication technique is an important aspect and should be specified at the first stage. The limits of the fabrication method determine the limits of the design. So, referring to the given information in Chapter 1, the surface micromachining technology was selected for fabrication and a recently very popular polymer in BioMEMS field, parylene was selected as the channel material for its number of advantages, such as being easily fabricated and allowing fabrication of small feature sizes.

Selecting the fabrication method and the structural material, the requirements and challenges were set at the very beginning of the design period in order to end up with successful designs. Relying on this basis, the challenges were:

Versatility: Despite the fact that problem specific designs give the highest performance in terms of the desired application, availability of multipurpose usage is always an important concern for any designed system. This gives the advantage of performing various different analyses with a single device. Considering the lab-on-a-chip concept, versatility of stand-alone devices makes the assembled system quite flexible and much simpler. It should be noted that, complexity is an important problem during the operation for the lab-on-a-chip systems, after assembling various devices.

Robustness and Durability: Since most of biological analyses, which are carried out with microsystems, need samples prepared in an external environment and need to be performed consecutively, robustness and durability are the major priorities in the structural design. So, the materials and therefore the fabrication techniques should be determined accordingly.

Easy fabrication: As well as the determination of the techniques, the easiness of the fabrication is also important in terms of decreasing the cost per device and high throughput fabrication. Especially, for disposable systems, which are favorable for hygienic conditions in genomic analyses, easy and rapid fabrication is crucial.

High throughput analyses: In addition to the fabrication of devices, their high throughput capabilities in experimentation are highly important. One of the most important advantages of microsystems over the conventional macrosystems are the ability of being adapted for high throughput analyses due to low consumption of sample and short analyses times with consecutive runs.

High performance and reliability: Designing and fabricating the most robust, cheapest and highest throughput systems has absolutely no meaning without yielding accurate and reliable results. Especially, reliability is a very challenging issue for microsystems in the field of biological applications, which will be discussed later. Accuracy and reliability are not the only performance metrics for microsystems, where they have been able to be the substitutes of the conventional systems with their ability of serving for higher performance analyses.

Novelty: Meeting all the above listed requirements is enough for a design to be successful, but not innovative; hence, does not yield in further advancement. So novelty is an important concern that should be considered during the design procedure.

Based on these requirements and challenges, single and double channel architecture design stages are discussed in the following sections.

3.2. Single Channel Architecture Design

The single channel layout with cross injection scheme, which is the most common micro CE architecture found in the literature [47-49] and the easiest technique to apply, was selected for the design process as a starting point. Several different alternatives were discussed and designed in order to gather practical knowledge about electrophoresis in micro scale and optimize the fabrication process flow.

At the first step, special focus was given into the injection techniques starting from the simplest one. Selecting the injection method and application techniques, the channel layouts were determined and geometry optimization was performed with flow simulations. Considering the available wafer area, all the desired alternatives were placed into the first mask set.

3.2.1. Injection Simulations

A comparative study and performance evaluation was carried out for several injection techniques, which are named as cross [50, 51], double-T [50, 52, 53], and double-L [50, 54] by performing flow simulations. Pullback [50] injection technique was also evaluated as an assisting method for increasing the injection performance.

For injection analyses, the simulations were performed for determining the concentration profile of the injected samples. The initial concentration values were selected arbitrarily. The simulations were carried out with a commercially available software package, CFD-ACE+ (ESI Group) using the Flow, Chemistry and Electric modules simultaneously. The diffusive and electrical parameters of the samples were specified closely as for dsDNA and the mobility was solved from diffusivity. The aim was to compare the different channel layouts in terms of the effect of the geometry on the injection performance.

Following sections include the details of the procedures applied for the flow simulations and their results.

3.2.1.1. Cross Injection

Cross injection is the most widely used technique due to its simplicity. Figure 1.2 illustrates the layout of the cross channel with dimensions used in the simulations.

Traditional Cross Injection Technique: After loading the sample into R1, the potential difference was applied on the injection channel. Therefore sample plug started to migrate from R1 to R2, where the higher potential was exerted. When the sample plug reached the junction, which is the area of intersection of the injection and the separation channels, the differential electric potential application was switched to the separation channel in order to perform the separation, while

both ends of the injection channel were kept at the same voltage with the buffer loading reservoir. This simple procedure is summarized in Table 3.1 and Figure 3.2 shows the flow simulation results for the application of this technique.

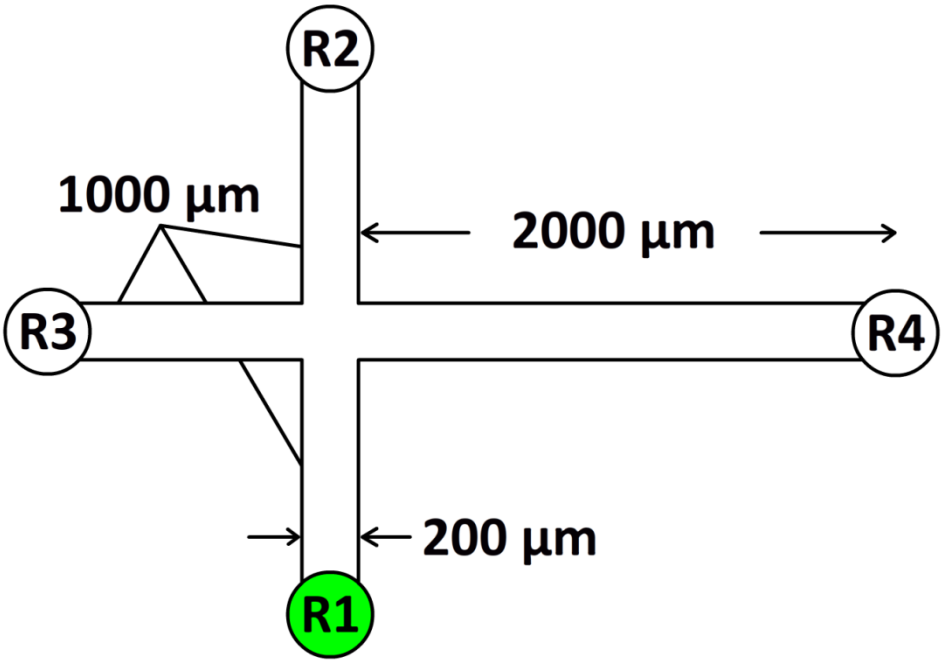

Figure 3.1: Schematic view of cross layout. R1: Sample loading reservoir, R2: Sample waste reservoir, R3: Buffer loading reservoir, R4: Separation waste reservoir.

Table 3.1: Applied voltages for the flow simulation of traditional cross injection technique.

	R1 (V)	R2 (V)	R3 (V)	R4 (V)
Injection	0	300	0	0
Separation	0	0	0	300

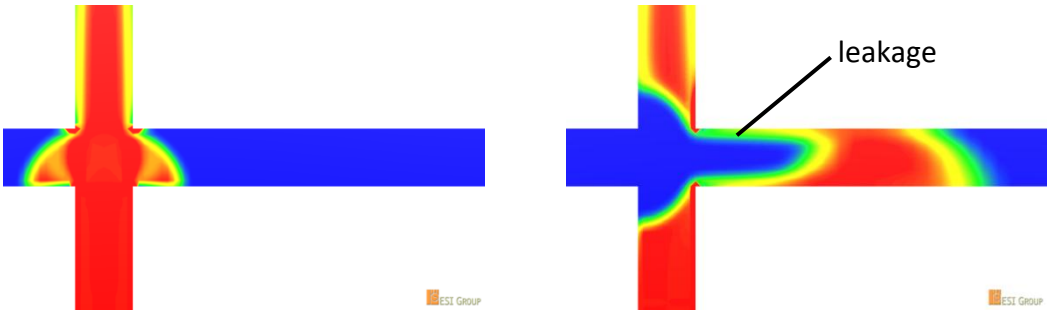

Figure 3.2: Flow simulation results for traditional cross injection technique. (a) Injection phase, (b) separation phase.

Despite the simplicity of this technique in application, it has a major drawback: *leakage*. As shown in Figure 3.2(b), leakage was observed after the phase change from injection to separation. This effect decreases the resolution dramatically, because the shape of the injected sample plug is very critical for the separation performance.

Pullback Injection Technique: In order to avoid the leakage, the pullback injection method was applied. This technique includes the application of the same electric potentials, which are higher than that of the buffer loading reservoir, to both ends of the injection channel during the separation phase. This forces the leaked sample to migrate back through the injection channel and then it no longer belongs to the injected sample plug in the separation channel. Avoiding the leakage effect, the shape of the sample plug becomes more compact and the resolution increases. Table 3.2 summarizes the applied voltages and Figure 3.3 shows the flow simulation results for this technique. As shown in Figure 3.3(b), application of pullback method avoided the leakage and resulted with more compact plug shape. Pullback potentials were applied at the same instant with the phase change.

Table 3.2: Applied voltages for the flow simulation of cross injection technique with pullback.

	R1 (V)	R2 (V)	R3 (V)	R4 (V)
Injection	0	300	0	0
Separation	50	50	0	300

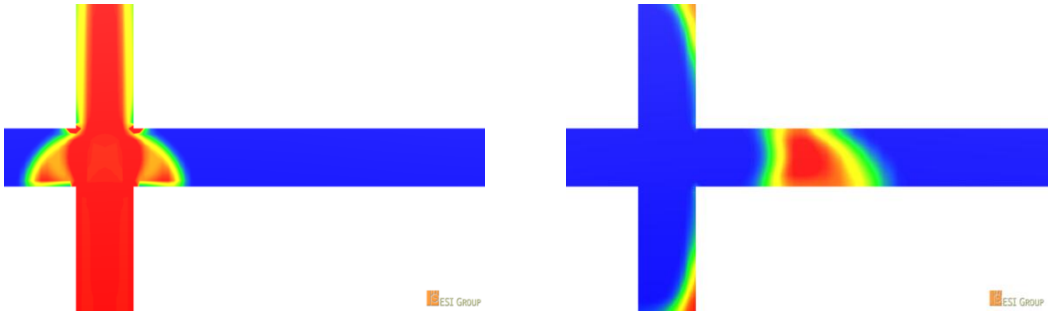

(a) (b)

Figure 3.3: Flow simulation results for cross injection technique with pullback. (a) Injection phase, (b) separation phase.

3.2.1.2. Double-T Injection

With the cross injection technique, the amount of the sample plug is determined by the cross-sectional area of the injection channel. Hence, the sample volume delivered to the separation is always constant. For applications requiring the supply of variable volume sample, this type of injection method is not suitable. As an alternative, double-T form injection method is applied. Figure 3.4 illustrates the layout of the double-T channel with dimensions used in the simulations.

Double-T Injection Technique: The application of the technique is similar to the traditional cross injection method. The procedure is summarized in Table 3.3 and Figure 3.5 shows the flow simulation results for the application of this technique.

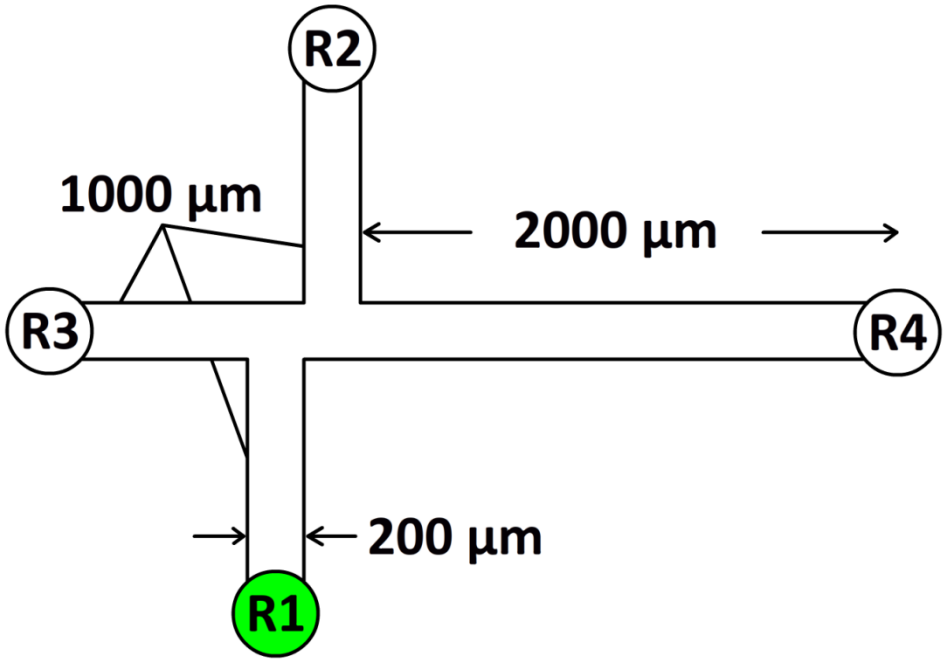

Figure 3.4: Schematic view of double-T layout. R1: Sample loading reservoir, R2: Sample waste reservoir, R3: Buffer loading reservoir, R4: Separation waste reservoir.

Table 3.3: The summary of the applied voltages for the flow simulation of double-T injection technique.

	R1 (V)	R2 (V)	R3 (V)	R4 (V)
Injection	0	300	0	0
Separation	0	0	0	300

Pullback Injection Technique: As shown in Figure 3.5(b), leakage was also observed with this technique. Similar to the cross injection technique, leakage problem for double-T injection was solved with pullback method. Table 3.4 summarizes the applied voltages and Figure 3.6 shows the flow simulation results for this technique.

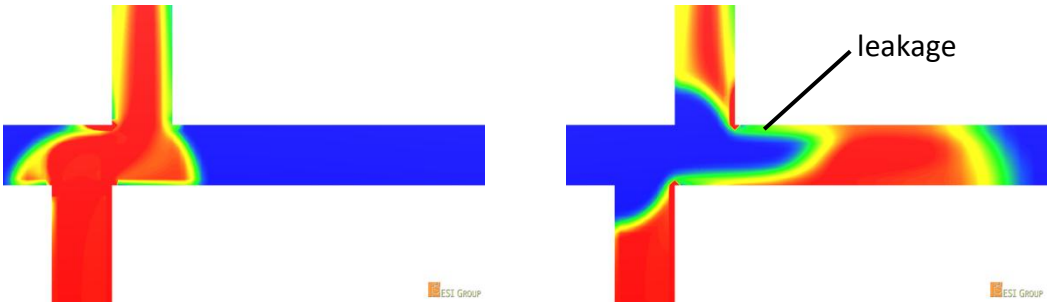

Figure 3.5: Flow simulation results for double-T injection technique.
(a) Injection phase, (b) separation phase.

Table 3.4: The summary of the applied voltages for the flow simulation of double-T injection technique with pullback.

	R1 (V)	**R2 (V)**	**R3 (V)**	**R4 (V)**
Injection	0	300	0	0
Separation	50	50	0	300

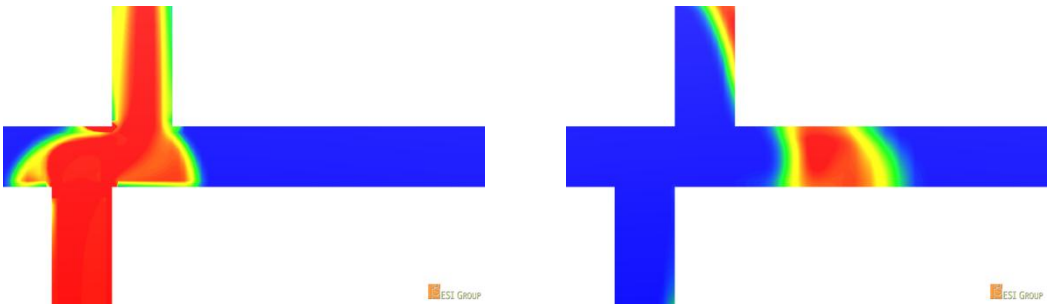

Figure 3.6: Flow simulation results for double-T injection technique with pullback.
(a) Injection phase, (b) separation phase.

3.2.1.3. Double-L Injection

This architecture is union of the cross and double-T layouts. So, both of the techniques can be applied with this alternative. Since flow simulations are performed for both cross and double-T injection methods, no further analyses were performed for this architecture. Figure 3.7 illustrates the layout of the double-L channel.

Although applications of different injection methods were reported with this architecture [50], performance of these methods in terms of the sample plug shape was not considered as satisfactory for this thesis work.

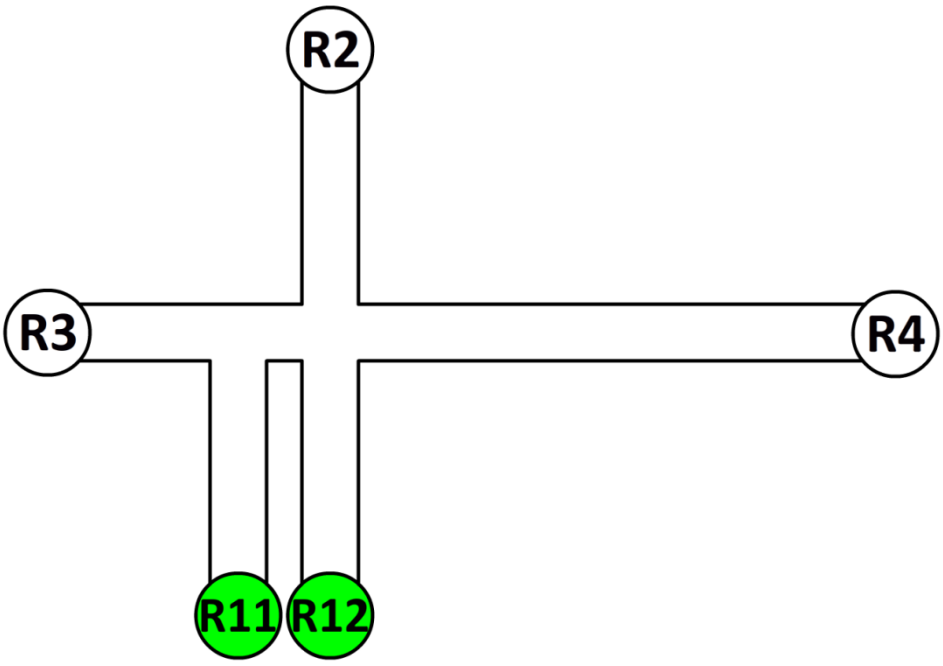

Figure 3.7: Schematic view of double-L layout. R11: Sample loading reservoir for double-T injection application, R12: Sample loading reservoir for cross injection application, R2: Sample waste reservoir, R3: Buffer loading reservoir, R4: Separation waste reservoir.

Comparatively evaluating these three injection techniques, the cross injection technique was selected as an only injection method for single channel arrangements because of its simplicity and ease of control. Since the single channel chips served for getting practical knowledge about electrophoresis and determining and/or optimization of the operational parameters rather than being designed for a specific analysis in this work, there was no need for more complicated injection techniques to be applied.

3.2.2. Channel Dimensions

All of the flow simulations performed in this work are two dimensional and parameters are evaluated always along the flow direction. Determining the width and height of the microchannels using the theory or flow simulations is a very complex and laborious work. It means expanding the solution domain with second and third dimensions. These types of simulations need high performance computing machines and/or takes very long time to get an accurate solution.

Since electrophoretic motion is a type of electrokinetically driven flow, with ignoring the effect of the electroosmotic flow (the charge carrier solution and sieving matrix are considered to be stationary), the movement of the sample plug is considered (as in Chapter 2) as independent of the above mentioned second and third dimensions. On the other hand, this assumption does not mean that channel width and height values can be selected arbitrarily. First of all, the “capillarity” should be preserved, in other words, the surface to volume ratio should be high enough. The most important concerns while selecting the channel width and height are the detection method and the capabilities of the detection system. For instance, for the fluorescently labeled DNA, the intensity of the fluorescence is needed to be enough to be caught by the camera.

Sticking with the above mentioned facts, three channel width alternatives, 50 µm, 100 µm, 200 µm were selected. Height of the channel was selected as 25 µm for the detection purposes.

3.2.3. Separation Channel Length

Referring the Equation (2.23), resolution is proportional to the square root of the separation length when other effects are not taken into consideration. On the other hand, the band broadening due to dispersion and diffusion affects the sample plug shape, so the resolution considerably. Therefore simply either lengthening the separation channel for higher resolution or shortening for less band broadening is not the proper approach. Hence, one of the simplest approaches for determining the separation channel length is defined as [12]

$$L_{req} = L_{sample} \frac{\mu_B}{\mu_A - \mu_B} \tag{3.1}$$

where L_{req} is the minimum required channel length for the successful separation of the analytes A and B, L_{sample} is the sample plug length, μ_A and μ_B are the mobilities. In order to achieve separation in the length of L_{req}, the injected sample plug length should not be longer than L_{sample}.

In a realistic point of view, Equation (3.1) is more likely indicates a derivation after experimentation, but not a pre-design parameter. In addition, the shape (length) of the sample plug depends on the exact dimensions of the fabricated device rather than the designed one. Moreover, the absolute evaluation of the electrophoretic mobility is a rather difficult (and very case specific) problem, especially for DNA, which is a flexible polyelectrolyte. Therefore it is a parameter, which is measured rather than calculated.

The concepts “separation channel length” and “separation length” have different meanings. In other words, fabricating the separation channel longer than needed does not affect the operation significantly, if the operational parameters (e.g. the applied voltages) are adjusted accordingly. The reported separation length (at which the separation is successfully observed) can be shortened by re-adjusting the parameters while having the same device. As a result, reported value for the separation length is the important parameter, not the fabricated channel length.

According to these facts, scientists prefer to make safe designs by making the separation channel length long enough for performing desired applications and for having versatile systems for further different applications. However, these length requirements are in the scale of centimeters, which is not favorable for a system still being called “micro”.

3.2.3.1. Serpentine Channels

In order to decrease the total area of the chips, serpentine channel designs were introduced [55, 56]. The serpentine arrangements are simply obtained by bending the separation channel. Figure 3.8 shows the two types of serpentine layouts.

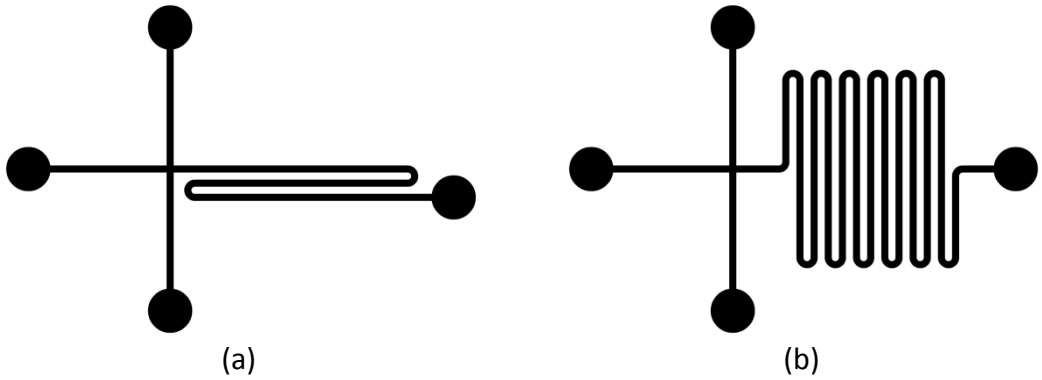

Figure 3.8: Schematic view of serpentine arrangements (a) first and (b) second type.

Although these designs save the chip area significantly, they introduce turning geometries, which cause dispersion, in the separation channel. The effect of these turns on the shape of the sample plug and the geometry optimizations for turning geometries are discussed in the following sections.

3.2.3.2. Turning Geometry Optimization

Dispersion is introduced as a consequence of the differences in length and field strength across the channel width in turning region. As the sample plug traverses a turn, the individual molecules in the band migrate different distances around the turn and experience different electric field strengths, depending upon their respective positions across the width of the channel [55]. This phenomenon is summarized in Figure 3.9.

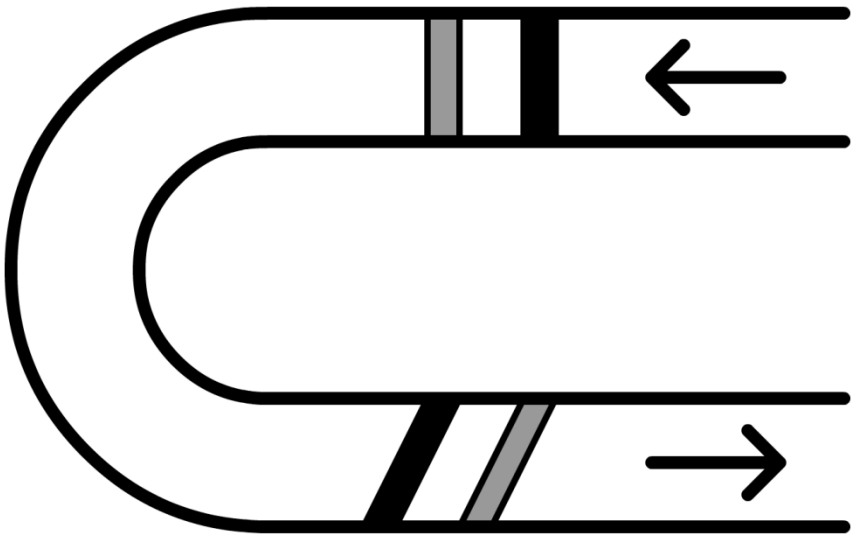

Figure 3.9: Dispersion in turning geometry [55].

The effect of the turning geometries on the resolution was investigated by the flow simulations. The first type and the second type of the serpentine arrangements were compared with the straight channel of the same length. The comparison was made depending on the sample dispersion. Therefore, the resulting sample plug sizes were compared. The channel length was set equal for all three arrangements for comparison. It was selected as 2000 µm. The channel width was 50 µm. Applied electric field strength was 1 kV/cm, therefore 200 V was applied to the outlet while inlet was kept at 0 V during the migration. As can be seen in all figures, initial sample plug size was selected as 50x50 µm. Figure 3.10, Figure 3.11 and Figure 3.12 show the flow simulation results after 0.43 s of migration for straight, serpentine of type 1, and serpentine of type 2, respectively. Resulting plug shape indicates the performance of the geometries. The highest performance was obtained with straight channel as expected. Although serpentine channel of type 2 had more turns than serpentine of type 2, its plug shape was more compact. In addition, type 2 was also more compact in term of its geometry and occupied area.

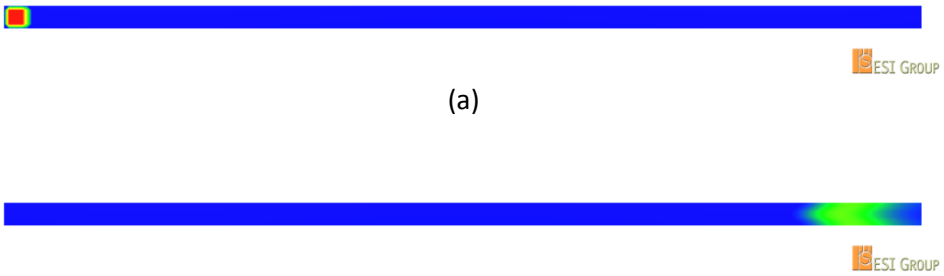

Figure 3.10: Flow simulation results of straight channel (a) before and (b) after migration.

(a)

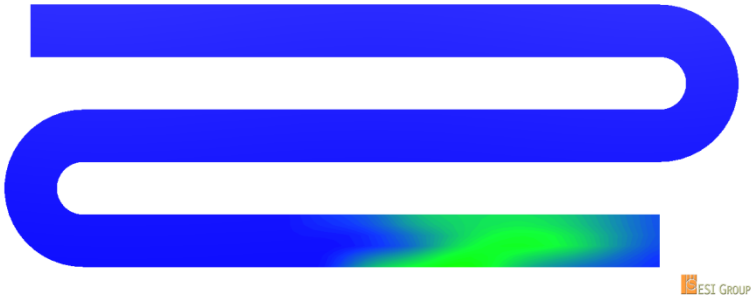

(b)

Figure 3.11: Flow simulation results of serpentine channel of type 1 (a) before and (b) after migration.

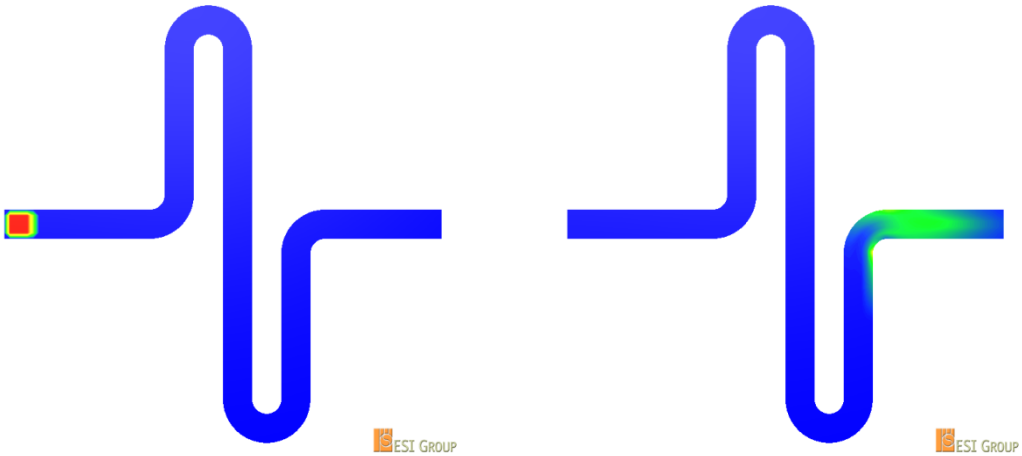

(a) (b)

Figure 3.12: Flow simulation results of serpentine channel of type 2 (a) before and (b) after migration.

In order to minimize the differential migration velocity, tapered turn method was applied as a geometry optimization technique. The turning part of the channel was all narrowed down according to the theory defined by Paegel and co-workers [56]. Figure 3.13 and Figure 3.14 show the layouts of the tapered turning geometries and flow simulation results for simple and tapered turn geometries, respectively.

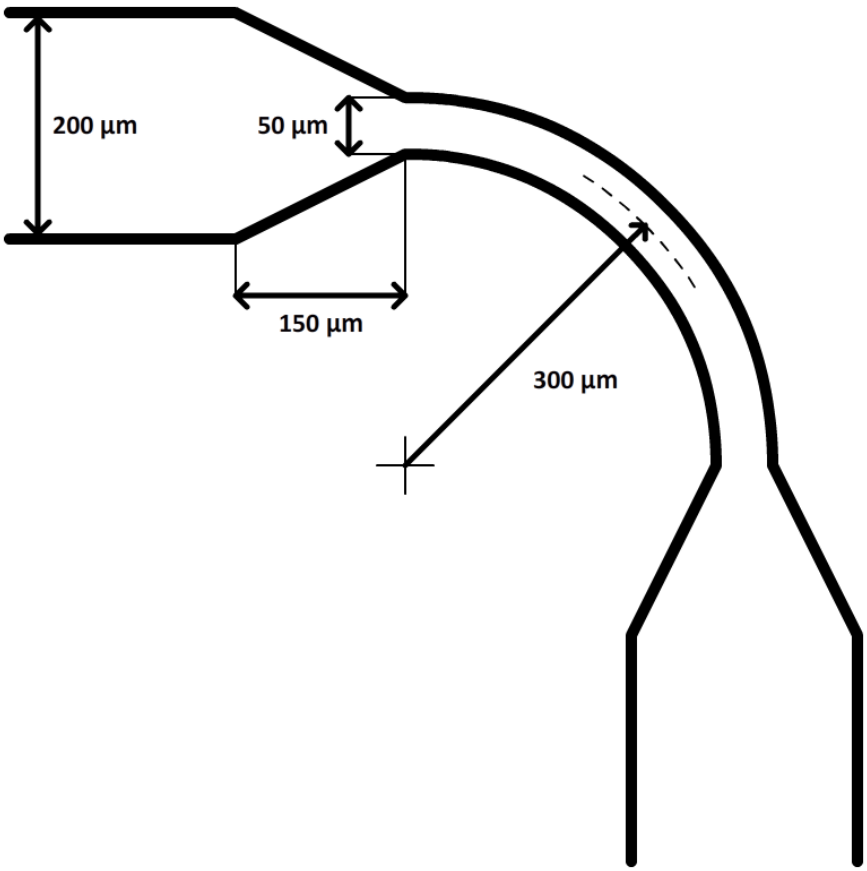

Figure 3.13: Tapered turn geometry.

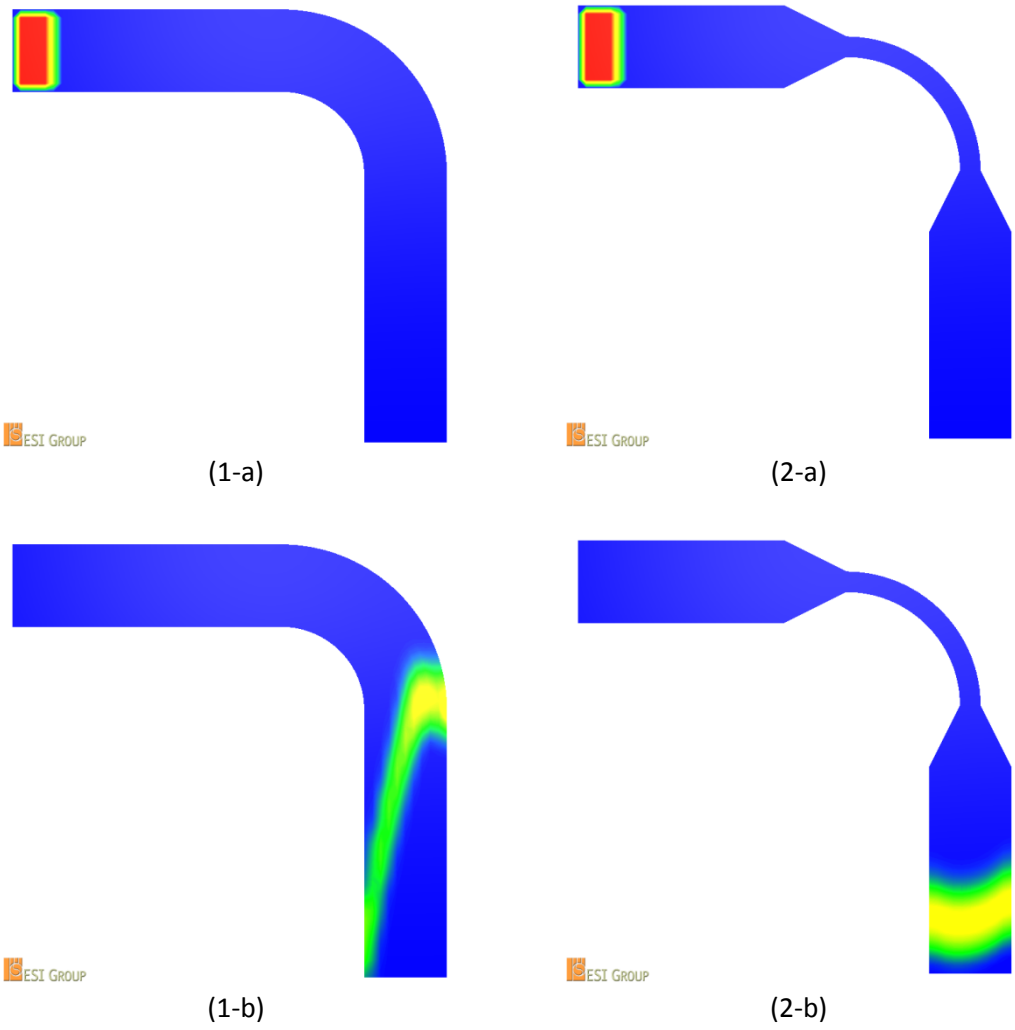

Figure 3.14: Flow simulation results for 90° turn geometry. (1) Simple turn geometry (1-a) before and (1-b) after migration, (2) tapered turn geometry (2-a) before and (2-b) after migration. E = 570 V/cm

The effect of tapered turn geometry on decreasing sample dispersion was observed obviously. According to the simulation results, this geometry optimization technique was applied for the serpentine channel designs.

For having safe designs, the separation channel length for straight channels was selected as 2 cm. In addition, for the evaluation of the performance of the serpentine geometries over straight channels with the same length, microchips with

the separation channel length of 4 cm were designed for all three alternatives. Moreover, 10 cm length separation channels were designed for both serpentine geometries.

3.2.4. Electrode Placement

In addition to the required electrodes on the reservoirs for performing sample injection and separation, several different electrode designs were implemented on the microchips for various purposes. These purposes were enabling electrode defined injection [57], moving electric field application [58], heating the device for further possible single stranded DNA (ssDNA) applications, and contact points for using thermocouples for temperature measurement. These electrodes are briefly described in Figure 3.15 for cross channel layout. Same procedure was applied for the other designs for electrode placements.

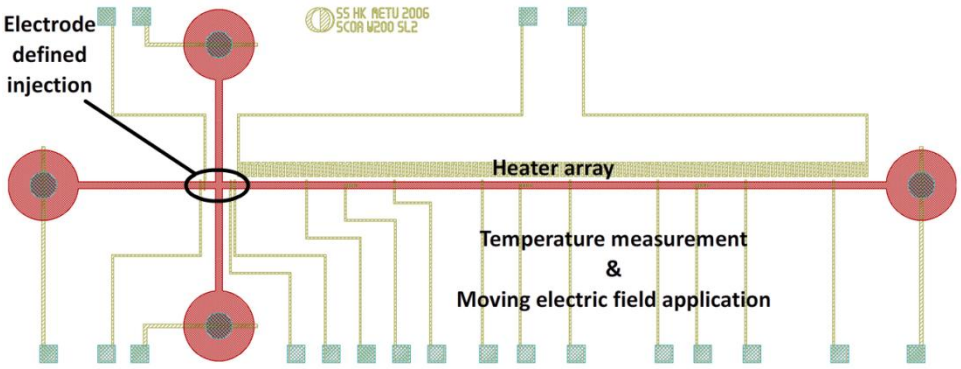

Figure 3.15: Electrodes placed on the chip.

3.3. Double Channel Architecture Design

As stated before, the double channel architecture was developed for the application of HDA. Although applications of HDA with single channel microchips were reported in the literature [24, 59, 60], these systems lack in reliability because of not having a control channel. The aim of this study was not only introducing a new design that can be used for HDA, but also yielding reliable results with its stand-alone applications.

Reliability in the application of HDA depends on having an additional control channel. Multichannel architecture is not a new concept introduced in this study. Several multichannel arrangements, so called capillary array electrophoresis (CAE) systems, were reported in the literature for various different applications including HDA [61-66]. Most of these CAE systems are constructed by arraying common single channel arrangements over the chip area, which makes the operation laborious and time consuming [61, 62]. The ones that have multi-channel structure on a single device need complex detection systems due to misaligned separation channels [64, 65]. Lastly, the remaining approaches utilize turning geometries in the separation channel in the purpose of aligning the separation columns for detection purposes, which cause dispersion, degrading the resolution dramatically [63, 66]. Moreover, these multichannel systems are mostly designed for high throughput analyses (especially sequencing), which in fact do not need multichannel arrangements for the application. In other words, these devices are used for performing same type of analyses simultaneously but separately.

The proposed design was a new double channel architecture for rapid mutation detection in a very short separation length and time with the application of HDA. This novel design has aligned separation channels, which have no turning geometries. In addition, a novel technique is applied for the sample injection, called

as u-turn injection. The design methodology for both the device layout and the injection method will be discussed in the following sections.

3.3.1. Double Channel Layout

The proposed system is derived from the traditional cross layout. Separation channel of the single cross channel layout with 200 µm width was divided into two parts by a thin wall, which is 20 µm in thickness. Then two identical separation channels, which are aligned side by side, with 90 µm width are obtained, while keeping the buffer loading and separation waste reservoirs common. This symmetrical structure guarantees that two identical separation processes can be performed simultaneously, under the same conditions.

The goals of dividing the separation channel, so the microchip into two parts, are having aligned separation channels for detection purposes and avoiding turning geometries, thus loss of resolution.

3.3.2. Injection System Design

The real challenge was to introduce an injection system for the split microchip. Similar to the separation channel, the injection channel was also divided into two parts with the same method. Then two more reservoirs were added for doubling the injection system. There were two sample loading and waste reservoir pairs located symmetrically. Figure 3.16 shows the designed system.

U-turn Injection Technique: With this new structure, a novel injection technique, named *u-turn injection method*, was applied. Since the injection channels have 180° turns at the junction, the loaded sample plug is injected while turning at the junction. The validity of this technique was proved with the flow simulations. The

similar procedure with single cross channel was applied for the double channel structure. Figure 3.17 shows the model used for the flow simulations.

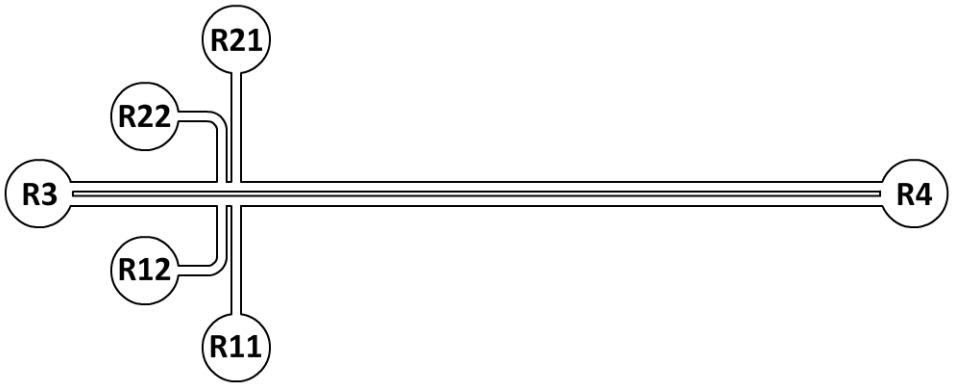

Figure 3.16: Schematic view of double channel structure. R11 & R21: Sample loading reservoirs, R12 & R22: Sample waste reservoirs, R3: Buffer loading reservoir, R4: Separation waste reservoir

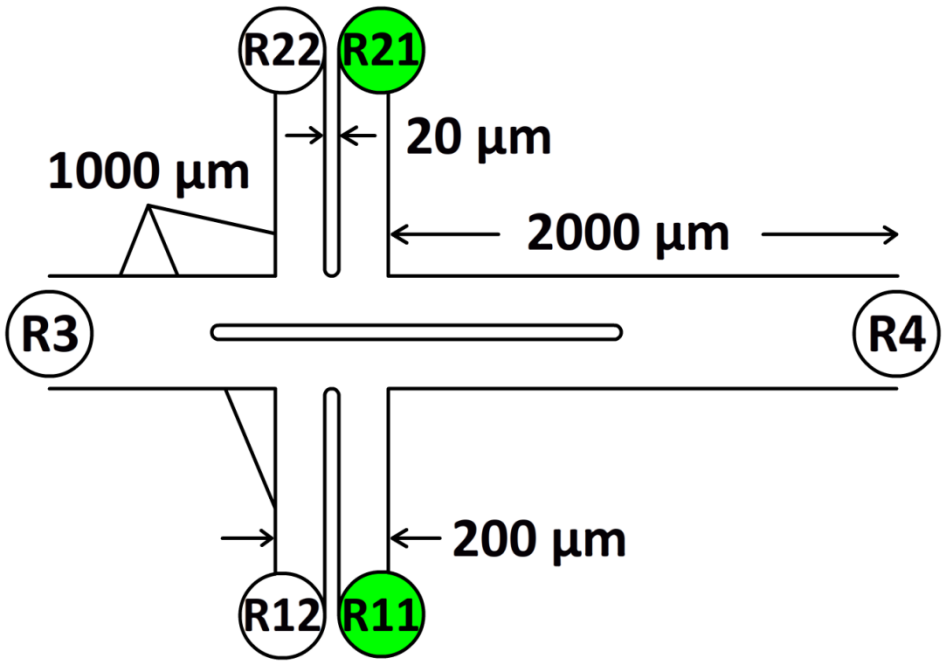

Figure 3.17: Model for flow simulations of double channel structure.

Table 3.5 summarizes the applied voltages. Figure 3.18 and Figure 3.19 show the flow simulation results for injection and separation, respectively.

Table 3.5: Applied voltages for the flow simulation of u-turn injection technique.

	R11 (V)	R12 (V)	R21 (V)	R22 (V)	R3 (V)	R4 (V)
Injection	0	100	0	100	0	0
Separation	0	0	0	0	0	150

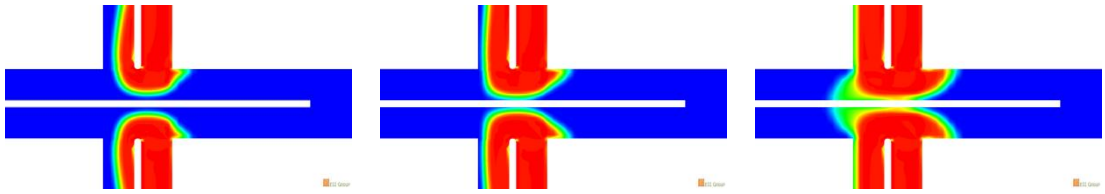

(a) (b) (c)

Figure 3.18: Flow simulation results for u-turn injection technique.
Injection after (a) 0.3 s, (b) 0.4 s, (c) 1 s.

As shown in Figure 3.18, injected sample amount can easily be controlled by adjusting the injection time with this injection method.

Figure 3.19 proves the feasibility of the injection technique. On the other hand, like all the previously discussed injection techniques in this study, leakage is also observed while the application of u-turn injection.

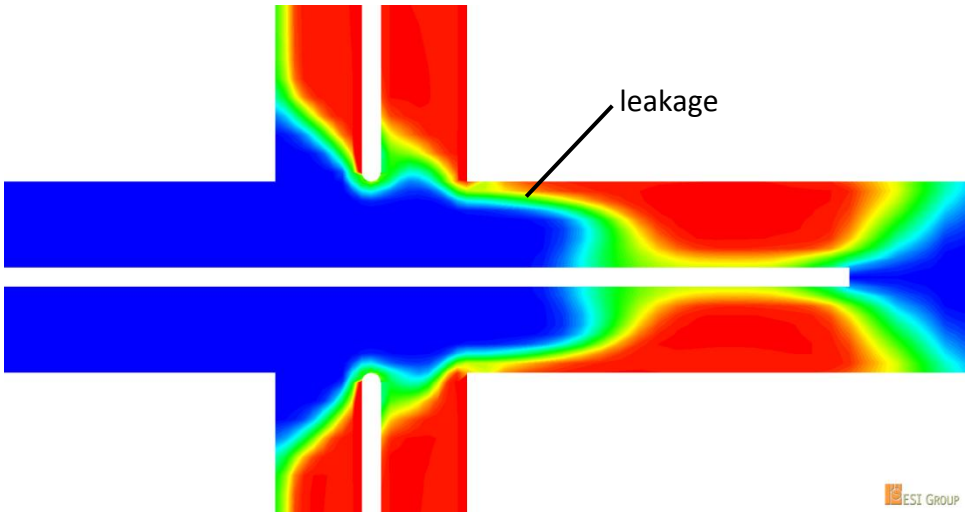

Figure 3.19: Flow simulation results for u-turn injection technique at separation phase.

Pullback Injection Technique: The pullback injection technique was also applied with this method for solving the leakage problem. Table 3.6 summarizes the applied voltages and Figure 3.20 shows the flow simulation results for the u-turn injection technique with pullback method.

Table 3.6: Applied voltages for the flow simulation of u-turn injection technique with pullback method.

	R11 (V)	R12 (V)	R21 (V)	R22 (V)	R3 (V)	R4 (V)
Injection	0	100	0	100	0	0
Separation	25	25	25	25	0	150

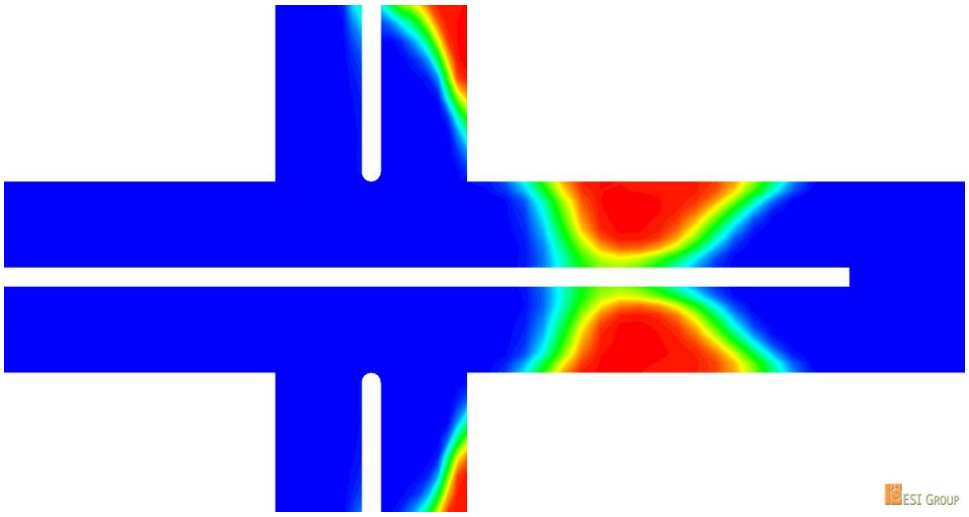

Figure 3.20: Flow simulation results for u-turn injection technique with pullback at separation phase.

As obviously seen in Figure 3.20, application of the pullback method completely solves the leakage problem and yields more compact plug shape.

3.3.3. Channel Dimensions

The channel dimensions of the double channel structures are exactly the same with the 200 µm wide single channel arrangements with divided channels and modified injection channels.

3.3.4. Separation Channel Length

The separation length was selected to be 2 cm for the straight double channel architecture. Serpentine arrangements with optimized turning geometries were also designed for this architecture.

3.4. Final Designs

According to the described techniques and optimization studies, totally 24 different devices were designed. Table 3.7 summarizes these devices.

Table 3.7: The summary of all of the designed devices with their types and properties.

Type	Channel Length (cm)	Channel Width (µm)
Single cross	2	50
Single cross	2	100
Single cross	2	200
Traditional. single cross	2	50
Traditional. single cross	2	100
Traditional. single cross	2	200
Traditional. single cross	4	200
Merged single cross	2	100
Merged single cross	2	200
Double-L	2	100
Single serpentine (type 1)	4	100
Single serpentine (type 1)	4	200
Single serpentine (type 1)	10	50
Single serpentine (type 1, tapered turn)	4	200
Single serpentine (type 2)	4	100
Single serpentine (type 2)	4	200
Single serpentine (type 2)	10	50
Single serpentine (type 2, tapered turn)	4	100
Single serpentine (type 2, tapered turn)	4	200
Double channel	2	90x2
Double channel	4	90x2
Double serpentine (type 1)	4	90x2
Double serpentine (type 2)	4	90x2
Double serpentine (type 2, tapered turn)	4	90x2

The wafer layout consists of totally 31 devices. Figure 3.21 shows the final 4” wafer layout.

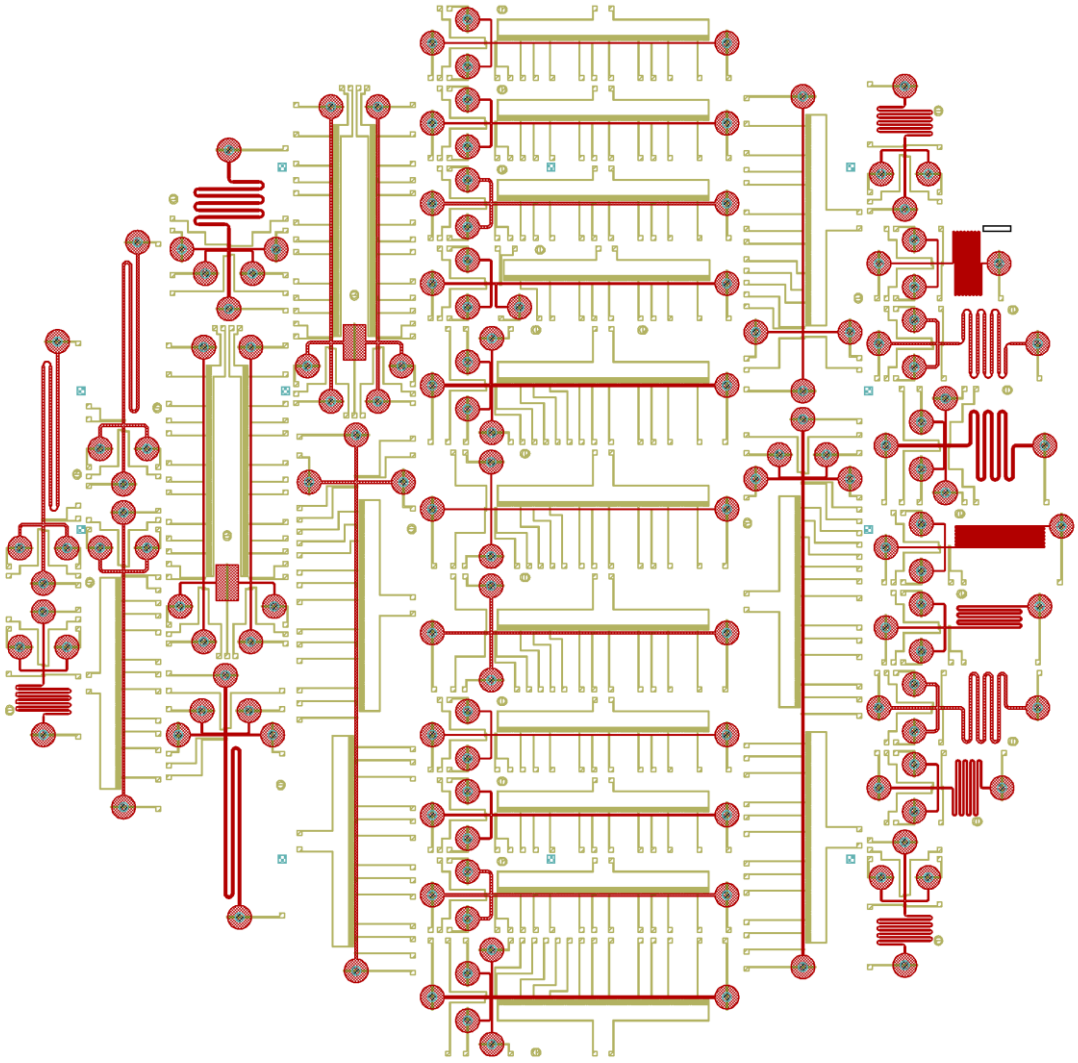

Figure 3.21: Final wafer layout.

3.4.1. Single Channel Architecture Designs

Several single channel arrangements were designed with various alternatives in terms of channel dimensions and placed into the wafer layout. The different types of single channels are described in this section briefly. For the channel dimensions, please refer to Table 3.7.

Figure 3.22 illustrates the layout of traditional single channel. This system was designed for size-based DNA separations and gathering knowledge and optimizing the operational parameters during experimentation.

Figure 3.23 illustrates the layout of single channel structure. It operates same as with traditional one, the only difference is its bended injection channel arms on both sides of the device for the purpose of saving the chip area.

Figure 3.24 illustrates the layout of merged single channels. In this design, two single channel chips were merged and their sample waste reservoirs were kept common. It was a pre-designed version of the novel double channel architecture.

Figure 3.25 illustrates the layout of double-L chip. Although it was stated in the previous sections that cross injection was selected as an only injection method, this single device was placed in the wafer layout for performance evaluation studies of investigated injection techniques other than cross injection.

Figure 3.26 and Figure 3.27 illustrate the layouts of serpentine geometries. As explained before, the purpose of these designs was saving the chip area and having a more compact microchip. Figure 3.28 shows the serpentine arrangement with tapered turns. This geometry optimization was applied for both types of serpentine arrangements.

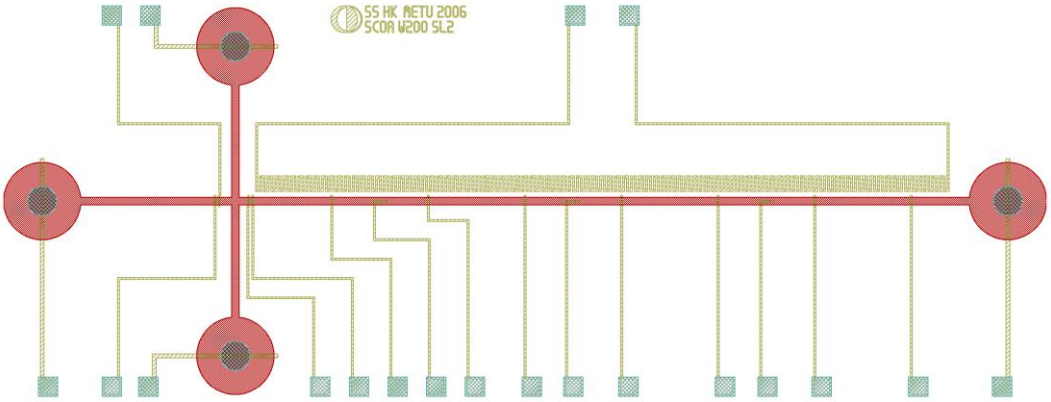

Figure 3.22: Traditional single channel cross layout.

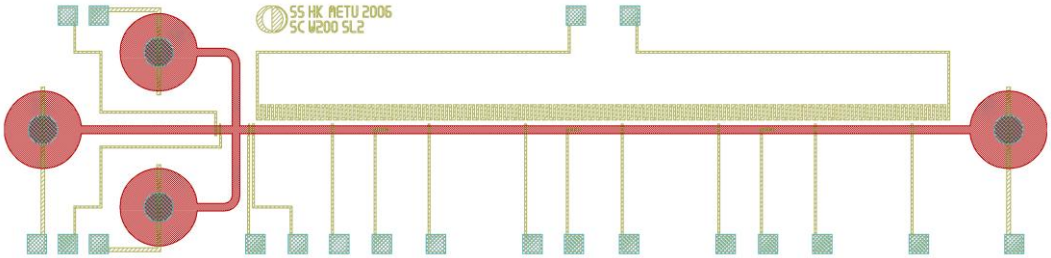

Figure 3.23: Single channel cross layout.

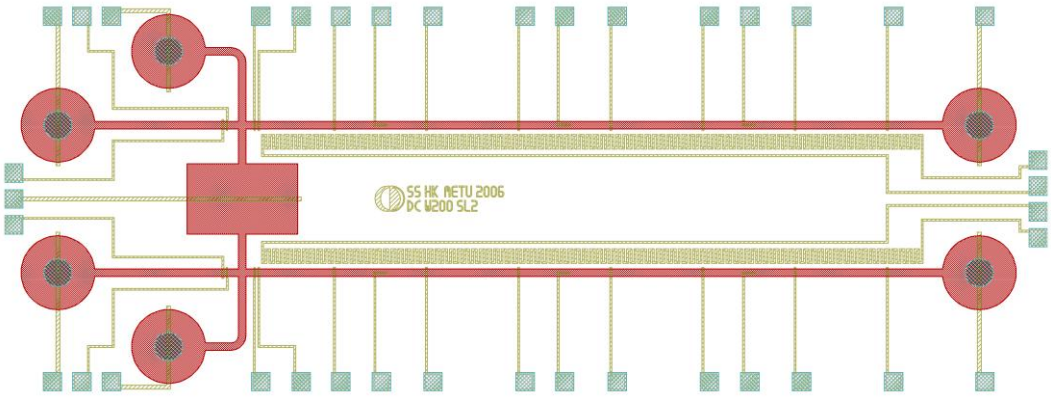

Figure 3.24: Merged single channel cross layout.

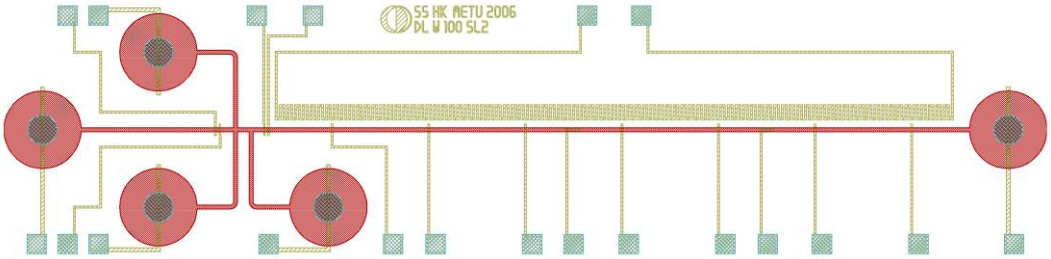

Figure 3.25: Double-L layout.

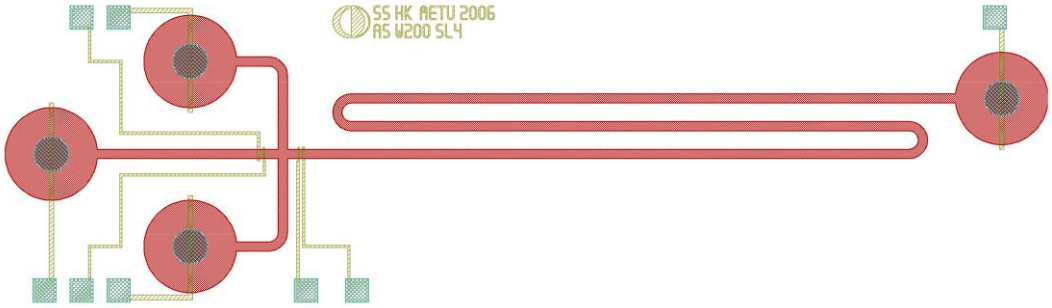

Figure 3.26: Single channel serpentine layout of 1st type.

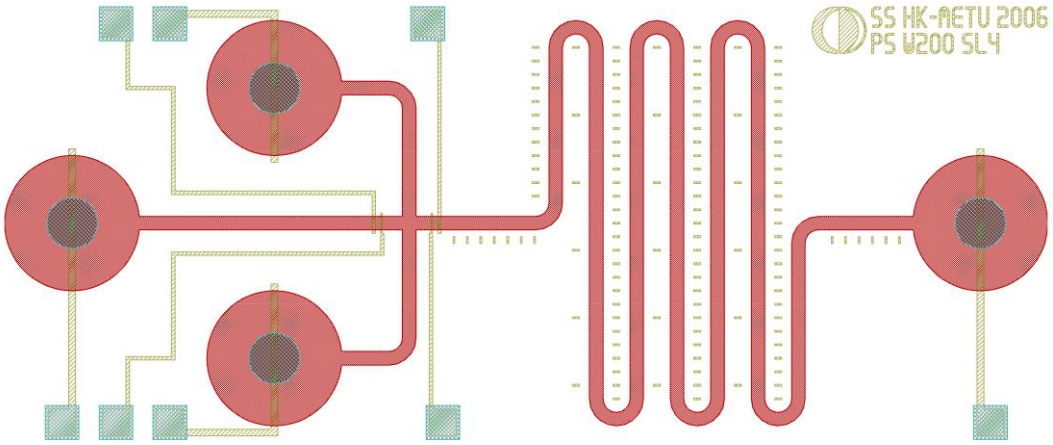

Figure 3.27: Single channel serpentine layout of 2nd type.

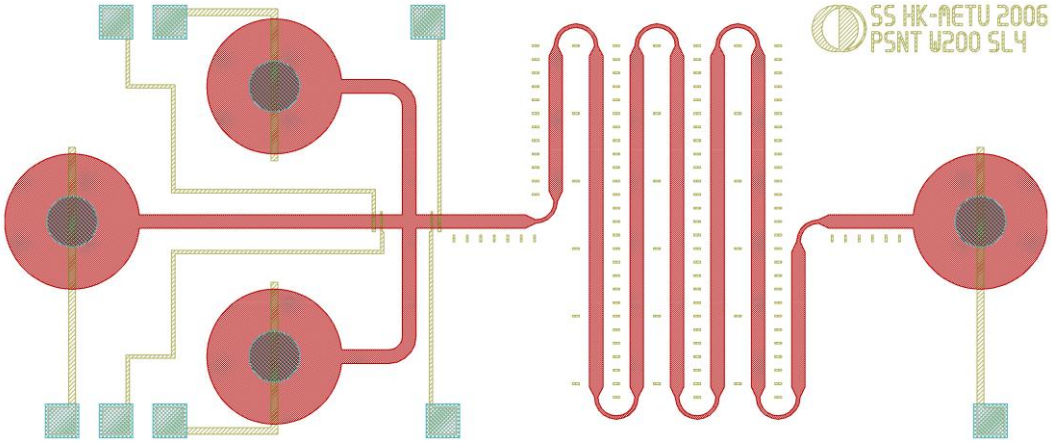

Figure 3.28: Single channel serpentine layout of 2nd type with tapered turn.

3.4.2. Double Channel Architecture Designs

Several double channel arrangements were designed with different alternatives in terms of channel lengths and placed into the wafer layout. The different types of double channels are described in this section briefly. For the channel dimensions, please refer to Table 3.7.

Figure 3.29 illustrates the layout of double channel. This system was designed for the application of HDA for rapid mutation detection.

Figure 3.30 and Figure 3.31 illustrate the layouts of serpentine geometries. Similar to the single channels, the purpose was saving the chip area. Figure 3.32 shows the serpentine arrangement with tapered turns. This geometry optimization was applied for both types of serpentine chips.

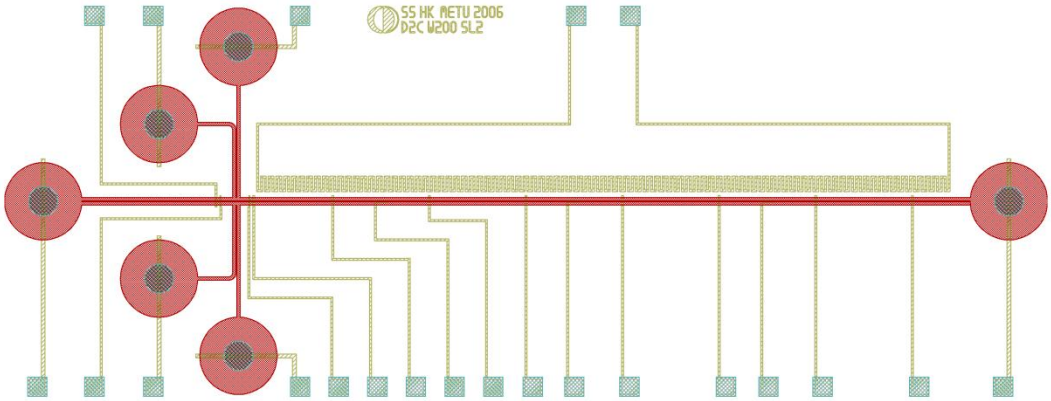

Figure 3.29: Double channel layout.

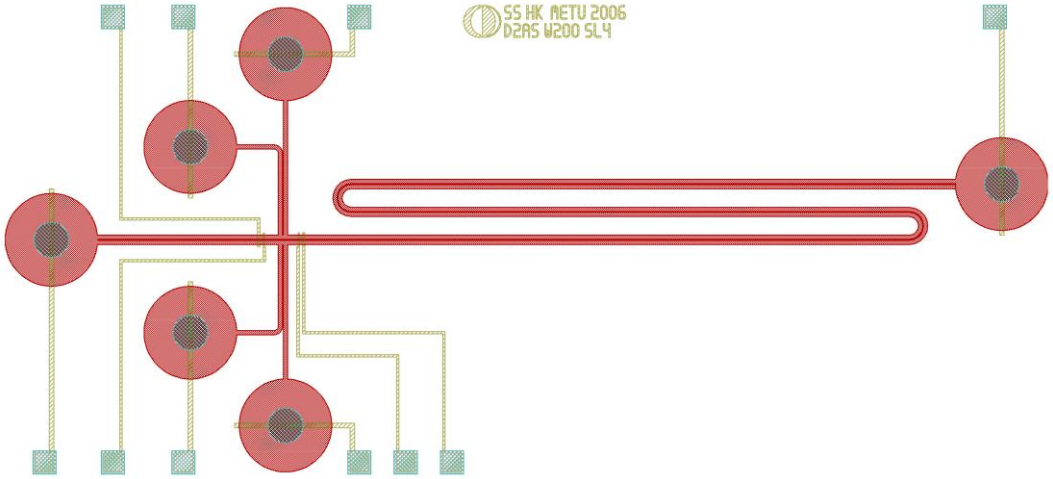

Figure 3.30: Double channel serpentine layout of 1st type.

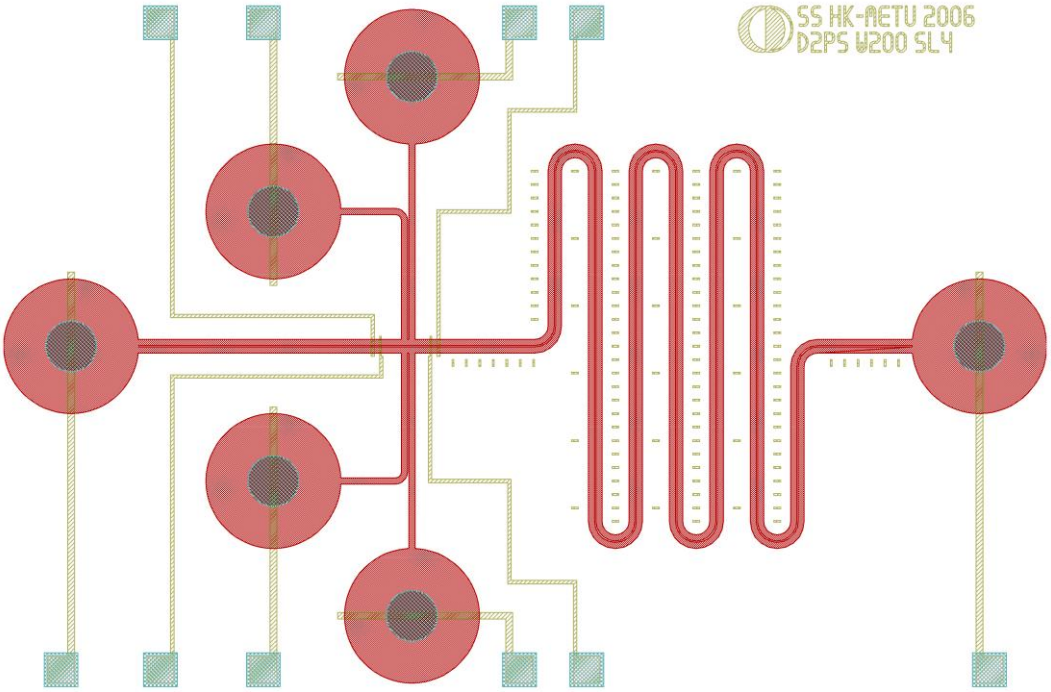

Figure 3.31: Double channel serpentine layout of 2nd type.

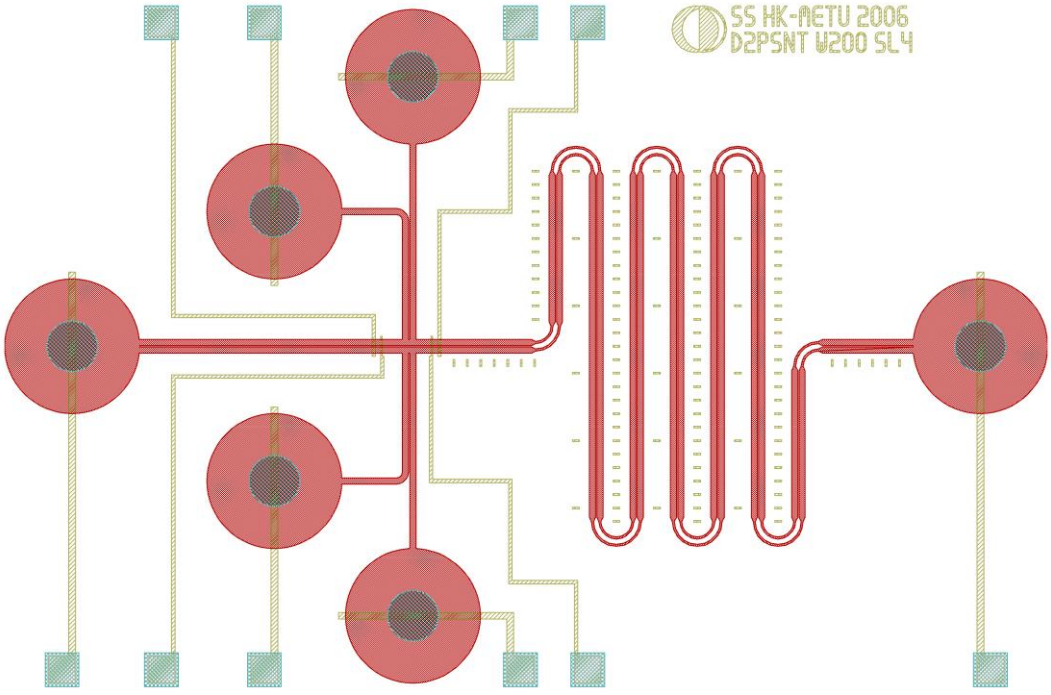

Figure 3.32: Double channel serpentine layout of 2nd type with tapered turn.

3.5. Conclusion

Stating the methodology and challenges, the design procedures of single and double channel structures were discussed. For the single channel architecture designs, injection method and device layouts were determined according to the flow simulations. Channel dimensions were selected due to the needs of easy detection. The separation channel lengths were set long enough for the purpose of having safe designs. For compaction of the geometries of the designs with long separation channels, serpentine arrangements were discussed. Since the turning geometries increase dispersion, a geometry optimization study was performed for the serpentine arrangements in order to increase the separation efficiency. Placing the electrodes for various purposes, the design procedure for the single channel architecture was completed.

The double channel system layout was derived from the traditional cross channel structure. Then the u-turn injection method was designed for this new double channel system. Channel dimensions and the separation channel length for double channel system were determined with the same methodology that for the single channel architecture. Finalizing the designs, according to the available area on a 4" wafer, the 24 different designs were placed into the layout of the wafer with totally 31 devices.

CHAPTER 4

FABRICATION

Fabrication method was selected according to the stated requirements in Chapter 3. In order to fabricate robust and durable devices with easy fabrication steps, surface micromachined polymer technology was selected. Using this technology, vertical and smooth sidewalls can be obtained with very small feature sizes.

Parylene-C was selected as a channel material because of its numerous advantages, which are listed below.

Transparency: Parylene is optically transparent and colorless. In testing and experimentation, transparent channels are essential for proof of concept, verification of fluidic properties, and operation.

Low background fluorescence: Parylene-C has very low background fluorescence from visual to infrared range. This property has a vital importance while using fluorescence based detection methods.

Easy fabrication: Fabrication technology of parylene is one of the easiest methods for constructing the microchannels when compared with other bulk or surface micromachining techniques.

Conformal deposition: Parylene is deposited conformally at any surface. Hence, it enables the construction of complex structures with very small feature sizes.

Low temperature processing: Parylene is deposited at room temperature in a vacuum chamber. Fluidic networks can be fabricated on top of virtually any substrate without affecting the performance of circuits or any thermally sensitive structures underneath. Plastic fluidic channels can be fabricated even on CMOS circuitry.

Biocompatibility: Parylene is biocompatible and biostable. In addition, its chemical inertness and non-toxicity characteristics have great importance when the corrosive environments of most of the biosystems are considered.

No surface treatment: Parylene requires no surface treatment during the operation like most materials used for forming microchannels, such as glass. Thus it makes the experimentation easier and yields with higher performance.

Mechanical strength: Parylene has high mechanical strength as it stands without collapse even with very low aspect ratios.

Following sections discuss the properties of parylene as the structural material, give information about the mask design and layout creation, and the fabrication.

4.1. Parylene: Material Properties and Methods

Parylene is a common name for a class of polymers called poly-xylylene. Four forms of parylene are currently commercially available. The basic structure of the parylene polymers are shown in Figure 1.2.

Parylene N, is poly-para-xylylene, a completely linear, highly crystalline material. Parylene N is a primary dielectric, exhibiting a very low dissipation factor, high dielectric strength, and a dielectric constant invariant with frequency. This form has the second penetrating power only to that of parylene HT.

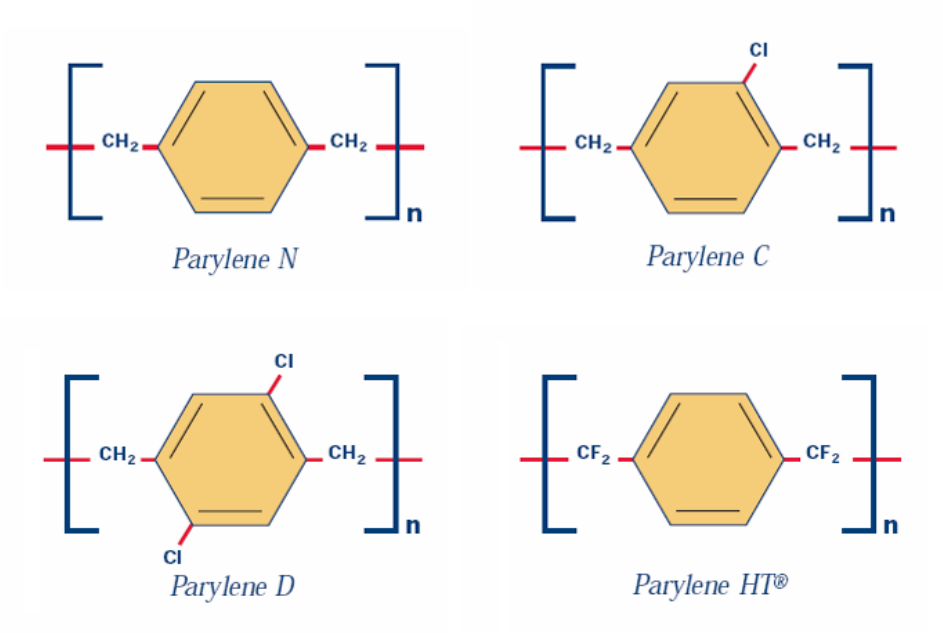

Figure 4.1: Chemical structures of different types of parylene [67].

Parylene C is produced from the same raw material (dimer) as parylene N, modified only by the substitution of a chlorine atom for one of the aromatic hydrogens. Parylene C has a useful combination of electrical and physical properties plus a very low permeability to moisture and other corrosive gases.

Parylene D is produced from the same raw material as parylene N, modified by the substitution of the chlorine atom for two of the aromatic hydrogens. Parylene D is similar in properties to parylene C with the added ability to withstand higher use temperatures.

Parylene HT, which is a quite new, replaces the alpha hydrogen atom of the N dimer with fluorine. This variant of parylene is useful in high temperature applications and those in which long-term UV stability is required. Parylene HT also has the

lowest coefficient of friction and dielectric constant, and the highest penetrating ability of all types.

4.1.1. The Deposition Process

Parylene polymers are deposited by vapor deposition at room temperature in a vacuum chamber. The parylene dimer (solid) is first sublimated at around 150 °C. The dimer is then split into two monomers at 680 °C. The monomers will then polymerize on surfaces at room temperature. Since the deposition is performed around 0.1 torr, the mean free path of the gas molecules in the deposition chamber is in the order of 0.1 cm. Therefore, all sides of the substrate are uniformly impinged by the gaseous monomer. This results with the highly conformal deposition. Figure 4.2 shows the diagram describing the deposition process [67].

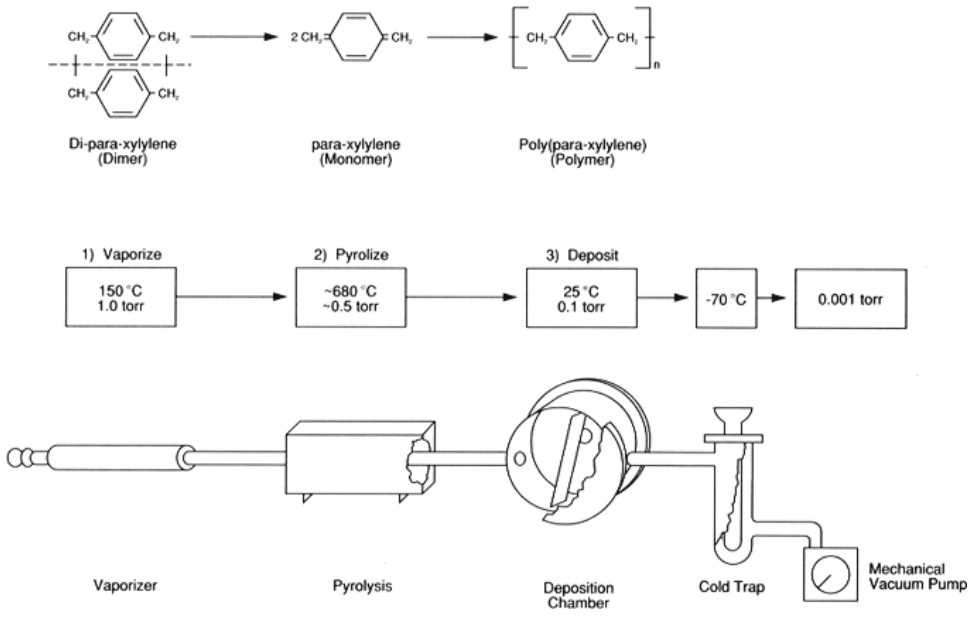

Figure 4.2: Deposition process for parylene [67].

The deposition rate is directly proportional to the square of the monomer concentration and inversely proportional to the absolute temperature.

4.1.2. Properties of Parylene

4.1.2.1. Permeability

A high permeability to water vapor means that water samples inside of the channels will dry more quickly. Furthermore atmospheric conditions may affect device performance and reliability. Gas permeability such as O_2 can limit reactions within these devices as well. Parylene exhibits lower permeability than the other polymers but still much higher than the inorganics.

4.1.2.2. Chemical Resistance

Parylene resists chemical attack at room temperature and are insoluble in all organic solvents up to 150 °C. Parylene C can be dissolved in chloro-napthalene at 175 °C and parylene N softens at the solvent's boiling point (265 °C). Both polymers are resistant to permeation by most solvents. Exposing parylene to different wet chemicals can change its surface property. For example, even though parylene is hydrophobic, after coating sacrificial photoresist with parylene and dissolving the sacrificial layer in acetone, parylene channel becomes hydrophilic because of the acetone treatment. For a long period (several weeks), the parylene channel should return back to its hydrophobic state. Furthermore, buffered hydrofluoric acid (BHF) and hydrofluoric acid (HF) fluorinates parylene's surface and make it more hydrophobic. This even spoils adhesion of the successive parylene deposition on parylene even after plasma ashing treatment. Chromium (Cr) etchant makes the parylene film hydrophilic during Cr etching on the surface areas, on which Cr layer lies. These observations are summarized in Table 3.1. Right after filling the parylene channel with water, consecutive water fills are faster because the parylene

absorbs water molecules [68]. This case can be returned back to the original state by treating the channel walls with acetone. Therefore treating parylene channels before using them with acetone gives better repeatability.

Although parylene has lower permeability to liquids and gases than the other polymers, it is still permeable. Therefore, once the parylene coated substrates are put inside a solution, the solution permeates through the parylene film. Then it attacks the adhesion layer between the parylene and the film underneath. No acid, base or solvent can dissolve the parylene film but by attacking the adhesion layer, they can peel it off. Hence, thicker parylene films will survive more in the strong solution. For example, potassium hydroxide (KOH) can etch oxide. If there is an oxide layer underneath the parylene layer, when KOH permeates through the parylene, it will etch oxide and make the parylene lose its adhesion. Accordingly, most photoresist developers like AZ400K and MF319 may etch oxide very slowly. If parylene is on top of the oxide layer and left inside these developers for long time, it may get delaminated. In addition, most of the photoresist strippers can also cause parylene to be peeled of when they are soaked by it. Acetone can also permeate through the parylene and dissolve the monolayer of silanol, which is formed by the adhesion promoter solution during the deposition process. Thus, soaking acetone for a long period of time causes delamination. As a result, a great care should be given on the sacrificial layer removal process in acetone. For thin layers of parylene, the releasing times should be kept as short as possible.

Table 4.1: Effects of some wet etchants on parylene film [69].

Chemical	Effect on surface	Effects adhesion
Au etchant	none	no
Chrome etchant	hydrophilic	no
BHF	hydrophobic	yes
HF	hydrophobic	yes
Acetone	none	no
IPA	none	no

4.1.2.3. Acetone Release

In order to form microchannels with parylene, photoresists are used as sacrificial layers. Since acetone can only be used for etching these sacrificial layers, the release process needs special care. Acetone release is a diffusion limited process. Therefore, the position of the dissolution front is approximately proportional to the square root of time. Taking the cross-section of the microchannel constant, the dissolution process can be expressed in one dimension, which is through the longitude of the microchannel, as [70]

$$\delta(t) = \sqrt{\frac{2D(C_S - C_B)}{\rho} t} \tag{4.1}$$

where $\delta(t)$ is the distance between the channel entrance and the dissolution front of the sacrificial photoresist, D is the diffusion constant of dissolved photoresist in acetone, C_S is the saturated concentration (maximum possible dissolution concentration) of dissolved photoresist in acetone, C_B is the concentration of dissolved photoresist in the bulk of the acetone solution, and ρ is the density of photoresist in its solid form. The dissolution process is described in Figure 4.3. For long channels (longer than 10 mm), the dissolving of photoresist process is problematic. In this case, either opening access holes on the channel in a repeated

manner or rinsing/re-dissolving in acetone cycles may solve the problem up to some specified lengths.

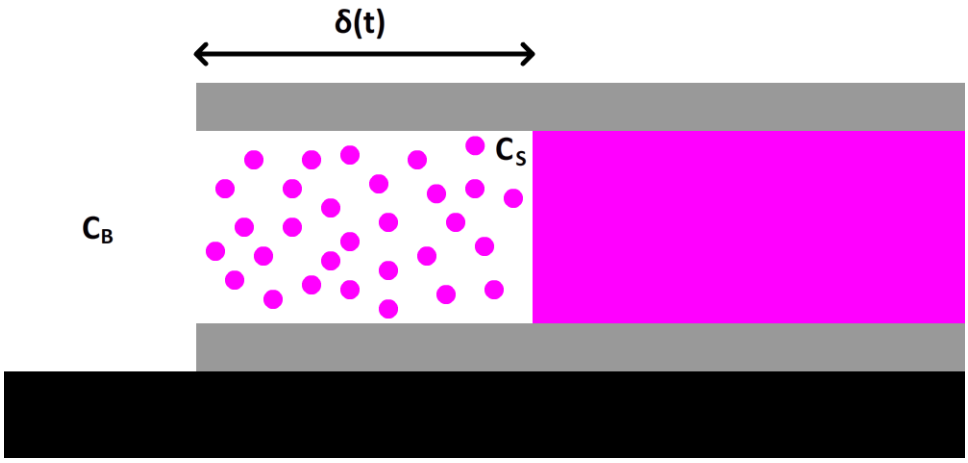

Figure 4.3: Sacrificial photoresist dissolution inside the parylene channel.

4.1.2.4. Releasing

The easiest alternative for releasing the parylene channels is rinsing with isopropyl alcohol (IPA) and/or methanol, then drying after acetone dissolution process. But this technique has some drawbacks. While liquid is drying, it forms a liquid-air interface under the free standing structures, then surface tension is created and this pulls the structures towards the bottom surface and cause stiction. Stiction is directly related to the surface energies. For instance, since the surface energy of the oxide layer is higher, parylene is ready to collapse to them. In addition, the thermal stress due to the previous fabrication steps is a driving force for occurring of stiction. Therefore, critical point drying (CPD) is a strong alternative for the

releasing process. It is the most effective technique that can be applied for releasing the free standing structures.

4.1.2.5. Adhesion

Substrates and oxide films: Successful adhesion of parylene to a wide variety of substrates (e.g. silicon, glass) and silicon based and/or oxide films can be achieved by a simple treatment with a solution of an organic silane prior to parylene coating. Silane can also be vapor phase applied if non-liquid application is needed.

Polymers: Adhesion of parylene to most polymers is improved by exposing the polymer surface to a short period of oxygen plasma ashing (typically for 1-2 minutes). This plasma treatment etches the surface of the polymer and exposes active polymer sites for parylene for bonding.

Metals to parylene: Adhesion of metals to parylene layers varies. While aluminum (Al) does not adhere well, Cr, gold (Au), and titanium (Ti) stick quite well. However, intrinsic stress is a major concern while metal coating. Adhesion of parylene to certain metals may be stronger than of the substrate. Then a high-stress metal layer can peel the parylene layer off from the substrate.

Parylene to Metals: Parylene-C has excellent adhesion when deposited on top of Al layers using the silanation process. Table 4.2 summarizes the adhesion characteristics of parylene.

4.1.2.6. Bonding

Wire bonding to metals on top of the parylene layers is quite a problematic process. Wire bonds tear the parylene since it is a soft material. Therefore, either parylene should be etched before metal layers are deposited on the surface, or the metal

thickness should be made as thick as possible (typically around 0.5 µm). During wedge bonding, bonds cannot stick to the metal layer well because of parylene's softness. To avoid this problem, the parylene layer under the metal layer should be coated thicker (at least 5 µm). Moreover, the adhesion of the parylene layer to the substrate should be strong enough in order not to peel the parylene off during the wedge bonding process.

Table 4.2: Adhesion of some films to parylene and parylene to them, and the methods used for promoting adhesion [69]. (A174 is a silane-based adhesion promoter).

Material	Adhesion: Film to Parylene-C	Adhesion: Parylene-C to film
Aluminum	poor	A174
Titanium	good	-
Chromium	good	-
Gold	good	poor
SiO_2 evaporated	good	A174
SiO_2 sputtered	good	A174
ITO DC sputtered	good	poor
AZO RF sputtered	poor	A174
Photoresist	good	plasma
Polyimide	plasma	plasma
Polycarbonate	-	plasma
Silicone rubber	plasma	-

4.2. Layout Creation

The sample process flow for parylene based surface micromachining was demonstrated in Chapter 1. Sticking with the same procedure, the fabrication process only includes three masks. Details of designed masks are given in the following sections for the single channel arrangement as an example. The fabrication process flow was exactly the same for all designs.

4.2.1. Mask 1: Electrode Definition

First mask was for defining the on-chip electrodes. This mask was selected to be clear-field, since positive photoresist was used for construction of the protective layer as an etch mask. Reservoir electrodes were designed wide enough for withstanding high voltages in kV range. Other electrodes were placed for special purposes, which were described in Chapter 3. Figure 4.4 shows the layout of the first mask.

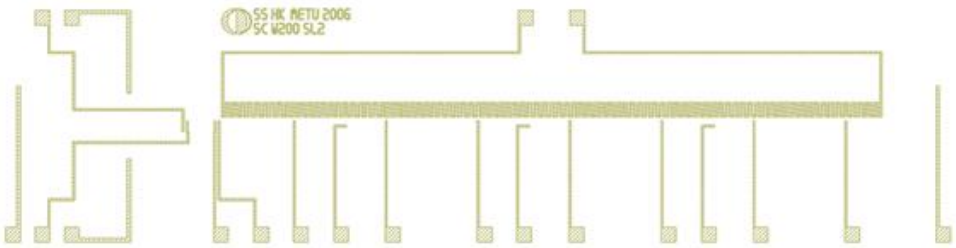

Figure 4.4: Layout of the first mask (electrode definition).

4.2.2. Mask 2: Channel Definition

Second mask was for defining the layout of the channel. This mask was clear-field since positive photoresist was used to define the microchannels. The photoresist layer constructed with using this mask is a sacrificial layer used for building up of microchannels with parylene deposition. Two dimensional shape of the channel was defined with this mask, and the height of the channel was determined with the thickness of the photoresist. Figure 4.5 shows the layout of the second mask.

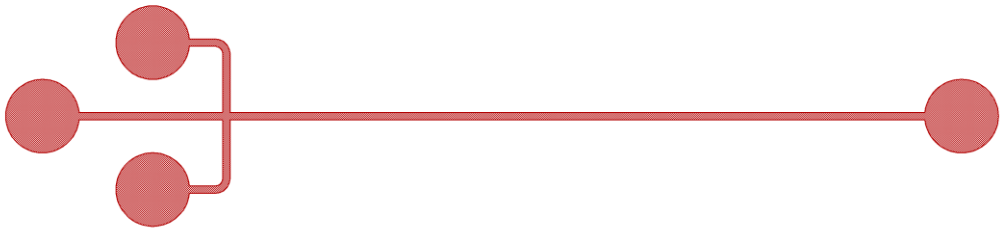

Figure 4.5: Layout of the second mask (channel definition).

4.2.3. Mask 3: Opening Definition

The third mask was for defining the openings for parylene etching. It was selected to be a dark-field mask, since positive photoresist was used as an etch mask. Different than the first mask, the drawn pattern defined the openings, where parylene layer was intended to be removed. The openings were drawn for reservoirs for the external fluidic connections, and for the electrodes for the external electrical connections. Figure 4.6 shows the layout of the third mask.

Figure 4.6: Layout of the third mask (openings definition).

4.3. Fabrication Process Flow

As stated before, the fabrication of the parylene microchips is only a three-mask process. Silicon or glass wafer can be used as a substrate. Previously described silanation process is applied for both substrate types. This treatment works perfectly with silicon substrates but parylene still does not stick well to the glass substrates. However, glass is preferable for a BioMEMS application as a substrate in terms of its transparency, biocompatibility and non-conductive behavior when the usage of the on-chip electrodes with high voltages in kV range is considered. In order to solve this adhesion problem, the wafers are immersed into the piranha and BHF solutions, respectively. Piranha solution, which is a mixture of sulphuric acid (H_2SO_4) and hydrogen peroxide (H_2O_2) with equal amounts, is used for the removal of the organic residues on the wafer. BHF treatment is used for increasing the surface roughness, making parylene sticks better to the substrate.

At the first step, a 5 µm thick parylene is deposited on the substrate for thermal and electrical insulation. Although an electrical insulation is not necessary for glass wafers, the insulation layer is required since the surface properties of parylene in terms of hydrophobicity and surface treatment requirements are favorable for the application.

At the second step, a Ti-Au layer is sputtered in a total thickness of 0.5 µm. Thick metal layer is required both for application of high voltages and solving the bonding problems. Then a thin layer of photoresist is spin-coated, exposed using the first mask and developed, respectively. This layer is used as an etch mask for wet etching of the metal layers in order to form the on-chip electrodes. Etching the metals, the photoresist is removed then.

At the third step, a 25 μm thick photoresist is spin-coated as a sacrificial layer. The microchannel layout is created by exposing using the second mask and developing the resist.

At the fourth step, a 20 μm thick parylene is deposited in order to form the microchannels.

At the fifth step, an etch mask is created with spin-coating the photoresist with a thickness more than 65 μm. This resist layer is exposed with the third mask and developed. This etch mask is used for dry etching of parylene with RIE for obtaining the reservoir and electrode pad openings. The photoresist is not hard baked in order not to bake the sacrificial layer. This makes the dissolution process in acetone easier. On the other hand, avoiding the hard baking, the etch rate of the photoresist becomes higher than expected when compared with the etch rate of parylene. Selecting the thickness of the etch mask in the order of 60 to 70 μm definitely enough for masking the parylene layer during the RIE process.

At the sixth step, parylene is dry etched with oxygen plasma RIE and completely removed in the area of the openings. The devices on the wafer then become ready for both fluidic and electrical connections.

At the final step, the wafers are diced and the stand alone devices are immersed into the acetone for dissolving the sacrificial layer for releasing the microchannels. The dissolving process typically takes 2 days for the specified thickness of the channels, which is consistent with the literature. For channel release, the devices were rinsed with IPA and methanol, respectively. Heating the devices, the methanol vaporizes quickly. Finally, released and dried microchannels are obtained. Figure 4.7 summarizes the fabrication process flow.

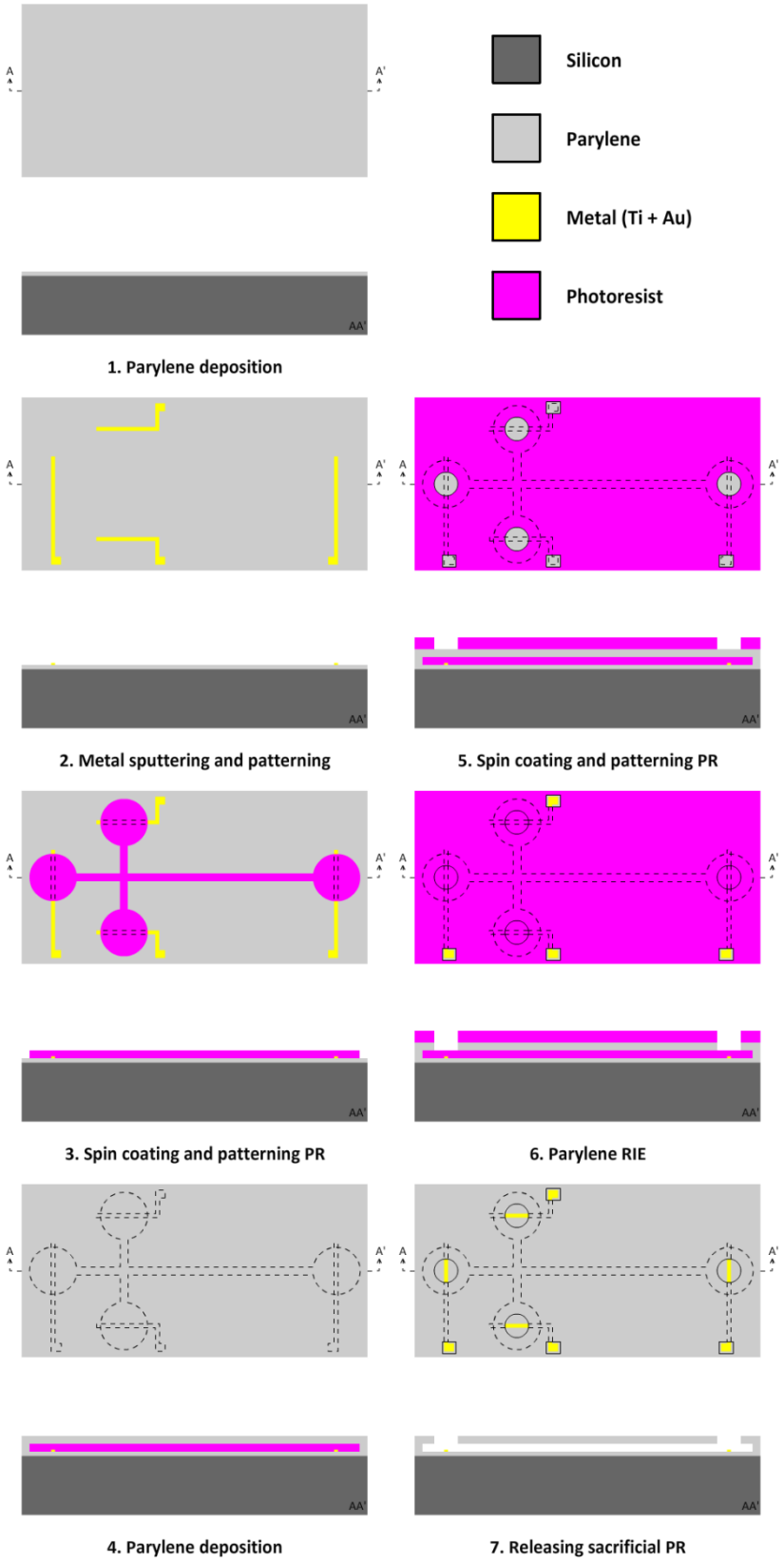

Figure 4.7: Fabrication process flow.

Figure 4.8, Figure 4.9, Figure 4.10, Figure 4.11, Figure 4.12, and Figure 4.13 show the diced glass wafer, fabricated single and double channel structures, and SEM pictures taken for detailed views, respectively.

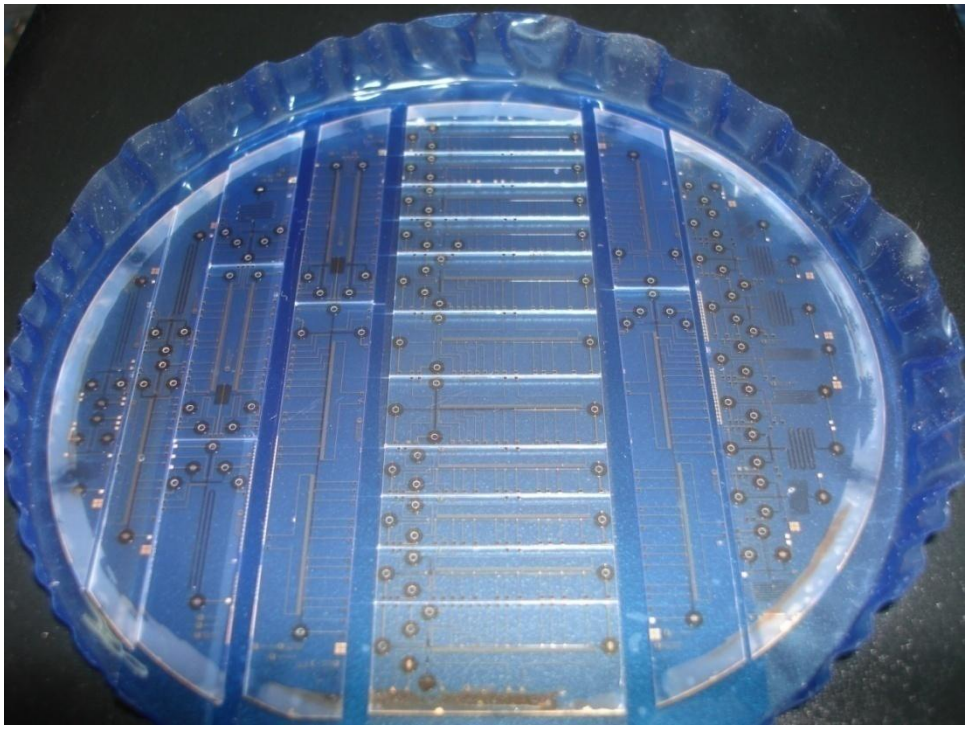

Figure 4.8: Diced glass wafer.

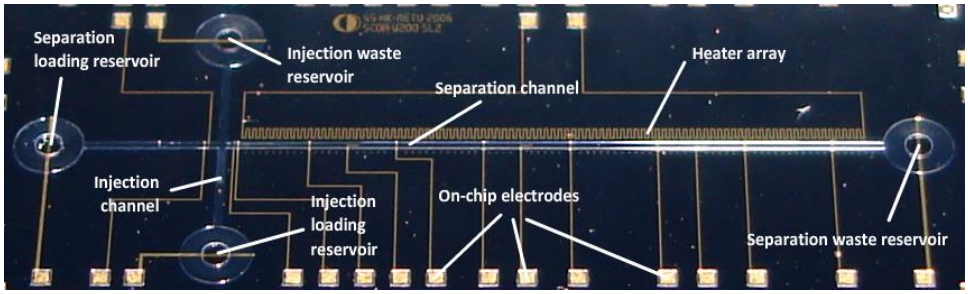

Figure 4.9: Fabricated cross channel device on silicon.

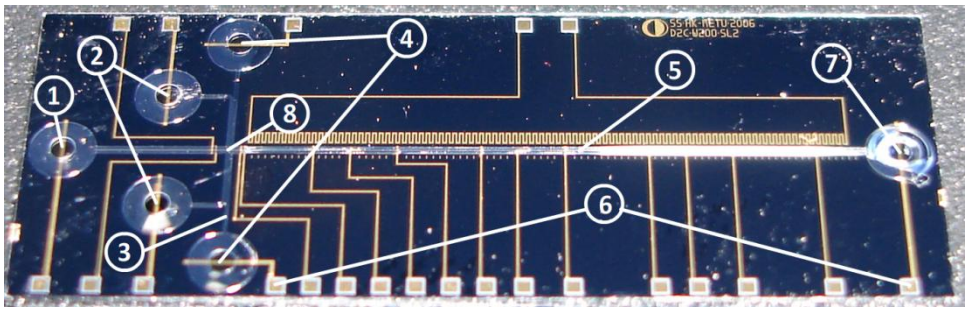

Figure 4.10: Fabricated double channel device on silicon. 1: Buffer loading reservoir, 2: Sample loading reservoirs, 3: Injection channels, 4: Injection waste reservoirs, 5: Separation channel, 6: Electrodes, 7: Separation waste reservoir, 8: Channel crossing.

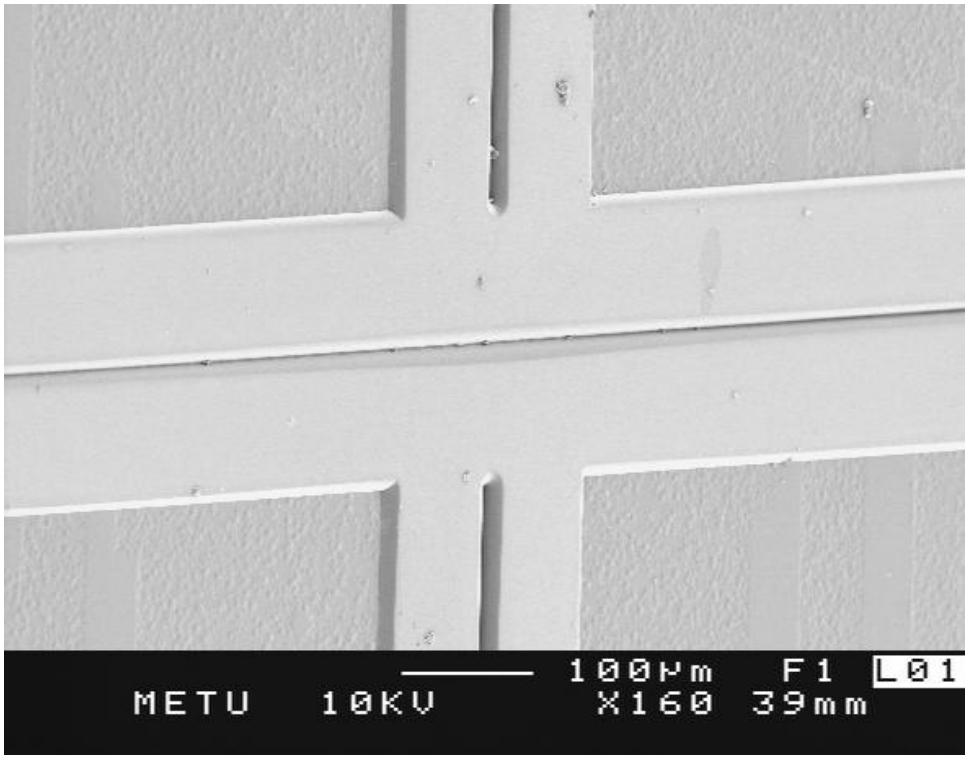

Figure 4.11: SEM picture of the junction of the double channel structure.

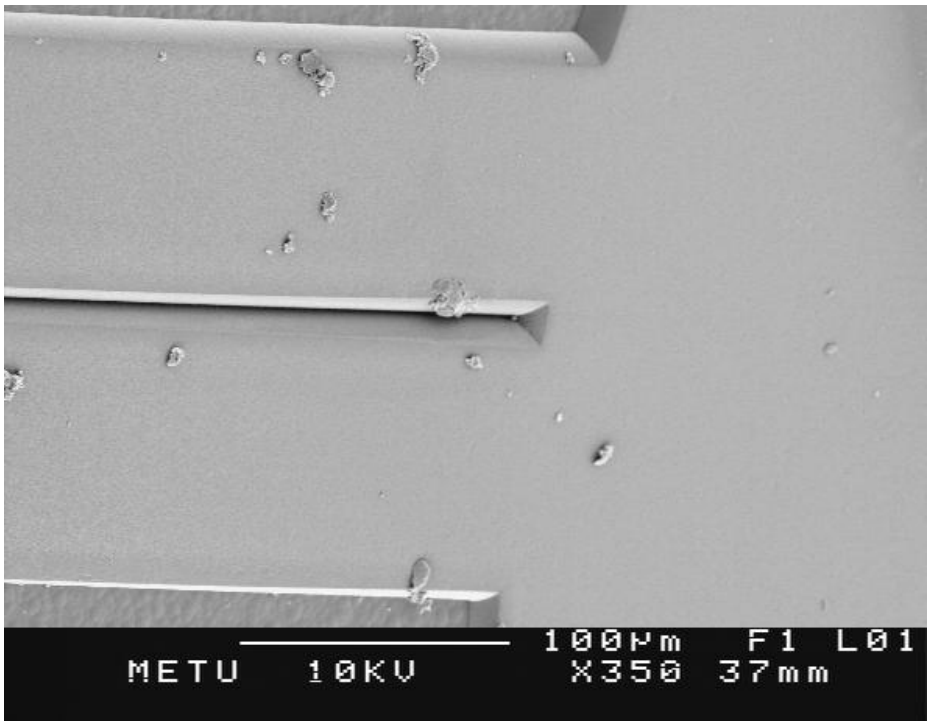

Figure 4.12: SEM picture of the reservoir entrance of double channel structure.

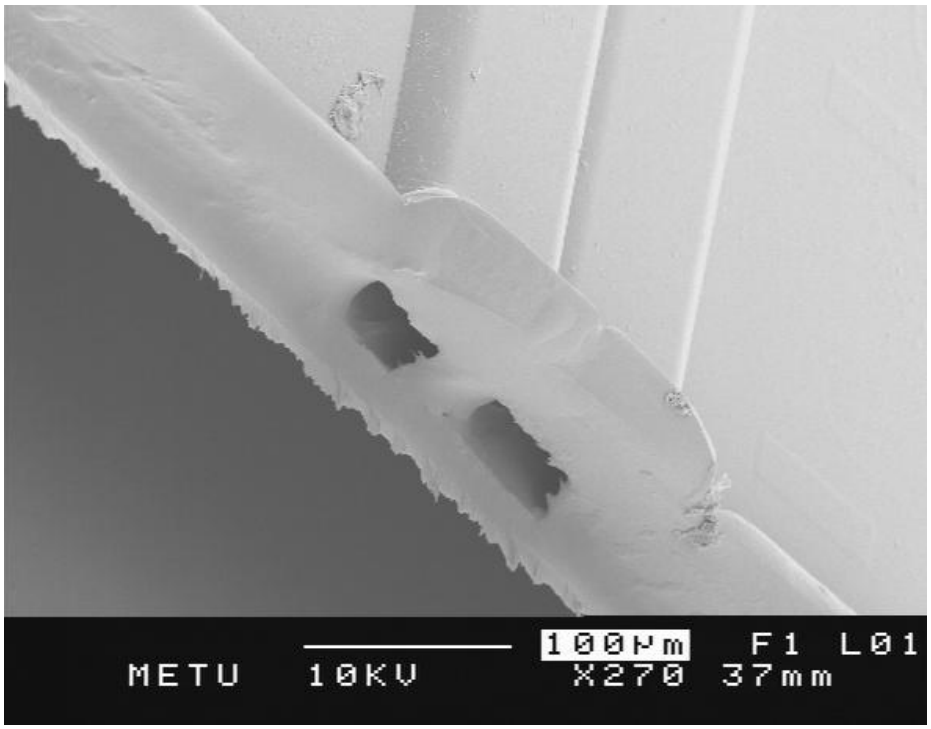

Figure 4.13: SEM picture of the cross-section of double channel structure.

Even though parylene thicknesses around 5 to 10 µm is enough for obtaining self standing microchannels for the channel height of 25 µm with applying CPD for releasing, the thickness of the parylene layer is selected as 20 µm. It was aimed to fabricate though devices for the used experimental setup, which is described in the next chapter.

Although it was not aimed, the fabricated structures are strong enough to be peeled off from the substrate without collapse after being released. Then flexible polymer micro devices can be fabricated with integrated electrodes. This unique feature gives the advantage of fabricating implantable microchips because parylene is a biocompatible material. Figure 4.14 shows the peeled off microchip.

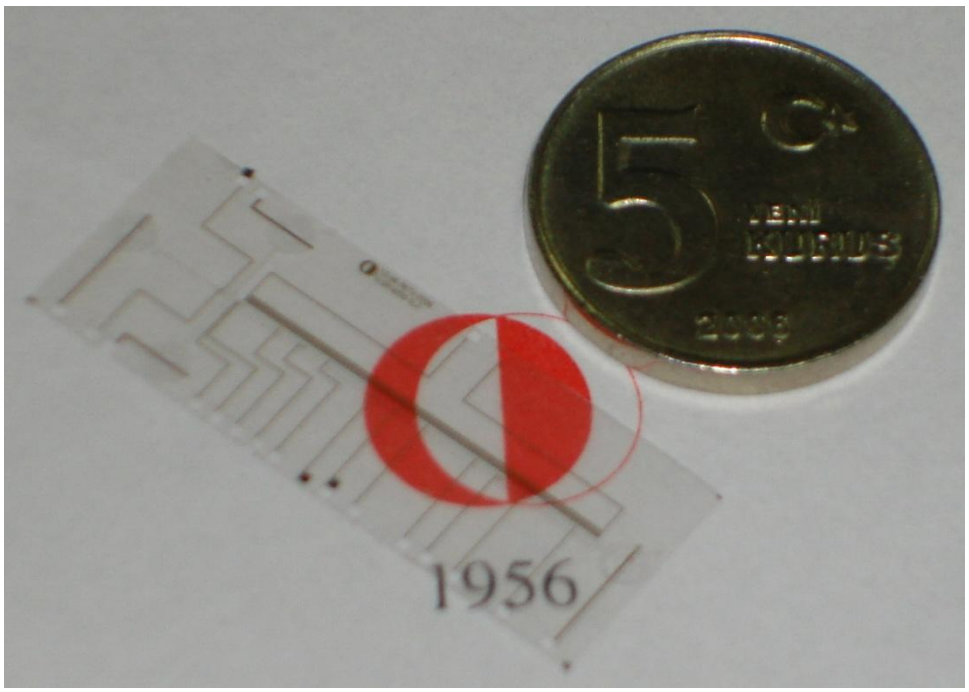

Figure 4.14: Peeled off parylene microchip.

4.4. Conclusion

In this chapter, the detailed discussion of parylene and the fabrication process flow was introduced. Using parylene-C, the microchips were fabricated with only a three-mask process. The thickness of the parylene was selected as 20 µm for constructing the channels where the height of the channel was 25 µm. Although Si was used as a substrate in early stages, adhesion problems with glass substrate was solved and the final microchips were fabricated on glass wafers. Optimizing the fabrication process flow, tough and durable polymer microchips were fabricated. During the release process, a unique feature of parylene was observed. It can be peeled off from the substrate when the bottom layer was selected thick enough for peeling off.

CHAPTER 5

EXPERIMENTAL WORK AND RESULTS

Experimental work is divided into three main sections: (i) Construction of test setup, (ii) single channel arrangement tests, and (iii) double channel arrangement tests. Single channel experiments were performed for sized based separation of dsDNA. According to the results and optimized parameters in single channel tests, double channel architecture was tested for the application of HDA. Following sections describe the experimental setup, carried out experimental work and the results.

5.1. Experimental Setup

The experimental setup was constructed for performing electrophoresis with high voltages and fluorescence based detection of the separation process. Online monitoring of the electrophoresis application was performed using the Olympus SZX12 stereo microscope (Olympus Inc.) with fluorescence attachment. The attachment has a 100 W mercury lamp for illumination. For monitoring of the process, a high resolution digital camera, Olympus DP70, which was directly connected to a computer, was used. For the illumination and monitoring, a filter set with 460 nm band-pass excitation filter, 495 nm long-pass emission filter, and 485 nm long-pass dichromatic mirror was placed into the microscope. Two high voltage power supplies were used for voltage application. Figure 1.1 and Figure 5.2 show the schematic of the test setup and the picture of the experimental setup, respectively.

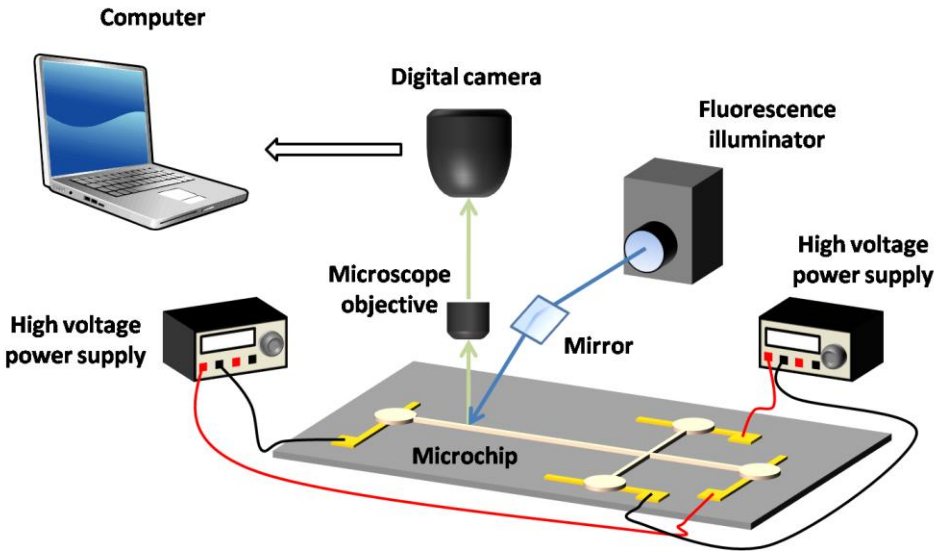

Figure 5.1: Schematic view of the electrophoresis test setup.

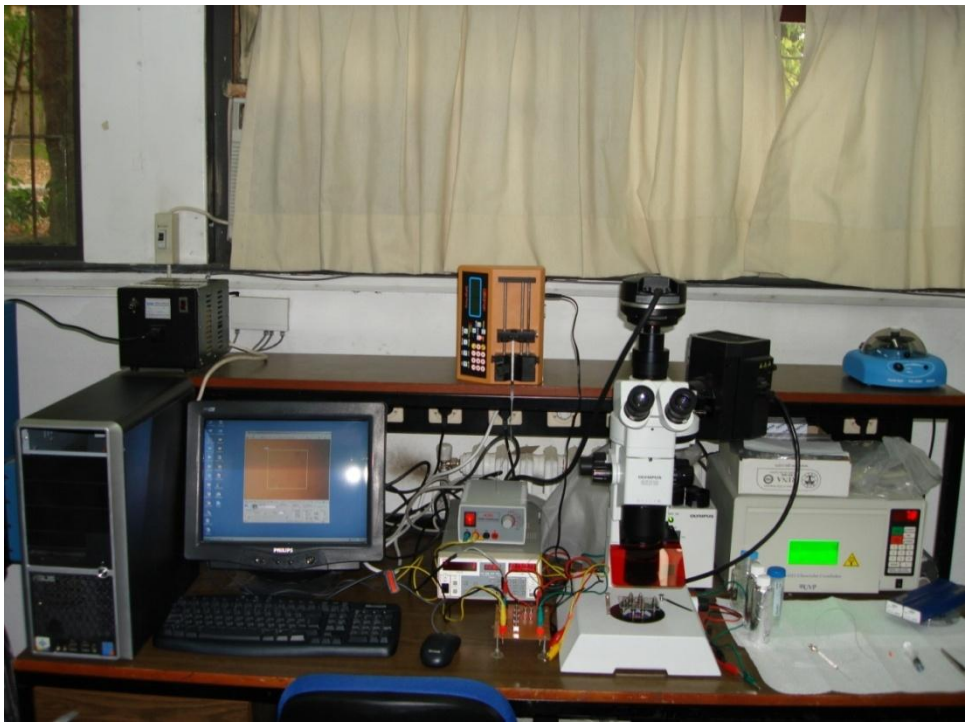

Figure 5.2: The picture of the whole experimental setup.

5.2. Separation of 100bp DNA ladder

In order to evaluate the performance of the devices and the reliability of the results, a DNA ladder was used instead of a PCR sample.

5.2.1. Sample Preparation

100bp DNA ladder (GeneRuler, Fermentas) with the concentration of 0.5 µg/µl was prepared for the separation. It was marked with a fluorescent dye, YOYO-1 (Invitrogen) for detection purposes with the DNA to dye ratio of 5:1. The ladder consists of 14 dsDNA fragments in different sizes changing from 100bp to 3000bp.

5.2.2. Microchip Preparation

Single straight channel microchip with 2 cm separation channel length and 200 µm channel width was selected for the desired application.

The first stage of microchip preparation is dispensing the sieving matrix. In order to achieve high resolution separations, entangled separation matrices should be used. High viscosity is the natural characteristic of entangled matrices because of their cross-linked behavior. Loading separation channels with high viscosity liquids in micro scale is a problematic issue. Capillarity is not sufficient as a driving force for filling microchannels with such liquids. Dispensing with pressure is not an appropriate way since high pressure is needed for filling, which can easily destroy the microchannels. In order to solve these problems, an ultraviolet (UV) photo-polymerized polyacrylamide was used as sieving material [57]. The gel was loaded in the microchannels in its linear (non-cross-linked) form easily since it is aqueous in this form. Then it was exposed to UV light and cross-linked.

Polyacrylamide gel (ReproGel High Resolution, Amersham Biosciences) was prepared as a mixture with a final concentration of 8% (w/v) acrylamide/bisacrylamide monomers and 1x TBE. Then microchip was loaded with the prepared gel mixture. Loading was performed by injecting 2-3 µl mixture with a microliter syringe in the separation waste reservoir and then channel was filled with the capillary action. Part of the microchip was covered with a mask leaving the separation channel unprotected and the device was exposed to UV light in a UV cross-linker (CL-1000M, UVP) with 8 W, 302 nm wave length illumination for 20 minutes. After the polymerization, the non-polymerized gel was vacuumed. The polymerization procedure is summarized in Figure 5.3.

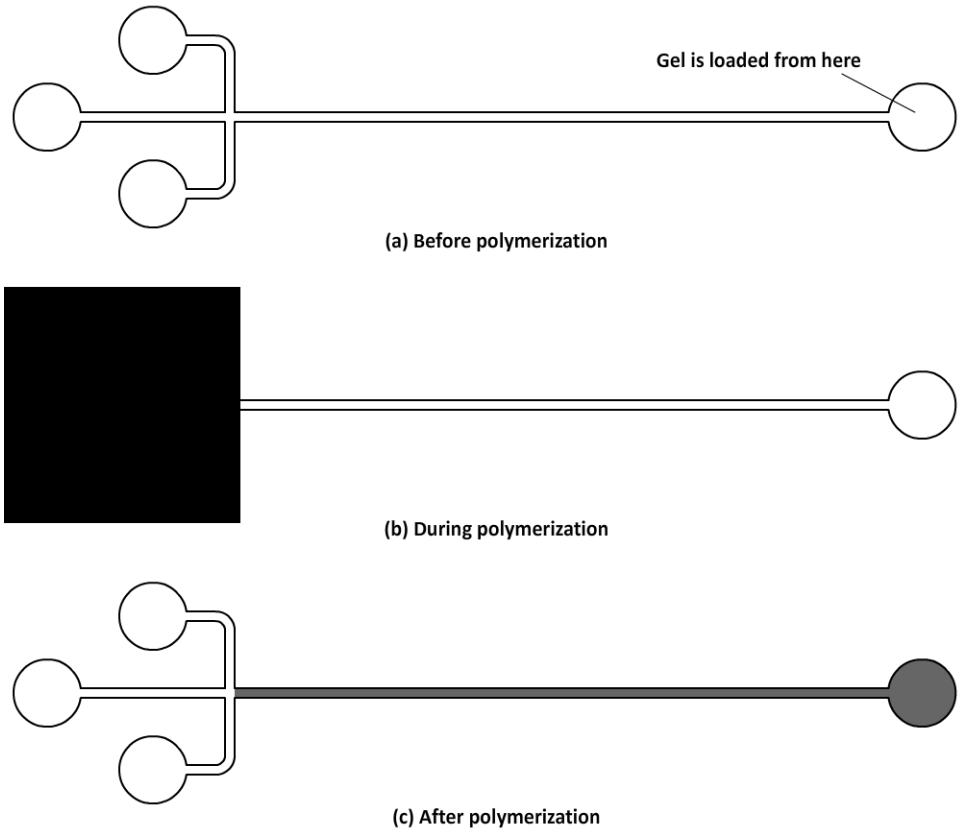

Figure 5.3: UV photo-polymerization of acrylamide.

After the polymerization process, the microchip was bonded to the ceramic package for external electrical connections. Figure 5.4 shows the microchip in ceramic package. Since the microchip was covered with the mask during polymerization, the gel loading and polymerization procedures were performed before the bonding process in order not to destroy the bonds.

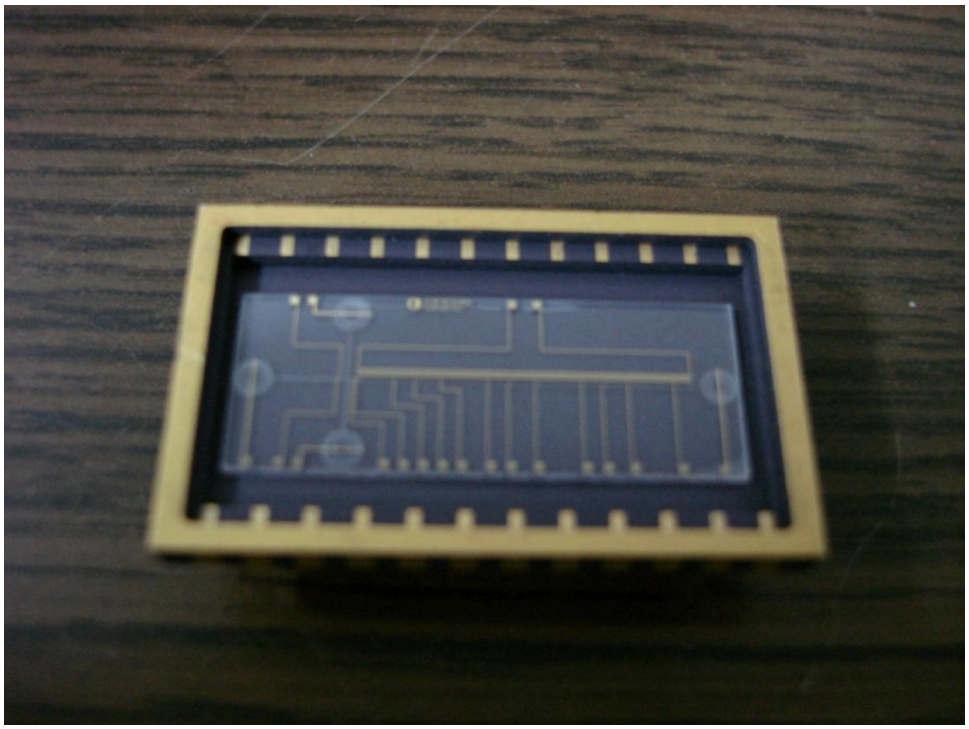

Figure 5.4: Microchip in ceramic package.

At the last stage, the microchip was filled with the running buffer, 0.5x TBE solution from the buffer loading reservoir. Similar to the gel loading, a 3-5 µl of buffer solution was injected into the reservoir with a microliter syringe.

5.2.3. Electrophoresis Procedure

After preparing the sample and the microchip, the electrical connections were made, in other words, ends of the injection and separation channels were connected to two high voltage power supplies separately. Sample of 1 µl was loaded from the sample loading reservoir again with the same technique as applied for both gel and buffer loading. Then the electrophoresis procedure was applied. In the electrophoresis run, the pullback method was applied in order to avoid leakage. The applied voltages in injection and separation phases are illustrated in Figure 5.5.

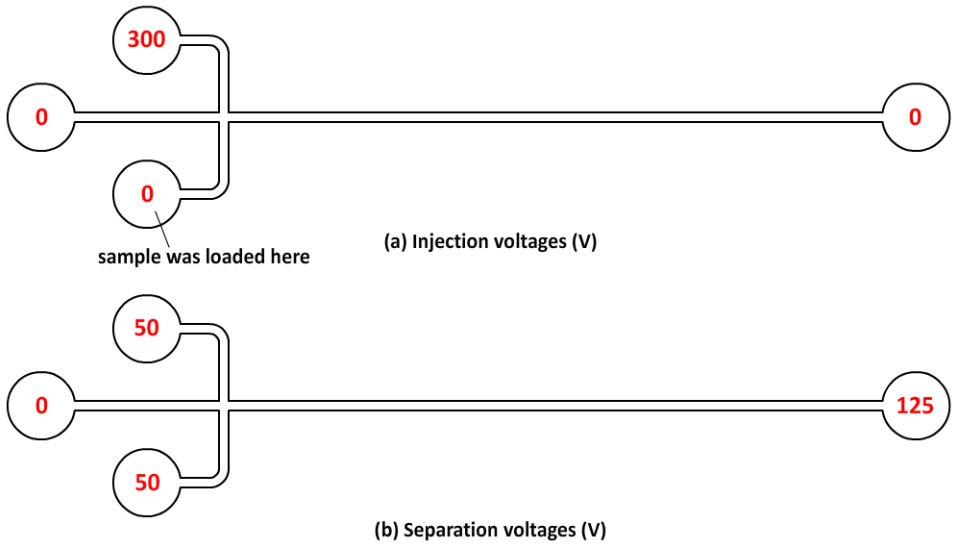

Figure 5.5: Applied voltages for 100 bp DNA ladder separation.

5.2.4. Results

The full separation of all 14 bands was observed after almost 13 minutes, which can be considered as a rapid separation. The whole separation process was recorded with the digital camera and the resulting video was processed with a commercially available image processing software (ImageJ). Figure 5.6 shows the intensity graph of separated bands through the channel. Since the sieving matrix is not suitable for the separation of long fragments (larger than 500bp), the separation performance decreases after 500bp.

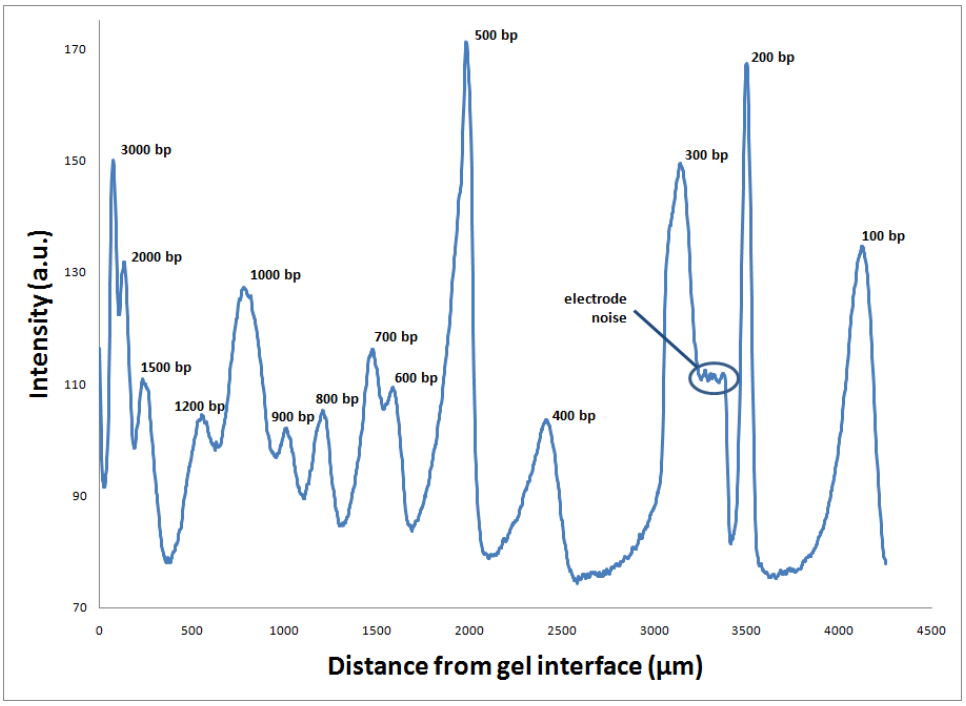

Figure 5.6: Intensity graph of separated bands with respect to their distance from the injection point after 12 min 36 sec of electrophoresis run.

The intensity graph of first four fragments, 100bp to 400bp was also plotted at the separation length of 1 mm and illustrated in Figure 5.7.

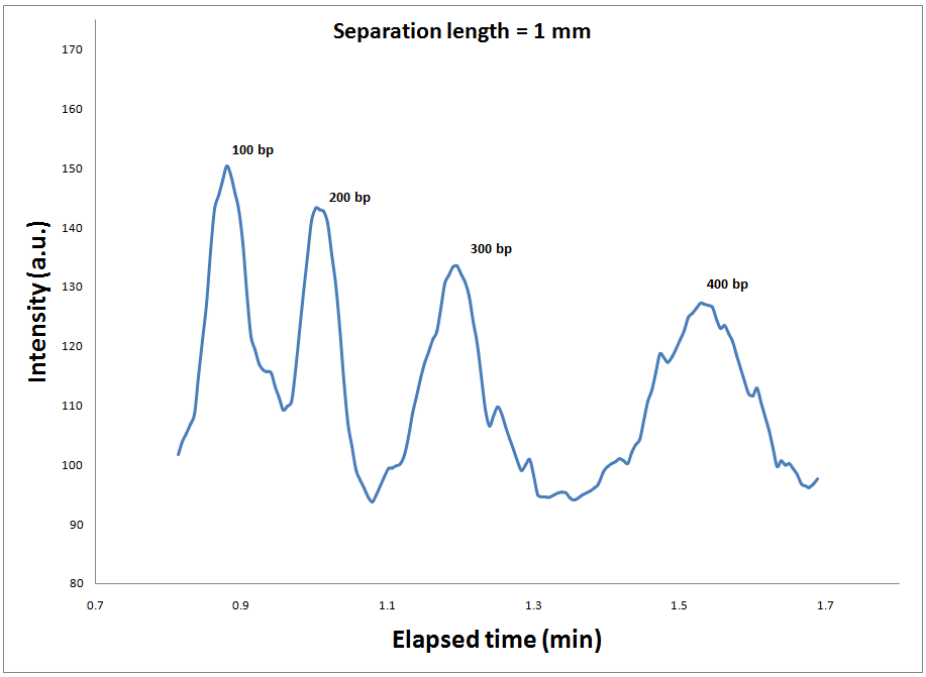

Figure 5.7: Intensity graph of first four separated bands with respect to time for the separation length of 1 mm.

Although the size range of the sample is quite broad, the full separation of 14 bands was accomplished successfully in a total length of 5 mm.

According to the Figure 5.6, the variation of mobility with respect to the fragment length was plotted in Figure 5.8. Mobility decreases linearly with increasing fragment length for relatively short fragments (up to 500bp), which was expected from the theory. Beyond this value, the trend turns to be polynomial, which was also expected for the longer fragments.

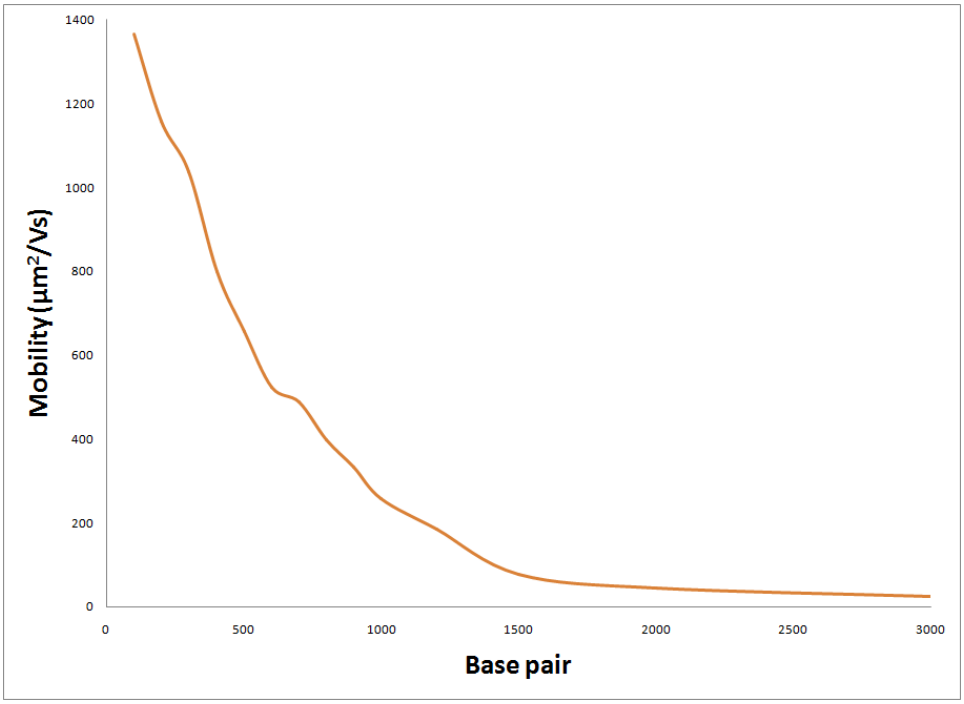

Figure 5.8: Variation of mobility with respect to fragment length.

5.3. Microchip Design Optimization

During the experimentation of first generation devices, two major problems arose. The first problem was formation of bubbles due to insufficient buffer amount. Since high electric field intensities were applied for very short channel lengths, the buffer solution evaporates rapidly. Therefore, the buffer solution has to be continuously fed into the channel for avoiding evaporation, so the formation of bubbles. The bubble formation was not only observed during electrophoresis runs, but also in the loading stage of buffer solution at the very beginning of the electrophoresis procedure. Since the solution was filled into the channel only by the capillary action, the air was stuck at the channel junction and stays there. This made the injection, and therefore separation impossible. The second problem was in bonding the chips after the polymerization. Since the polyacrylamide gel should be used

immediately after the polymerization, waiting for the bonding process after the polymerization causes crack initiations in the gel composition during the runs.

In order to solve the above mentioned problems, second mask set was prepared for the same fabrication process flow with optimized designs of 200 µm width single straight channel and double channel architectures with 2 cm separation channel lengths.

Design optimization was performed in two steps. First, the diameter of buffer loading reservoir was enlarged according to the footprint of the nanoports (Upchurch), which are used for interconnecting the external fluidic components to the microfluidic chips. Moreover, all other reservoirs were also enlarged according to the footprint of Luer Lok compatible adapters, on which the commonly used luer syringes can fit. Second, omitting all other electrodes, the contact pads of the electrodes placed at the reservoirs are enlarged enough so that bonding became unnecessary. In order to avoid the overlapping of the interconnections, the separation channel of the microchips was lengthened 0.5 cm. Figure 5.9 and Figure 5.10 show the optimized single and double channel structures, respectively.

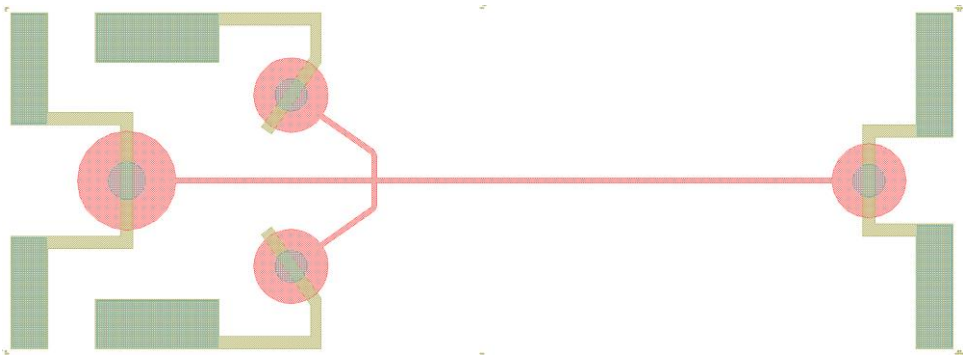

Figure 5.9: Optimized single channel design.

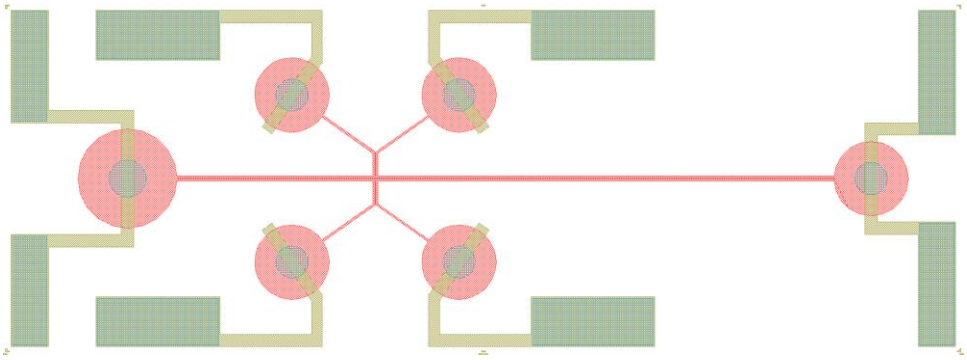

Figure 5.10: Optimized double channel design.

5.4. Separation of Heteroduplex Control Sample with Single Channel Microchip

Optimizing the design of the microchips, HDA was tested with the single channel architecture.

5.4.1. Sample Preparation

For performing heteroduplex analysis, the commercially available heteroduplex control sample (Cambrex Biosciences), which contains 350bp homoduplex and heteroduplex fragments was selected. It was marked with YOYO-1 for detection purposes with the DNA to dye ratio of 5:1.

5.4.2. Microchip Preparation

Different from the previous designs, the fluidic interconnections were fixed on the respective reservoirs with white epoxy. The nanoport was bonded on the buffer loading reservoir, and the luer lok adapters were bonded on the sample loading and injection waste reservoirs. No interconnection was bonded on the sample waste

reservoir. After fixing the interconnections, following a curing process white epoxy makes a permanent and rigid layer, which avoids leakage perfectly. Figure 5.11 shows the picture of the optimized single channel device with fluidic interconnections.

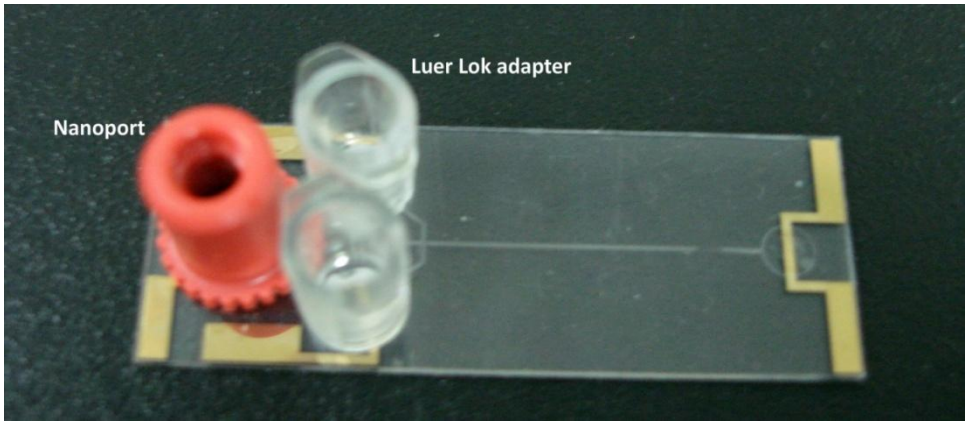

Figure 5.11: Optimized single channel structure with fluidic interconnections.

Then gel loading and polymerization steps were performed with the same method described in the previous sections. The buffer solution, 0.5x TBE, was dispensed into the microchip with a syringe pump through the nanoport. Filling the microchannels with pressure driven flow avoided the bubble forming.

5.4.3. Electrophoresis Procedure

Since bonding was no longer necessary, the microchip was placed and fitted onto a plastic piece with metal connections as shown in Figure 5.12. The electrical connections and voltage control were made through the voltage panel as shown in Figure 5.13.

Figure 5.12: Plastic piece with metal connections for microchip placement.

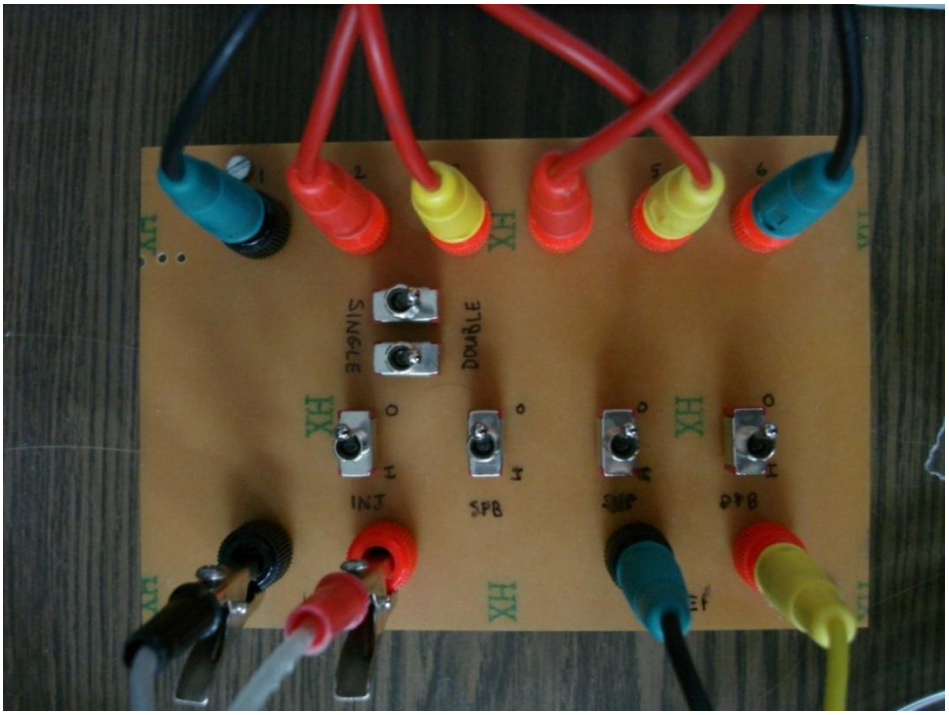

Figure 5.13: Voltage control panel for injection and separation.

Following the same procedure explained in the previous sections, the electrophoresis run was completed for HDA. The applied voltages are illustrated in Figure 5.14.

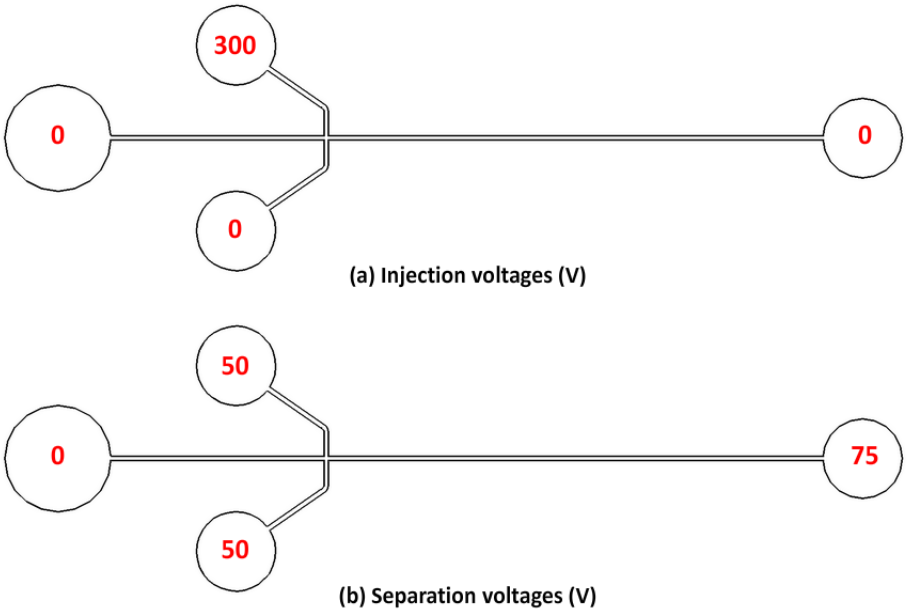

Figure 5.14: Applied voltages for single channel HDA.

5.4.4. Results

The heteroduplex control sample contains two bands: a slower moving heteroduplex DNA and a faster moving homoduplex band (heteroduplex bands often run as a single band). Homozygous normal or mutant samples are expected to migrate as a single band (homoduplex). Depending on the mutation, the PCR products of heterozygous DNA will form up to four bands: mutant/mutant, normal/normal homoduplexes, plus two mutant/normal heteroduplexes.

Therefore, the expected two bands were observed in a very short separation length, which is around 300 µm, as shown in Figure 5.15.

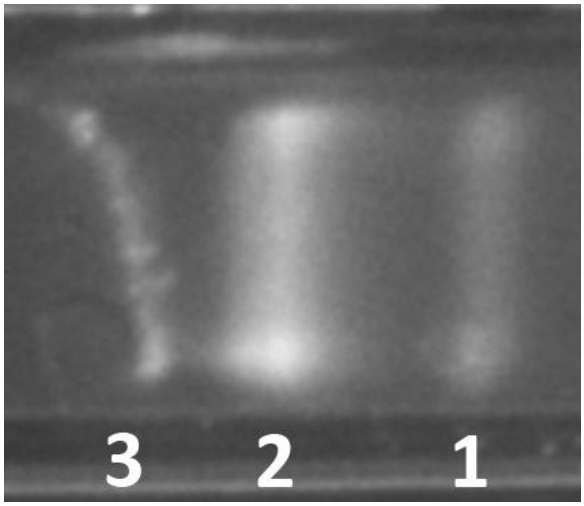

Figure 5.15: Separation result for HDA with single channel chip. 1: Homoduplexes, 2: Heteroduplexes, 3: Gel interface. Migration direction is from left to right (E = 25 V/cm). Note that soon after the samples passed through the gel interface, separation of heteroduplexes from homoduplexes were observed. Channel width is 200 µm.

Figure 5.15 proves that the heteroduplex analysis was successfully applied with the single channel microchip in a very short separation length.

5.5. Separation of Heteroduplex Control Sample with Double Channel Microchip

Optimizing the design of the microchips, successfully applying HDA with single channel microchip, application of HDA was tested with double channel architecture.

5.5.1. Sample Preparation

Heteroduplex control sample was selected to be separated for the application of HDA. Sample preparation procedure was the same as single channel microchips.

5.5.2. Microchip Preparation

Similar to the sample preparation procedure, the microchip preparation procedure was same as for single channel architecture. But this time the luer lok adapters were not used since masking during the polymerization stage was not possible with them. Figure 5.16 shows the double channel device with fluidic interconnection.

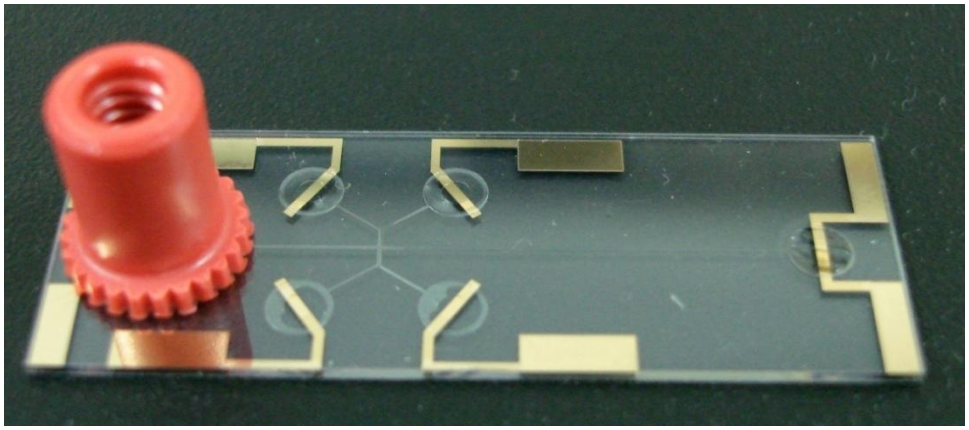

Figure 5.16: Double channel structure with fluidic interconnection.

Gel loading, polymerization and buffer dispensing were performed with same procedure as previously mentioned.

5.5.3. Electrophoresis Procedure

Electrophoresis run was completed for HDA with similar procedure as described in previous sections. The applied voltages are illustrated in Figure 5.17.

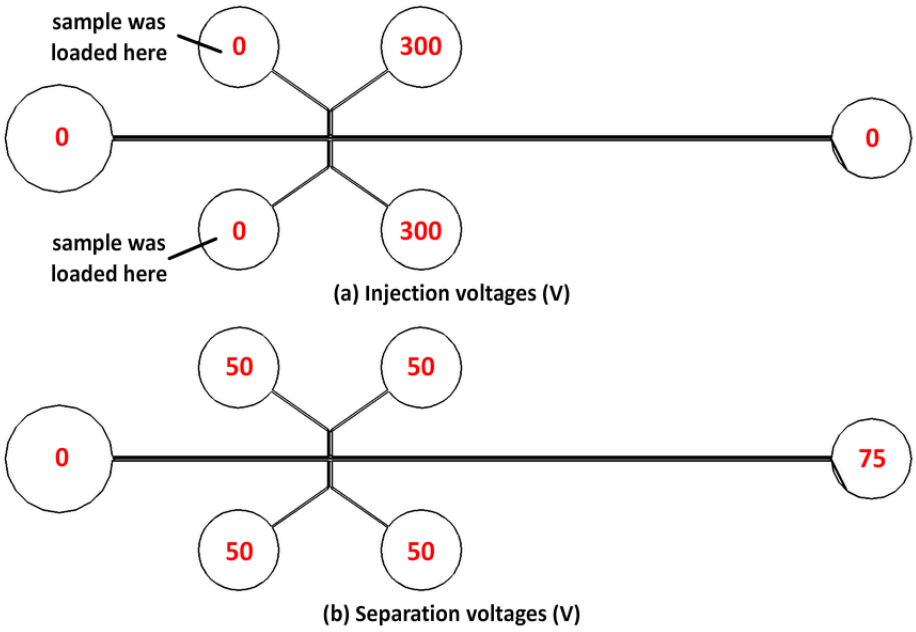

Figure 5.17: Applied voltages for HDA with double channel structure.

5.5.4. Results

5.5.4.1. Injection

During the sample injection, novel u-turn method, which was described in Chapter 3, was applied. The experimental results were better than expected. Sample injection was successfully applied with this method.

The most important drawback of the u-turn injection technique was the resulting sample plug shape, which was directed to the separation channel after the phase change. As stated earlier, the sharpness of the sample plug shape has a critical role in the separation performance. This disadvantage was eliminated with the usage of the cross-linked polyacrylamide. Since the part of the channel was protected from UV excitation during the polymerization, a sharp gel interface was formed at the entrance of the separation channel. Taking into account the entangled characteristic of the cross-linked polyacrylamide, the sample plug compacted at the buffer-gel interface, just before entering the separation channel.

An important advantage of the u-turn injection technique is its ability to control the sample amount during the injection by adjusting the time of operation. In other words, shorter injection time yields less amount of sample, whereas a longer time yields more. Although low sample amount is favorable for sharp sample plug shapes in most applications, it is difficult to detect the low concentration samples. Increasing the sample amount by lengthening the injection time and making it compacted at the gel interface increases the sample concentration, which makes the detection easier. The application of time-controlled injection and the sample plug compaction are illustrated in Figure 5.18.

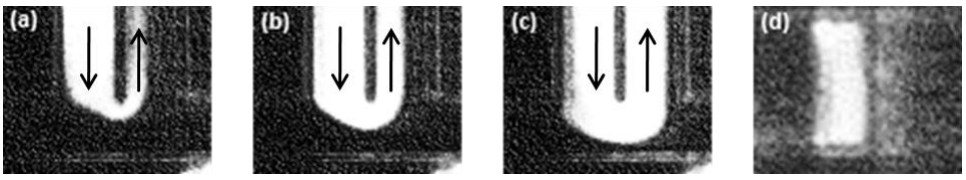

Figure 5.18: Injected sample amounts for U-Turn injection method after (a) 28s, (b) 33s, (c) 100s. (d) Compacted sample at the gel interface.

5.5.4.2. Separation

Performing the injection, HDA analysis was applied successfully with double channel structure in a very short separation length, less than 200 µm. Figure 5.19 shows the separated fragments. Separating the same sample in both microchannels proved that the identical conditions were obtained for the two separation process. This fact indicated the reliability of the system. In addition to this fact, accomplishing the separation in a very short separation length indicated that HDA can be applied with this system in a very short separation length and time with reliable results.

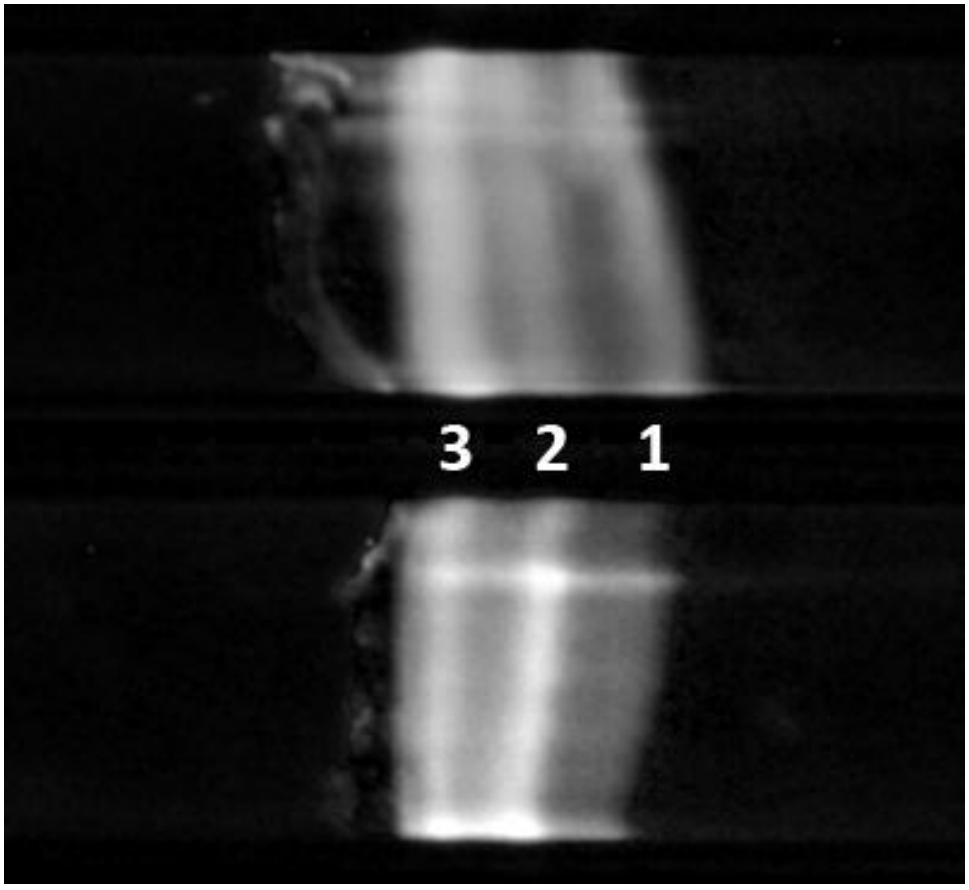

Figure 5.19: Separation result for HDA with double channel chip. 1: Homoduplexes, 2: Heteroduplexes, 3: Gel interface. Migration direction is from left to right (E = 25 V/cm). Channel width is 90 µm for each.

5.6. Heteroduplex Analysis with Double Channel Microchip

After the successful separation of heteroduplex control sample with the double channel structure, finally HDA was applied with a double channel structure with purified PCR samples. 590 bp long PCR samples with 3 bp mutations were analyzed.

5.6.1. Sample Preparation

For heteroduplex analysis, 590 bp long, gel purified PCR products were used. The PCR products were generated from vectors that either contained a wild type human gene or a mutant version of the same gene (site directed 3bp mutation). The wild type sequence contained TGC which were replaced by GCA. For homoduplexes and heteroduplexes, the sequence verified normal sequence was mixed up with the mutant sample (each around 140 ng/ul), heat denatured at 95 °C for 5 minutes and were annealed at 68 °C for 30 minutes.

5.6.2. Microchip Preparation

This stage is the same as with the heteroduplex control sample separation using double channel structure.

5.6.3. Electrophoresis Procedure

Following again the same procedure with previous experiment, the applied voltages are illustrated in Figure 5.20.

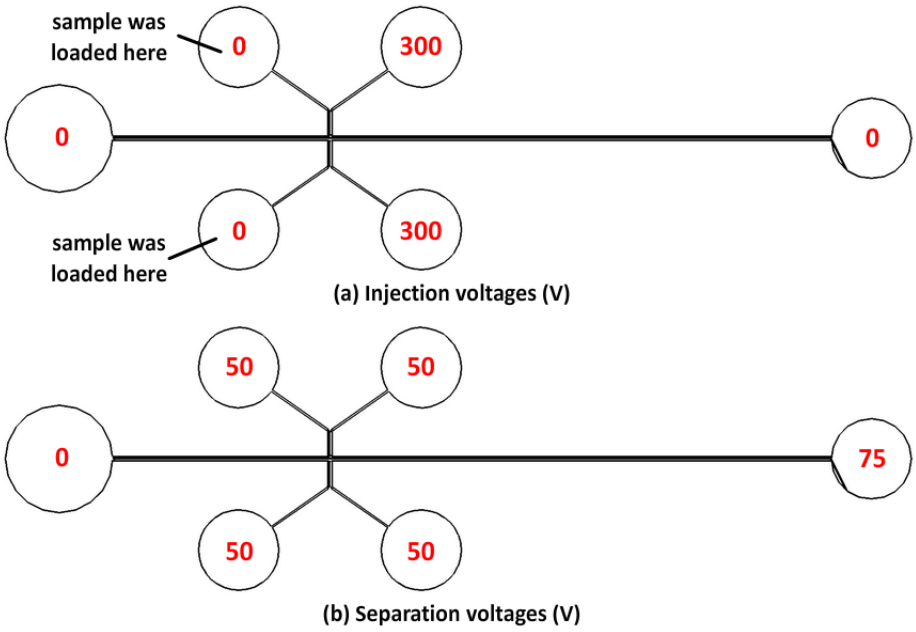

Figure 5.20: Applied voltages for HDA with double channel structure.

5.6.4. Results

HDA analysis was performed successfully with double channel structure in a very short separation length, around 50 µm in less than 3 minutes. In addition, using the control channel, reliable results were obtained. Having a control channel not only gives the advantage of having reliable results, but also avoiding the need of performing high resolution separations because it is enough to see the additional heteroduplex band between the homoduplex and the gel interface bands, which are aligned with their counterparts in the control channel. This yields with observing the desired results before reaching high resolution separation and thus ending up with very short separation length and time. As a result, high throughput mutation detection applications can be performed easily and practically.

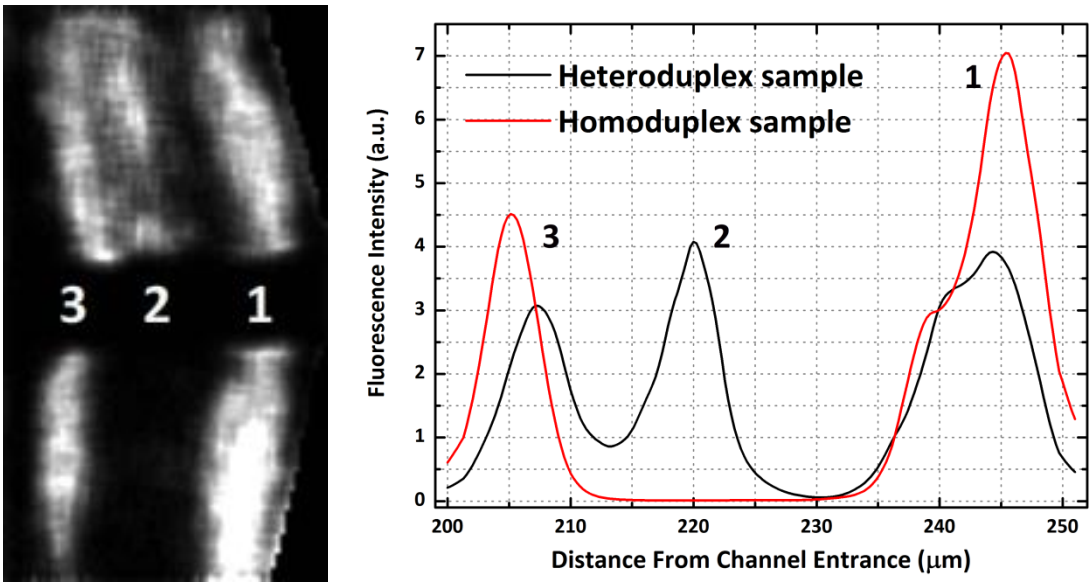

(a) (b)

Figure 5.21: (a) Separation result for HDA with double channel chip. (b) Intensity graph of separation result for HDA with double channel chip. 1: Homoduplexes, 2: Heteroduplexes, 3: Gel interface. Migration direction is from left to right (E = 25 V/cm). Channel width is 90 μm for each.

5.7. Conclusion

The objectives of the experimental work were accomplishing successful separations with the single channel architecture and therefore applying HDA with the double channel structure. After a number of experiments, parameter optimizations, such as applied voltages for injection and separation, gel polymerization time, used buffer concentration etc. were completed. In addition to sized based separation of DNA ladder, HDA was successfully performed with the control sample with the single and double channel architectures within a very short separation length. Separating the same sample in both channels simultaneously also proves that identical conditions can be provided with two separation channels of this novel design. Finally HDA was performed with a purified PCR sample with 3 bp mutations within 50 μm separation length in less than 3 minutes. These results indicate

potential uses of the proposed system for HDA for even single base mismatches, because the separation length and time are very short. This structure can also be used for the size determination of PCR products like applied in slab-gel electrophoresis by running DNA ladder in the control channel simultaneously. After size determination, the PCR products can be investigated for the mutations and therefore this design can be used as a stand-alone system for the mutation detection applications with high throughput and reliable analyses.

CHAPTER 6

CONCLUSION AND FUTURE WORK

The research performed within the framework of this thesis contains design, fabrication and implementation of all polymer micro scale electrophoresis systems for DNA separations using MEMS technology. Throughout this study, it was aimed to perform development and application of micro scale electrophoresis system for the first time in Turkey and try to participate in construction of BioMEMS technology, which is quite new for the country. Having this ultimate goal, the following objectives were completed:

1. **Development of all polymer micro electrophoresis systems with different single channel architectures:** A comparative study including performance evaluation was performed for the cross, double-T and double-L injection methods with flow simulations. Due to the leakage problem, the pullback injection technique was applied successfully with flow simulations. Cross injection technique was selected as the only injection method due to its highest performance. Determining the injection technique, channel dimensions and separation channel length were determined according to the needs of application. Channel height was selected as 25 µm for easy detection. Channel widths were selected as varying from 50 to 200 µm. Separation channel length was selected as 2 cm. In order to make safe designs, serpentine arrangement microchips were designed with longer separation channels, 4 cm and 10 cm, with decreased chip area. Due to the performance decrease in separation, geometry optimizations were performed with tapered turns for serpentine

layouts. Finalizing the designs, the first mask set was created and 24 different systems were included on the wafer layout.

2. **Development of a novel double channel microchip for the application of heteroduplex analysis:** According to the need of having an additional control channel for reliability of the results, a geometrical derivation from the traditional single channel layout was performed to create double channel layout. The 200 μm wide separation channel was divided into two parts with a 20 μm thick wall at the center. Therefore two identical side-by-side separation channels of 90 μm width were designed. A new, u-turn injection method was designed for this new architecture. The feasibility of the injection technique was proved with the flow simulations. Doubling the sample loading and injection waste reservoirs, the construction of the double channel layout was completed.

3. **Development of fabrication process flow for parylene:** The desired fabrication process flow was determined for a parylene based all polymer microchip construction with on-chip electrodes. All steps and parameters of microfabrication were optimized. Channel wall thickness was selected as 20 μm in order to have robust and durable devices. Solving all the problems with fabrication, polymer microchips were successfully fabricated on glass substrates.

4. **Constructing the experimental setup and tests:** Experimental setup was constructed for testing the fabricated devices with fluorescence based on-line detection system. Single channel arrangements were tested and operational parameters were determined and optimized with all constraints, including the injection/separation voltages, gel polymerization time etc. Determining the parameters, successful size based separations were performed with the single channel microchips. Two main problems were observed during the experimentation of the single channel microchips, first was the bubble

formation because of the insufficient feeding of buffer solution during the operation; second was bonding of the microchips to the ceramic packages for external electrical connections. In order to solve these problems, the designs were optimized for the usage of fixed fluidic interconnections and avoiding the bonding procedure with enlarged on-chip electrodes. Solving all the problems related to fabrication and operation, HDA was first performed with single channel architecture successfully with a very short separation length. The parameters for HDA were set and optimized for double channel architecture experiments.

5. **Testing the new double channel design and successful application of HDA:** Taking the advantage of successful application of HDA with single channel architecture, HDA was performed with the set parameters with double channel architecture. Using the gained experience form the experiments of single channel microchips, successful application of HDA with heteroduplex control sample was performed with the novel double channel design. Separating the same sample in both channels simultaneously also proved that identical conditions can be provided. HDA was carried out in a very short separation length. Then 590 bp long PCR product with 3 bp mutations was analyzed. The mutation was detected in less than 3 minutes within a separation length of 50 µm. These successful results indicate potential uses of the proposed system for HDA for even single base mismatches, because the separation length is very short compared to the total channel length.

The most important aspect of the double channel system is that under the same conditions, electrophoresis can be performed for both channels simultaneously. This gives the chance of having a control channel, which is very critical for the accuracy and reliability of the results in genetic analyses. In addition to HDA, this system can be applied for a number of applications such as various other

mutation detection systems for determining the length of a PCR product with running a ladder in the control channel.

Although an extensive effort spent for achieving these objectives, there are still some challenges that can be stated as future work:

1. All designed and fabricated channel architectures can be tested for performance evaluation of different geometries.

2. Using the additional electrodes, electrode defined sample injection and moving electric field separations can be performed for increasing the separation performance.

3. Using the heater array, single-stranded DNA (ssDNA) separations can be performed for the purpose of sequencing.

4. High-throughput mutation detection applications can be performed applying HDA with double channel structures for the genetic screening of some diseases.

5. Advanced flow simulations can be performed for the gel medium for the separation process for the aim of developing more efficient systems.

REFERENCES

[1] C. R. Fiers W, Duerinck F, Haegeman G, Iserentant D, Merregaert J, Min Jou W, Molemans F, Raeymaekers A, Van den Berghe A, Volckaert G, Ysebaert M., "Complete nucleotide sequence of bacteriophage MS2 RNA: primary and secondary structure of the replicase gene," *Nature,* vol. 260, pp. 500 - 507, 1976.

[2] J. Kohn, "A cellulose acetate supporting medium for zone electrophoresis," *Nature,* vol. 180, pp. 986-988, 1957.

[3] H. Scherz, "Thin-layer electrophoretic separation of monosaccharides, oligosaccharides and related compounds on reverse phase silica gel," *Electrophoresis,* vol. 11, pp. 18-22, 1990.

[4] S. Hjerten, "High-performance electrophoresis: The electrophoretic counterpart of high performance liquid chromatography," *J. Chromatogr.,* vol. 270, pp. 1-6, 1983.

[5] J. W. Jorgenson and K. D. Lukacs, "Zone electrophoresis in open-tubular glass capillaries," *Anal. Chem.,* vol. 53, pp. 1298-1302, 1981.

[6] E. Carrilho, A. W. Miller, M. C. Ruiz-Martinez, L. Kotler, J. Kesilman, and B. L. Karger, "Factors to be considered for robust high-throughput automated DNA sequencing using a multiple-capillary array instrument," *Proc. SPIE-Int. Soc. Opt. Eng.,* vol. 2985, pp. 4-18, 1997.

[7] M. A. Q. X. C. Huang, R. A. Mathies, "Capillary Array Electrophoresis Using Laser-Excited Confocal Fluorescence Detection," *Anal. Chem.,* vol. 64, pp. 967 - 972, 1992.

[8] S. C. Terry, J. H. Jerman, and J. B. Angell, "A gas chromatograph air analyzer fabricated on a silicon wafer," *IEEE Trans. Electron. Devices,* vol. ED-26, p. 1880, 1979.

[9] A. Manz, N. Graber, and H. M. Widmer, "Miniaturized total chemical analysis systems: a novel concept for chemical sensing," *Sensors and Actuators, B: Chemical,* vol. B1, pp. 244-248, 1990.

[10] A. Manz, D. J. Harrison, and E. M. J. Verpoorte, "Planar chips technology for miniaturization and integration of separation techniques into monitoring systems. Capillary electrophoresis on a chip," *J. Chromatogr.,* vol. 593, pp. 253-258, 1992.

[11] S. C. Jacobson, R. Hergenroder, L. B. Koutny, and J. M. Ramsey, "High-speed separations on a microchip," *Anal. Chem.,* vol. 66, pp. 1114-1118, 1994.

[12] V. Dolnik, S. Liu, and S. Jovanovich, "Capillary electrophoresis on microchip," *Electrophoresis,* vol. 21, pp. 41-54, 2000.

[13] J. S. R. Matthew A. Roberts, Paul Bercier, and Hubert Girault, "UV Laser Machined Polymer Substrates for the Development of Microdiagnostic Systems," *Anal. Chem.,* vol. 69, pp. 2035 - 2042, 1997.

[14] R. J. N. Randy M. McCormick, M. Goretty Alonso-Amigo, Dominic J. Benvegnu, and Herbert H. Hooper, "Microchannel Electrophoretic Separations of DNA in Injection-Molded Plastic Substrates," *Anal. Chem.,* vol. 69, pp. 2626 - 2630, 1997.

[15] G. J. M. B. Carlo S. Effenhauser, Aran Paulus, and Markus Ehrat, "Integrated Capillary Electrophoresis on Flexible Silicone Microdevices: Analysis of DNA Restriction Fragments and Detection of Single DNA Molecules on Microchips," *Anal. Chem.,* vol. 69, pp. 3451 - 3457, 1997.

[16] L. E. L. Larisa Martynova, Michael Gaitan, Gary W. Kramer, Richard G. Christensen, and William A. MacCrehan, "Fabrication of Plastic Microfluid Channels by Imprinting Methods," *Anal. Chem.,* vol. 69, pp. 4783 - 4789, 1997.

[17] R. Srinivasan and B. Braden, "Ultraviolet laser ablation of organic polymers," *Chem. Rev.,* vol. 89, pp. 1303-1316, 1989.

[18] L. G. Reyna and J. R. Sobehart, "Laser ablation of multilayer polymer films," *J. Appl. Phys.,* vol. 76, pp. 4367-4371, 1994.

[19] J. R. Webster, M. A. Burns, D. T. Burke, and C. H. Mastrangelo, "An inexpensive plastic technology for microfabricated capillary electrophoresis chips," in *International Conference on Miniaturized Systems for Chemistry and Life Sciences (μ-TAS)*, 1998, pp. 249-252.

[20] C. W. Kan, C. P. Fredlake, E. A. S. Doherty, and A. E. Barron, "DNA sequencing and genotyping in miniaturized electrophoresis systems," *Electrophoresis,* vol. 25, pp. 3564-3588, 2004.

[21] F. Sanger, S. Nicklen, and A. R. Coulson, "DNA sequencing with chain-terminating inhibitors," *Proc. Natl. Acad. Sci.,* vol. 74, pp. 5463-5467, 1977.

[22] M. Orita, H. Iwahana, H. Kanazawa, K. Hayashi, and T. Sekiya, "Detection of polymorphisms of human DNA by gel electrophoresis as single-strand conformation polymorphisms," *Proc. Natl. Acad. Sci.,* vol. 86, pp. 2766-2770, 1989.

[23] C. Jespersgaard, L. A. Larsen, S. Baba, Y. Kukita, T. Tahira, M. Christiansen, J. Vuust, K. Hayashi, and P. S. Andersen, "Optimization of capillary array electrophoresis single-strand conformation polymorphism analysis for routine molecular diagnostics," *Electrophoresis,* vol. 27, pp. 3816-3822, 2006.

[24] T. Footz, M. J. Somerville, R. Tomaszewski, K. A. Sprysak, and C. J. Backhouse, "Heteroduplex-based genotyping with microchip electrophoresis and dHPLC," *Genetic Testing,* vol. 7, pp. 283-293, 2003.

[25] E. Szántai and A. Guttman, "Genotyping with microfluidic devices," *Electrophoresis,* vol. 27, pp. 4896-4903, 2006.

[26] A. Tiselius, "A new apparatus for electrophoretic analysis of colloidal mixtures," *Trans. Faraday Soc.,* vol. 33, p. 524, 1937.

[27] J. L. Viovy, "Electrophoresis of DNA and other polyelectrolytes: Physical mechanisms," *Reviews of Modern Physics,* vol. 72, pp. 813-872, 2000.

[28] A. Sartori, V. Barbier, and J. L. Viovy, "Sieving mechanisms in polymeric matrices," *Electrophoresis,* vol. 24, pp. 421-440, 2003.

[29] E. Hückel, "The electrophoresis of spherical colloid," *Phys. Zeit,* vol. 25, pp. 204-210, 1924.

[30] M. von Smoluchowski, "Contribution à la théorie de l'endosmose électrique et de quelques phenomènes corrélatifs," *Bulletin International de l'Academie des Sciences de Cracovie,* vol. 8, pp. 182-200, 1903.

[31] J. A. Luckey, T. B. Norris, and L. M. Smith, "Analysis of resolution in DNA sequencing by capillary gel electrophoresis," *The Journal of Physical Chemistry,* vol. 97, pp. 3067-3075, 1993.

[32] K. A. Ferguson, "Starch-gel electrophoresis-Application to the classification of pituitary proteins and polypeptides," *Metabolism,* vol. 13, pp. 985-1002, 1964.

[33] H. Benoit and P. Doty, "Light scattering from non-gaussian chains," *The Journal of Physical Chemistry,* vol. 57, pp. 958-963, 1953.

[34] P. D. Grossman and D. S. Soane, "Experimental and theoretical studies of DNA separations by capillary electrophoresis in entangled polymer solutions," *Biopolymers,* vol. 31, pp. 1221-1228, 1991.

[35] J.-L. Viovy and T. Duke, "DNA electrophoresis in polymer solutions: Ogston sieving, reptation and constraint release," *Electrophoresis,* vol. 14, pp. 322-329, 1993.

[36] D. Broseta, L. Leibler, A. Lapp, and C. Strazielle, "Universal properties of semidilute polymer solutions: a comparison between experiments and theory," *Europhysics Letters,* vol. 2, pp. 733-737, 1986.

[37] A. G. Ogston, "The spaces in a uniform random suspension of fibres," *Trans. Faraday Soc,* vol. 54, pp. 1754–1757, 1958.

[38] M. Doi and S. F. Edwards, *The theory of polymer dynamics*. Oxford: Oxford University Press, 1986.

[39] P. G. de Gennes, *Scaling concepts in polymer physics*. Ithaca, NY: Cornell University Press, 1979.

[40] O. J. Lumpkin and B. H. Zimm, "Mobility of DNA in gel electrophoresis," *Biopolymers,* vol. 21, pp. 2315-2316, 1982.

[41] L. S. Lerman and H. L. Frisch, "Why does the electrophoretic mobility of DNA in gels vary with the length of the molecule?," *Biopolymers,* vol. 21, pp. 995-997, 1982.

[42] T. Duke, J. L. Viovy, and A. N. Semenov, "Electrophoretic mobility of DNA in gels. I. New biased reptation theory including fluctuations," *Biopolymers,* vol. 34, pp. 239-247, 1994.

[43] T. A. J. Duke, A. N. Semenov, and J. L. Viovy, "Mobility of a reptating polymer," *Physical Review Letters,* vol. 69, pp. 3260-3263, 1992.

[44] A. N. Semenov, T. A. J. Duke, and J. L. Viovy, "Gel electrophoresis of DNA in moderate fields: The effect of fluctuations," *Physical Review E,* vol. 51, pp. 1520-1537, 1995.

[45] C. Heller, T. Duke, and J. L. Viovy, "Electrophoretic mobility of DNA in gels. II. Systematic experimental study in agarose gels," *Biopolymers,* vol. 34, pp. 249-259, 1994.

[46] G. T. Barkema, J. F. Marko, and B. Widom, "Electrophoresis of charged polymers: Simulation and scaling in a lattice model of reptation," *Physical Review E,* vol. 49, pp. 5303-5309, 1994.

[47] J. J. Lu and S. Liu, "A robust cross-linked polyacrylamide coating for microchip electrophoresis of dsDNA fragments," *Electrophoresis,* vol. 27, pp. 3764-3771, 2006.

[48] Y. Shi and R. C. Anderson, "High-resolution single-stranded DNA analysis on 4. 5 cm plastic electrophoretic microchannels," *Electrophoresis,* vol. 24, pp. 3371-3377, 2003.

[49] V. M. Ugaz, R. Lin, N. Srivastava, D. T. Burke, and M. A. Burns, "A versatile microfabricated platform for electrophoresis of double-and single-stranded DNA," *Electrophoresis,* vol. 24, pp. 151-157, 2003.

[50] C. H. Tsai, R. J. Yang, C. H. Tai, and L. M. Fu, "Numerical simulation of electrokinetic injection techniques in capillary electrophoresis microchips," *Electrophoresis,* vol. 26, pp. 674-686, 2005.

[51] M. Tabuchi, Y. Kuramitsu, K. Nakamura, and Y. Baba, "A 15-s protein separation employing hydrodynamic force on a microchip," *Anal. Chem,* vol. 75, pp. 3799-3805, 2003.

[52] U. Backofen, F. M. Matysik, and C. E. Lunte, "A chip-based electrophoresis system with electrochemical detection and hydrodynamic injection," *Anal. Chem,* vol. 74, pp. 4054-4059, 2002.

[53] G. Ocvirk, M. Munroe, T. Tang, R. Oleschuk, K. Westra, and D. J. Harrison, "Electrokinetic control of fluid flow in native poly (dimethylsiloxane) capillary electrophoresis devices," *Electrophoresis,* vol. 21, pp. 107-115, 2000.

[54] L. M. Fu and C. H. Lin, "High-resolution DNA separation in microcapillary electrophoresis chips utilizing double-L injection techniques," *Electrophoresis,* vol. 25, pp. 3652-3659, 2004.

[55] C. T. Culbertson, S. C. Jacobson, and J. M. Ramsey, "Dispersion sources for compact geometries on microchips," *Anal. Chem,* vol. 70, pp. 3781–3789, 1998.

[56] B. M. Paegel, L. D. Hutt, P. C. Simpson, and R. A. Mathies, "Turn geometry for minimizing band broadening in microfabricated capillary electrophoresis channels," *Anal. Chem,* vol. 72, pp. 3030-3037, 2000.

[57] S. N. Brahmasandra, V. M. Ugaz, D. T. Burke, C. H. Mastrangelo, and M. A. Burns, "Electrophoresis in microfabricated devices using photopolymerized polyacrylamide gels and electrode-defined sample injection," *Electrophoresis,* vol. 22, pp. 300-311, 2001.

[58] L. M. Fu and R. J. Yang, "Low-voltage driven control in electrophoresis microchips by traveling electric field," *Electrophoresis,* vol. 24, pp. 1253-1260, 2003.

[59] T. Footz, M. J. Somerville, R. Tomaszewski, B. Elyas, and C. J. Backhouse, "Integration of combined heteroduplex/restriction fragment length polymorphism analysis on an electrophoresis microchip for the detection of hereditary haemochromatosis," *Analyst,* vol. 129, pp. 25-31, 2004.

[60] H. Tian, L. C. Brody, and J. P. Landers, "Rapid detection of deletion, insertion, and substitution mutations via heteroduplex analysis using capillary-and microchip-based electrophoresis," *Genome Res.,* vol. 10, pp. 1403-1413, 2000.

[61] C. Backhouse, M. Caamano, F. Oaks, E. Nordman, A. Carrillo, B. Johnson, and S. Bay, "DNA sequencing in a monolithic microchannel device," *Electrophoresis,* vol. 21, pp. 150-156, 2000.

[62] J. S. Buch, C. Kimball, F. Rosenberger, W. E. Highsmith Jr, D. L. DeVoe, and C. S. Lee, "DNA mutation detection in a polymer microfluidic network using temperature gradient gel electrophoresis," *Anal. Chem,* vol. 76, pp. 874-81, 2004.

[63] N. J. Munro, K. Snow, J. A. Kant, and J. P. Landers, "Molecular diagnostics on microfabricated electrophoretic devices: From slab gel-to capillary-to microchip-based assays for T-and B-cell lymphoproliferative disorders," *Clinical Chemistry,* vol. 45, pp. 1906-1917, 1999.

[64] Y. Shi, P. C. Simpson, J. R. Scherer, D. Wexler, C. Skibola, M. T. Smith, and R. A. Mathies, "Radial capillary array electrophoresis microplate and scanner for high-performance nucleic acid analysis," *Anal. Chem,* vol. 71, pp. 5354-5361, 1999.

[65] P. C. Simpson, D. Roach, A. T. Woolley, T. Thorsen, R. Johnston, G. F. Sensabaugh, and R. A. Mathies, "High-throughput genetic analysis using microfabricated 96-sample capillary array electrophoresis microplates," *Proc. Natl. Acad. Sci.,* vol. 95, pp. 2256-2261, 1998.

[66] A. T. Woolley, G. F. Sensabaugh, and R. A. Mathies, "High-speed DNA genotyping using microfabricated capillary array electrophoresis chips," *Anal. Chem,* vol. 69, pp. 2181-2186, 1997.

[67] "http://www.scscoatings.com/parylene_knowledge/specifications.aspx," in *Parylene Specifications*: SCS Coatings, 8/31/2007.

[68] L. J. Yang, T. J. Yao, and Y. C. Tai, "The marching velocity of the capillary meniscus in a microchannel," *Journal of Micromechanics and Microengineering,* vol. 14, pp. 220-225, 2004.

[69] J. R. Webster, "Monolithic structures for integrated capillary electrophoresis systems," Ph.D. Dissertation: University of Michigan, 1999.

[70] K. N. Walsh and J. Y. C. Tai, "Photoresist as a sacrificial layer by dissolution in acetone," *The 14th IEEE International Conference on Micro Electro Mechanical Systems, 2001 (MEMS 2001),* pp. 114-117, 2001.

APPENDIX

DETAILED FABRICATION PROCESS FLOW

STEP	PROCESS	SPECIFICATION
1	GLASS WAFERS WITH FLAT	4" Wafers
2	**WAFER CLEANING**	1. Immerse in piranha solution
	Piranha Solution (1:1 H2SO4:H2O2)	2. Wait for 15 min.
		3. DI-Water rinsing, 7 cycles
		4. Dry by N_2
	Buffered Hydrofluoric Acid (BHF)	5. Immerse in BHF
		6. Wait for 1 min.
		7. DI-Water rinsing, 5 cycles
		8. Dry by N_2
2	**PARYLENE DEPOSITION**	Dimer: 10 gr
	Use silanation	Set Point: 15
		PLA_I: 9
		Meas: ~ 5 um thickness
3a	**TITANIUM SPUTTERING**	Flow: 2.5 sccm Ar (Pressure: 2e-3 mbar)
		Power: 300 W Distance: 135 mm
		Time: 180 secs
		Meas: ~ 500 A thickness

3b	**GOLD SPUTTERING**	Flow: 6.2 sccm Ar (Pressure: 5e-3 mbar) Power: 300 W Distance 130 mm Time: 400 secs Meas: ~5000 A thickness
4	**LITHOGRAPHY** MASK #1 for Metal Etching Mask name: **METAL**	1. Primer(HMDS), 500rpm 7 sec. + 4000rpm 30 sec. 2. S1813 PR, 500rpm 7 sec. + 4000rpm, 30 sec. 3. Softbake 115°C, 70 sec., hotplate 4. Align & Expose, 5 sec (12 mW/cm2 @CP) 5. Develop, MF-319, 50 sec. 6. DI-Water Rinse, 1.5 min + 1.5min. 7. Dry by N_2 8. Inspection 9. Hardbake, 10 min @ 110 °C.
5a	**GOLD ETCH** Gold Etchant: Transene Type TFA	1. Etch in Au Etchant (Duration depends on the etchant, 2-2.5 mins with fresh etchant) 2. DI-water rinse, 3 cycles 3. Dry by N_2 4. Inspection
5b	**TITANIUM ETCH** Ti Etchant: 1:1:640 HF:H2O2:DI-Water	1. Etch in Ti Etchant for ~4.5-5 min 2. DI-water rinse, 3 cycles 3. Dry by N_2 4. Inspection

6	**STRIP PHOTORESIST** With Teflon Holder	1. ACE 2. IPA 3. DI-water rinse. 4. Dry by N_2 5. Inspection
7	**LITHOGRAPHY** MASK #2 for Channel Forming Mask name: **CHANNEL**	1. Primer(HMDS), 500rpm 10 sec. + 900rpm 20 sec. 2. AZ9260 PR, 500rpm 10 sec. + 900rpm, 20 sec. 3. Wait for 15 min. 4. Pre-Bake 95°C, 90 sec., hotplate 5. Edge bead removal, 500rpm 10 sec. + 900rpm 20 sec. 6. Softbake Start at RT raise the temperature to 95°C, 30 min at 95 °C. 7. Rehydration (3 pipettes of DI-Water in blue box, 1 hr) 8. Align & Expose, 45 sec (12 mW/cm2 @CP) 9. Develop, AZ826-MIF, 10 min. 6. DI-Water Rinse, 1.5 min + 1.5min. 7. Dry by N_2 8. Inspection
8	**PARYLENE DEPOSITION** Do not use silanation	Dimer: 40 gr Set Point: 25 PLA_I: 10 Meas: ~ 20 um thickness
9	**LITHOGRAPHY** MASK #3 for Parylene Etching Mask name: **OPENING**	1. Primer(HMDS), 500rpm 10 sec. + 750rpm 20 sec. 2. AZ9260 PR, 500rpm 10 sec. + 750rpm, 20 sec. 3. Wait for 15 min. 4. Pre-Bake 90°C, 3 min., hotplate

		5. Edge bead removal, 500rpm 10 sec. + 750rpm, 20 sec. 6. AZ9260 PR, 500rpm 10 sec. + 750rpm, 20 sec. (Second spin) 7. Wait for 15 min. 8. Pre-Bake 90°C, 5 min., hotplate 9. Edge bead removal, 500rpm 10 sec. + 750rpm, 20 sec. 10. Softbake Start at RT raise the temperature to 90°C, 60 min at 90 °C. 11. Rehydration (4 pipettes of DI-Water in blue box, 2 hrs) 12. Align & Expose, 55 sec (12 mW/cm2 @CP) 13. Develop, AZ826-MIF, 30 min. 14. DI-Water Rinse, 1.5 min + 1.5min. 15. Dry by N_2 16. Align & Expose, 55 sec (12 mW/cm2 @CP) 17. Develop, AZ826-MIF, 20 min. 18. DI-Water Rinse, 1.5 min + 1.5min. 19. Dry by N_2 20. Inspection
10	**PARYLENE RIE**	1. Etch Parylene in RIE for 45 + 40 min with Paryle_1 recipe 2. Inspection
11	**DICING**	1. Dice the wafers
12	**RELEASE**	1. Immerse in Acetone, wait for 48 hrs 2. IPA Rinse 3. Methanol Rinse 4. Vaporize Methanol with 0.5 cm proximity on hotplate @60°C